DESIGN OF MULTILAYERED SLOT AND YAGI-UDA-BASED LINEARLY AND CIRCULARLY POLARIZED TRANSMITARRAYS

CHEW HOO BENG

MASTER OF ENGINEERING SCIENCE

LEE KONG CHIAN FACULTY OF ENGINEERING AND SCIENCE
UNIVERSITI TUNKU ABDUL RAHMAN
FEBRUARY 2016

DESIGN OF MULTILAYERED SLOT AND YAGI-UDA-BASED LINEARLY AND CIRCULARLY POLARIZED TRANSMITARRAYS

By

CHEW HOO BENG

A dissertation submitted to the Institute of Postgraduate Studies and Research,

Lee Kong Chian Faculty of Engineering and Science,

Universiti Tunku Abdul Rahman,

in partial fulfillment of the requirements for the degree of Master of

Engineering Science

February 2016

ABSTRACT

DESIGN OF MULTILAYERED SLOT AND YAGI-UDA-BASED LINAERLY AND CIRCULARLY POLARIZED TRANSMITARRAYS

Chew Hoo Beng

Transmitarray has been proven to be a viable architecture for achieving high directivity in antenna to make it suitable for satellite and wireless communication systems, remote sensing, and radar applications. The demand of high-gain antennas is ever-increasing for radar and long-distance communications. A transmitarray consists of an illuminating feed source and a flat transmitting surface with one or multiple layers. Usually, its feeding source can be placed directly in front of the aperture without causing blockage losses or affecting the radiation patterns that are inherent in a conventional reflectarray configuration. Also, the flexibility to be implemented into reconfigurable apertures is one of the major advantages of the transmitarray.

In my first project, a wideband transmitarray was analyzed by implying the design concept of Yagi-Uda antenna which requires the use of feeder, directors and reflectors, operating at 6 GHz. This transmitarray has achieved an antenna gain of 17 dBi at the desired frequency and it has 1-dB bandwidth of 11.86%. It has significantly improved the bandwidth limitation of the microstrip transmitarray. Also, the design of a circularly polarized transmitarray has been demonstrated. Again, the concept of Yagi-Uda was

applied. In this case, the directors between any two layers have an offset of 5 degrees. A total of 8 layers of director are required to achieve a 3-dB axial ratio of 7% and 1-dB bandwidth of 4.06% at the operating frequency of 10 GHz.

For my second project, the conventional annular ring-slot resonator is selected for designing a high-gain transmitarray. The unit cell has 3 layers of transmitting elements. The unit element was first simulated and analyzed using the Floquet method, and the generated S-curve was later used to transform it into a full-fledge transmitarray. The proposed transmitarray antenna has been designed, fabricated, and measured in free space environment at the operating frequency of 7.8 GHz. The measured gain of the prototype transmitarray is 22.4 dBi and it has a 1-dB bandwidth of 2.58%.

CST Microwave Design Studio was used to simulate all the configurations, with experiments done for verification. Good agreement is found between the simulated and measured results. Parametric analysis has been performed to understand the effects of all the design parameters.

ACKNOWLEDGEMENT

First of all, I would like to thank Dr. Lim Eng Hock and Dr. Lo Fook Loong for their valuable guidance and advices throughout all stages of my research project. Stimulating conversation and discussion have been a constant source of valuable ideas in the development of these new devices. In addition, they were always ready to give consultation all the time.

Also, I would like to express my gratitude to Mr. Ho, who guided me on fabrication process. With his guidance, I was able to fabricate my design precisely. Besides that, I also like to extend my gratitude to my course mates for their assistances during experiments.

Special thanks to UTAR for providing all the necessary equipment, facilities, and research materials. Moreover, the online database such as ProQuest and IEEE Xplore are very helpful where most of the important literatures are available.

APPROVAL SHEET

This dissertation entitled **'DESIGN OF MULTILAYERED SLOT AND YAGI-UDA-BASED LINEARLY AND CIRCULARLY POLARIZED TRANSMITARRAYS'** was prepared by CHEW HOO BENG and submitted as partial fulfillment of the requirement for the degree of Master of Engineering Science at Universiti Tunku Abdul Rahman.

Approved by:

(Assoc. Prof. Dr. Lim Eng Hock) Date:……………..
Supervisor
Department of Electrical and Electronic Engineering
Lee Kong Chian Faculty of Engineering Science
Universiti Tunku Abdul Rahman

(Assoc. Prof. Dr. Lo Fook Loong) Date:……………..
Co-supervisor
Department of Electrical and Electronic Engineering
Lee Kong Chian Faculty of Engineering Science
Universiti Tunku Abdul Rahman

LEE KONG CHIAN FACULTY OF ENGINEERING SCIENCE

UNIVERSITI TUNKU ABDUL RAHMAN

Date: 23 February 2016

SUBMISSION OF DISSERTATION

It is hereby certified that **CHEW HOO BENG** (ID No: **14UEM01306**) has completed this dissertation entitled "**DESIGN OF MULTILAYERED SLOT AND YAGI-UDA-BASED LINEARLY AND CIRCULARLY POLARIZED TRANSMITARRAYS**" under the supervision of Dr. Lim Eng Hock (Supervisor) from the Lee Kong Chian Department of Electrical and Electronic Engineering, Faculty of Engineering and Science (FES), and Dr. Lo Fook Loong (Co-Supervisor) from the Lee Kong Chian Department of Electrical and Electronic Engineering, Faculty of Engineering and Science (FES).

I understand that University will upload softcopy of my dissertation in pdf format into UTAR Institutional Repository, which may be made accessible to UTAR community and public.

Yours truly,

(CHEW HOO BENG)

DECLARATION

I hereby declare that the thesis is based on my original work except for citations and quotations which have been duly acknowledged. I also declare that it has not been previously and concurrently submitted for any other degree or award at UTAR or other institutions.

(CHEW HOO BENG)

Date: 23 February 2016

TABLE OF CONTENTS

LIST OF TABLES

LIST OF FIGURES

CHAPTER 1

INTRODUCTION

1.1 Background and Issues

Antenna is an intrinsic part of all wireless communication and sensing systems. It transforms electromagnetic (EM) energy from a wave-guiding structure into free-space. The physical layout of the antenna can be designed into different shapes and sizes depending on its applications. A satellite antenna has to be designed to have high gain, broad bandwidth, light weight, and easy implementation by standard printed-circuit-board manufacturing processes. For radar and long-distance communications, particularly, the demand for high-gain antenna is increasing as the radiated power has to be focus in a specific direction so that it is able to travel farther. A high-gain antenna enables long range EM wave transmission with minimum amount of transmitting power.

Traditionally, the high-gain applications have been heavily relied upon parabolic reflectors or antenna arrays (Jasik, 1961). *Figure 1.1* depicts the parabolic disc of the reflector antenna. It is able to focus EM power into a certain direction for enhancing antenna gain. However, the disc is usually made of metallic materials, making it very bulky, and it appears to be impractical for space-borne applications, especially on beam scanning feature. A mechanical rotator has to be incorporated with a parabolic reflector antenna to perform beam scanning by changing the direction of radiation aperture without affecting the feeding angle of the illuminating source. But scanning the beam mechanically is too slow for capturing the fast-changing signals in the wireless systems.

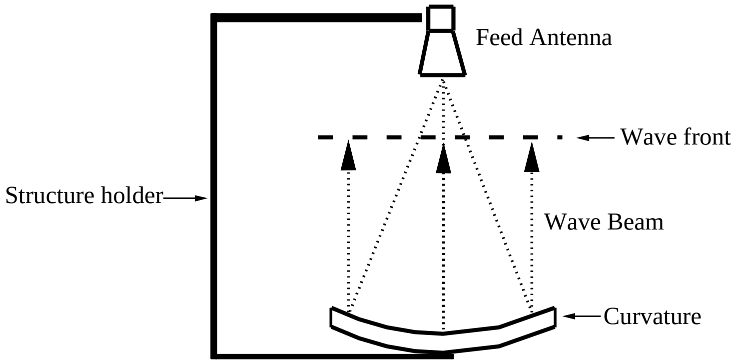

Figure 1.1: Parabolic reflector with broadside feed.

To overcome the limitations of the parabolic reflector antenna, phased array has been introduced. It functions by combining multiple antennas into array form. Phased array is directly fed by different input phases that enable beam scanning easily. The design theory and techniques of the phased arrays have already been well developed and studied by Bhattacharyya (2006) and Hansen (2009). *Figure 1.2* shows the prototype of a conventional reconfigurable phased array. To drive all the transmitting antennas, multiple power dividers are used to split the input signal and a number of phase shifters are deployed for controlling the phases of the radiating waves. However, phase array design can be quite complicated, especially for a large-scale one, as it may involve the use of a cascade of power dividing networks, which can introduce high insertion loss. (Reinhart et. al., 2003 and Ku et. al, 2014)

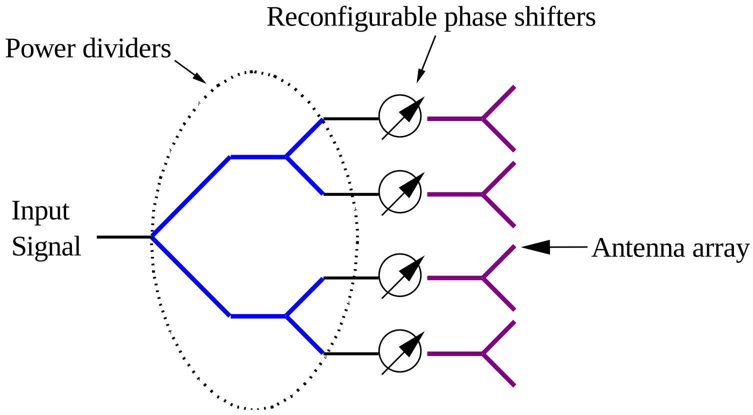

Figure 1.2: Reconfigurable phased array.

To overcome the shortcomings of the phased array, a new type of antenna called reflectarray has been introduced. Reflectarray is a latest technology that combines some of the good features of both the conventional parabolic reflector antenna and the phased array. It consists of either a flat or slightly curved reflecting surface illuminated by a feeder, as shown in *Figure 1.3*, where all of the radiating elements are pre-designed to be excited by an incident wave and to re-radiate into a certain direction. The first reflectarray was proposed by Berry et al. (1963). Similar to parabolic reflector, reflectarray can obtain good antenna efficiency for a large aperture due to the implementation of spatial feeding techniques (Huang and Encinar, 2007). All the radiating elements of the reflectarray are spatially excited by the feeding source, as it does not require any complicated power dividing networks. However, the position of the feeding source does affect and interrupt the reflected waves in the broadside direction. This is because the feeding source is usually made of conductive material, which can scatter waves and degrade the radiation performances.

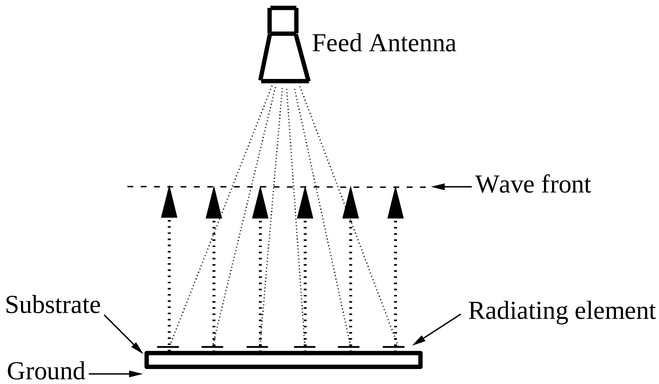

Figure 1.3: A typical reflectarray with multiple wave beams reflected by the radiating elements.

As a remedy, the offset-fed reflectarray has been proposed to avoid potential feed blocking loss, as shown in *Figure 1.4* (Encinar, 2001; Ahmadi et al., 2013). Such structure may be lighter and lower in profile than the conventional parabolic reflector as it needs less supporting fixtures. That makes it popular for space-borne applications, especially in spacecrafts or satellite systems. The antenna gain of a reflectarray can be easily enhanced by hosting more radiating elements. Nevertheless, this offset geometry gives rise to higher cross polarization, feed image lobes, and beam squint (Yu et al., 2009; Almajali et al., 2014).

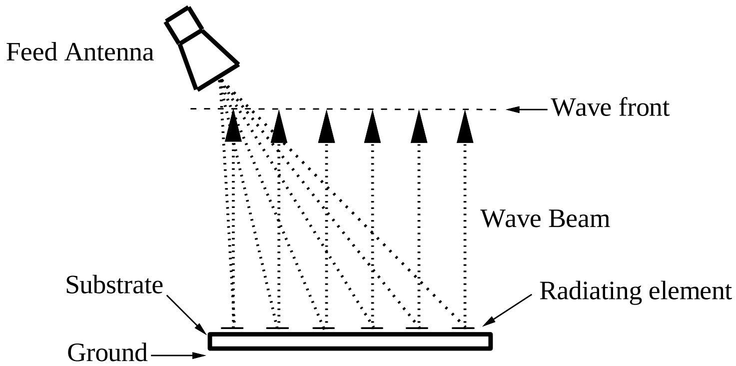

Figure 1.4: A typical offset-fed reflectarray with multiple wave beams reflected by the radiating elements.

In order to improve the shortcomings of reflectarray, a new type of antenna called transmitarray has been introduced. Transmitarray is a type of antenna which has many unit elements arranged in array form, with the neighboring elements having equal or unequal separation distances depending on the structure of the transmitting element. It is a structure that combines the features of dielectric lens and phased array. For a transmitarray, the incident electromagnetic wave coming from the feeding source transmits through the transmitting layers and it can be converted from a spherical wave front into any others (Lam et al., 1997).

Figure 1.5 shows the geometry of a conventional four-layer microstrip transmitarray, where the feeding horn is placed on the opposite side of the radiating aperture to avoid potential blockage. A transmitarray usually has a better efficiency when the source is fed at the broadside direction without any inclination angle (Almajali, 2014). Comparing to the conventional reflectors and lenses, the transmitarray structure has one obvious advantage of being planar, making it easy to integrate with other structures such as roof-tops and walls. A transmitarray can also be made steerable, which is useful for point-to-point and satellite-based communication systems.

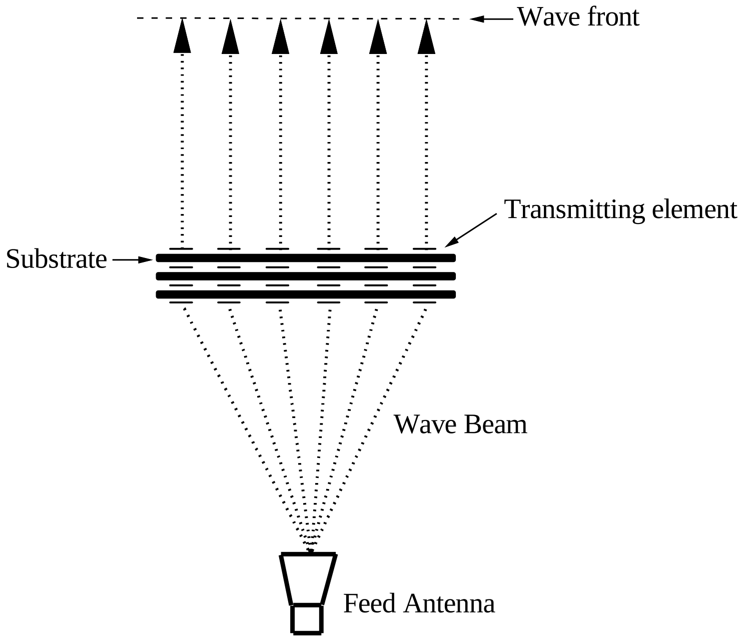

Figure 1.5: Geometry of a four-layer microstrip transmitarray.

1.2 Research Objectives and Motivation

Limited by their unit elements, most of the transmitarrays have narrow bandwidth. The main objective of the proposed projects is to explore new low-Q resonators for designing transmitarrays so that they able to produce broad phase range and wide bandwidth. In this dissertation, two projects have been conducted to achieve the same research objectives. Different types of unit elements have been explored for the design of either linearly- or circularly-polarized transmitarrays. For both cases, different resonances of the unit elements have been identified to obtain low insertion loss and high phase range concurrently.

In the first project, the concept of Yagi-Uda is deployed for designing a high-gain linearly polarized transmitarray for the first time. A transmitarray element, which is composed by six strips stacked in parallel, can be used as the director of the feeder at the same time. It was found that the unit element can be made to generate circularly polarized wave by introducing angular rotation into the strips.

The second project is devoted to studying the resonances of the annular ring-slot resonator, which can be used to design a linearly-polarized transmitarray. To demonstrate the design idea, a total of 81 unit elements have been deployed to design a 9×9 microstrip transmitarray, working at 7.8 GHz. Experiment was carried out and parametric analysis was performed to understand the effects of design parameters.

1.3 Thesis Overview

In this dissertation, the operating principles and design procedures for two high-gain transmitarrays will be explored systematically and numerically in the following chapters. In this section, an overview of the thesis will be provided. There are 5 chapters in this thesis and a complete reference list has also been appended.

Chapter 1 introduces the design concept of the transmitarray, along with introduction of high-gain antennas. In the final part, the research objectives and motivation of this research are ensued.

Chapter 2 discusses the recent development and design methodology of the transmitarray. This includes the simulation method and design procedures for analyzing transmitarray. Brief explanations of some of the key performance indicators are also presented in this chapter.

Chapter 3 presents the linearly and circularly polarized transmitarrays which are designed using the Yagi-Uda concept. The design procedures are described, with the simulation and measurement results studied.

Chapter 4 explores the design of a C-band transmitarray with the annular-slot resonator. Details on the fabrication, layout, and analysis are presented, along with simulated and experimental results. Parametric analysis is performed on the key design parameters.

Chapter 5 summarizes the research works done in this dissertation. Discussion on the key findings is included.

CHAPTER 2

BACKGROUND AND DEVELOPMENT

2.1 Development History

Transmitarray, a new type of antenna which is originated from dielectric lens, is a practical radiating structure that is able to achieve a high gain, broad bandwidth and low profile. Lenses can be used to redirect, converge, and diverge electromagnetic wave to or from a feeding source. A brief introduction of lens is given here. In one of its earliest applications, homogeneous lens was designed to perform wide-angle scanning (Friedlander, 1946). It was found that homogeneous lenses could also be used as a phase-front corrector for horn antenna (Khoury and Heane, 1991). In this case, Snell's law can be used to describe the dielectric constant of the lens to the incidence and refraction angles. As illustrated in *Figure 2.1*, the refracted waves converge at a focal point after passing through a shaped lens.

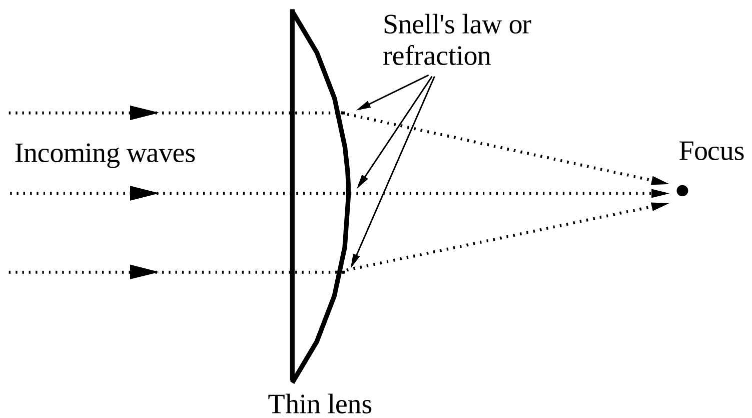

Figure 2.1: **A** thin lens for converging wave beams.

Reflection mismatch or dielectric losses are two unavoidable factors when designing a dielectric lens. To minimize them, dielectric materials with low loss and low permittivity such as Teflon, polyethylene, and quartz are commonly used to reduce the material loss to a negligible level (Thornton and Huang, 2013). As a result, dielectric lenses that operate at low frequencies are usually bulky and expensive to manufacture. A wide range of techniques can be used to design the curvature of the lenses at microwave frequencies (Ruze, 1950; Ikonen et al., 2006; Petosa et al., 2006; Lyer and Eleftheriades, 2007; Yijing et al., 2010). Fabricating an accurate curvature may require sophisticated tooling, which can be very expensive.

Microstrip transmitarray, appearing as planar microwave lenses, has received considerable attention (McGrath, 1986; Pozar, 1996; Hollung et al., 1997; Zhou et al., 2005; Abbaspour-Tamijani et al., 2007) because it is mechanically simple to make. It can be designed using printed elements such as loop, patch, and dipole, which can be easily mounted on a supporting substrate (Lam et al., 1997 and Ryan et al., 2010). To provide sufficient compensating phase, a transmitarray element is required to generate a transmission phase of at least 360^{o}, while maintaining low transmission loss in the desired frequency passband. Since a single layer of transmitarray element is usually able to yield a 3-dB transmission phase of less than 90^{o} (Abdelrahman et al., 2014), multilayer structures have been commonly used for increasing the phase range of the transmitarray.

2.2 Design Procedure of Transmitarray

There exist two types of design methods for the designing transmitarray elements - Generalized Direct Optimization Technique (GDOT) and Phase-Only Synthesis (POS) method. The first technique employs Spectral-Domain Method of Moments (SDMoM) and it is suitable for arbitrarily-shaped elements which do not have a fixed orientation or position (Zhou et al., 2013). This technique is time-consuming as it requires a lot of computational resources to simulate and analyze all the possible combinations when arranging the locations of the unit elements. The POS approach is much more convenient and effective, where all of the unit elements are arranged in square or symmetrical grid systematically. Also, the unit elements can have equal or unequal spacing. Such design method is much more direct and definitive and it avoids the needs for performing numerous computational simulations. In fact, this technique has been extensively used to design various types of transmitarrays as well as reflectarrays (Huang and Encinar, 2007; Arrebola, 2008; Capozzoli, 2010; Ryan et al., 2010; Shaker et al., 2014).

In my dissertation, the POS technique is adopted for designing the proposed transmitarrays. *Figure 2.2* illustrates a brief and concise design procedure for the POS. First of all, the transmission response of the unit element is simulated either using the waveguide method or Floquet cell where the phase-shifting parameter of the unit element is identified. The curve that relates the geometrical change to the transmission phase, also known as S-curve, is established for normal incidence. Next, the constellation of the full transmitarray is defined by placing multiple elements close to each other, where wave path lengths from the feeder to all elements can be easily determined. By taking one of the unit elements as reference, the path difference between a particular element and the reference are then calculated in phase angle. Usually, the element located in the shortest path length is selected as the reference. The phase difference is then mapped to S-curve for extracting the geometrical dimension that is required to generate it. Finally, the full-fledge transmitarray is constructed and simulated using the CST Microwave Studio. Key performance indicators such as antenna gain, 1-dB bandwidth, and axial ratio will be analyzed. Here, optimization will be performed to further improve the radiation performance.

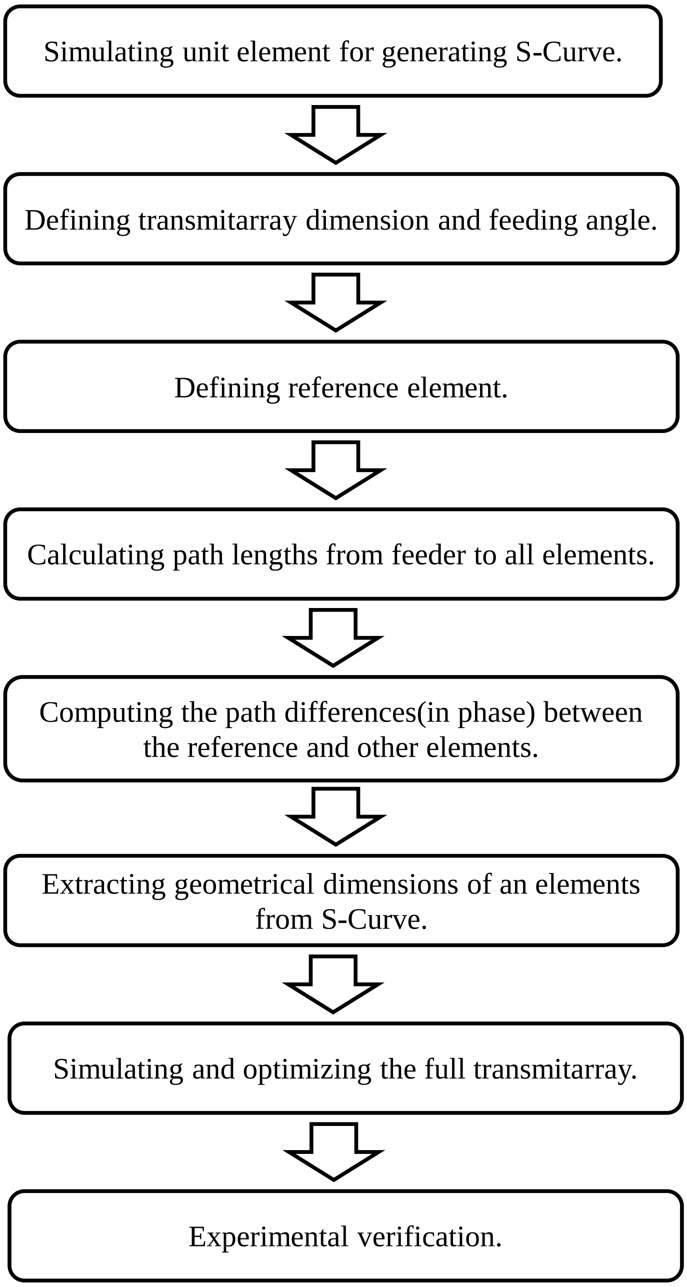

Figure 2.2: Design procedure of a transmitarray by using the phase-only synthesis (POS) technique.

2.3 Key Performance Indicators for Transmitarray

In this section, the key performance indicators that are used to describe the performances of a transmitarray are discussed. A transmitarray is usually designed to have high gain and broad bandwidth.

2.3.1 Antenna Gain

Antenna gain is a measure that takes into account of the antenna efficiency as well as its directional characteristics in a particular direction. Generally, it is measured in dBi (the gain of the antenna with respect to the gain of an isotopic radiator). The maximum gain of an antenna is simply defined as the product of the directivity to the antenna efficiency, as defined in *equation (2.1)*. Antenna gain is usually less than its directivity due to the inclusion of antenna efficiency.

$$\text{Antenna Gain} = \text{Directivity} \times \text{Antenna Efficiency} \tag{2.1}$$

Similar to reflectarray, the gain of a transmitarray is primarily affected by the number of unit elements as well as the separation distances between them in the transmitting aperture. The separation distance between the transmitting elements is usually designed to be 0.5λ to 0.6λ to minimize the unwanted side-lobes effects. *F / D* ratio is another design parameter which can be optimized for enhancing the antenna gain of a transmitarray. Theoretically, the *F / D* ratio does take into account of the spillover losses, taper losses, and quantization losses simultaneously (Kaouach et al., 2011 and Clemente et al., 2012). Typical F / D ratio for the microstrip transmitarray usually falls in the range of 0.5 to 1.

2.3.2 1-dB Gain Bandwidth

Another useful measure for describing the performance of a transmitarray is its 1-dB gain bandwidth. It is defined as the range of frequencies which the antenna gain drop is less than 1-dB. For a transmitarray, its gain bandwidth is mainly limited by the characteristics of unit element and the elements' separation distance, which is designed at one frequency only.

2.3.3 Axial Ratio Bandwidth

The polarization of a transmitarray is mainly depending on the polarization of the feeding source as well as the characteristics of the unit elements. With the use of the element rotation and rotational symmetry techniques, the transmitarray elements can be easily made to provide Left Hand Circularly Polarization (LHCP) or Right Hand Circularly Polarization (RHCP), with minimum insertion loss and sufficient transmission phase (Dussopt et al., 2011). Axial Ratio (AR) is a key indicator for measuring the circular polarization performance. Usually, the axial ratio of a circularly polarized antenna has to be kept below 3dB. The spectrum in which the transmitarray is able to provide an AR ratio of lower than 3dB is defined as the axial ratio bandwidth (Toh et al., 2003; Gao et al., 2014).

2.3.4 Losses and Side-lobes

Ideally, it is desirable that the input signal that reaches the receiving surface of a transmitarray will wholly be transmitted. However, the transmitting signal can be affected by unwanted losses such as dissipative loss, reflection loss, and spillover loss, as depicted in *Figure 2.3*.

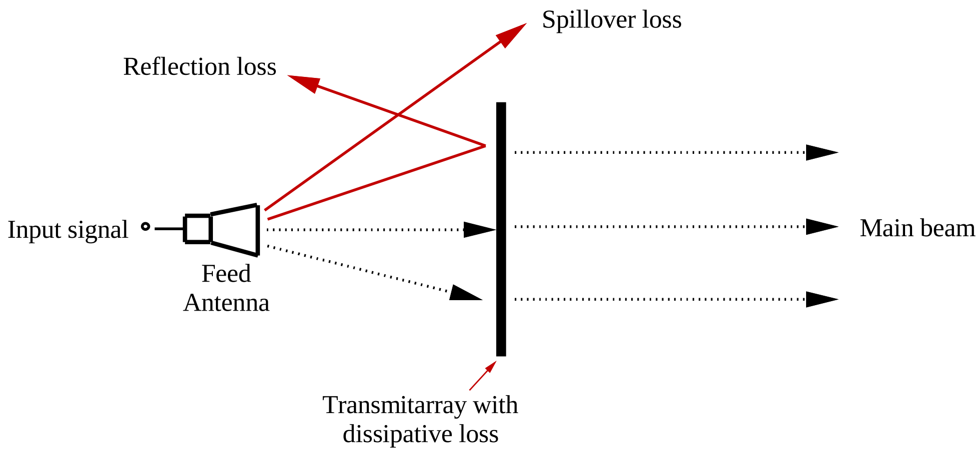

Figure 2.3: Losses of transmitarray.

Dissipative loss is introduced by conductive and dielectric losses in the transmitarray elements. Conductive loss is caused by the ohmic dissipation that exists in the metallic parts that are used for designing the elements. On the other hand, dielectric loss is found in dielectric materials with non-zero conductivity. Summing up the two losses may degrade the radiation efficiency of the transmitarray. To further reduce the dielectric loss, a transmitarray that does not have any dielectric substrate was explored and implemented by Abdelrahman et al. (2014). This makes the manufacturing costs lower as it does not require any expensive substrate materials. Dissipative loss can also be caused by parasitic resistances found in lumped components such as capacitors, varactors and inductors that may exist in an antenna. The feeding source of the transmitarray plays an important role in manipulating the amount of spillover loss. Since the dimension of transmitarray is finite, the feeding source (*F / D* ratio) cannot be placed too far from the transmitting surface. Research has been studied by Clemente et al. (2012) and Kaouach et al. (2010) on the optimization of the *F / D* ratio. Usually, a transmitarray with smaller *F / D* ratio can have poorer 1-dB bandwidth performance due to taper and quantization losses. While having a large *F / D* ratio, on the other hand, may introduce spillover losses and unwanted side-lobes. With reference to *Figure 2.3*, reflection loss can be caused by the specular reflection from the ground plane (Rajagoplan et. al. 2012).

2.4 Unit Element Simulation

It is obvious that finding a unit element that is able to provide sufficient phase range is crucial in the designing a transmitarray. There are two ways to simulate and analyze the characteristics of a unit element, namely, the waveguide method and Floquet method. Both of the Ansoft HFSS and CST Microwave Studio are able to accomplish the computational modeling (infinite array approach) process, which will be elaborated in the following subsections.

2.4.1 Waveguide Method

Waveguide method is useful because experiment can be conducted to verify the simulation model. Such model is composed by a unit element placed at the center between two sections of waveguides, along with all four walls defined to be perfect electrical conductors (PEC), as illustrated in *Figure 2.4*. Electromagnetic wave is launched at Port 1, and the transmitted wave is observed at the other end (Port 2). The transmission response is simulated using the CST Microwave Studio, and S-curve can be easily extracted from the transmission phase by varying the phase-shifting parameter. However, the size of the unit element is restricted by the waveguide dimension, making this method to be less practical for designing a full-fledge transmitarray. For a waveguide dimension, the incident angle of the incoming wave is also an unchangeable number at a certain operating frequency.

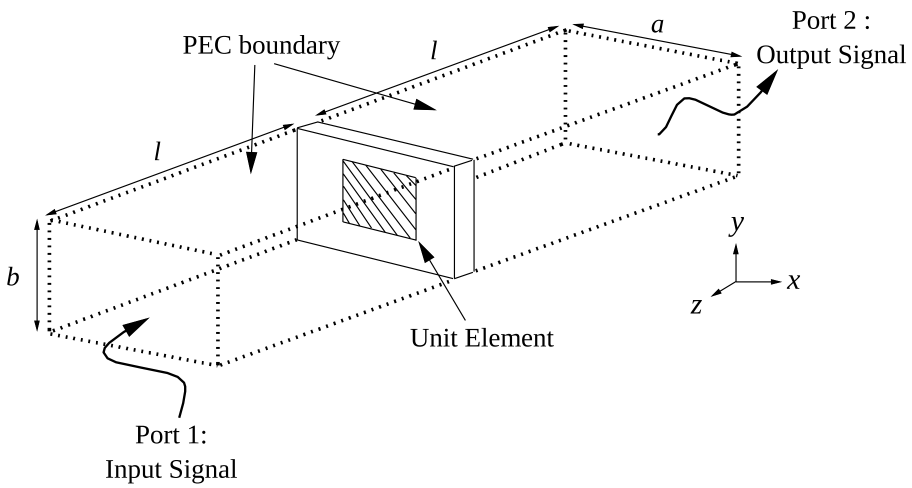

Figure 2.4: Waveguide model with a unit element placed at the center.

2.4.2 Floquet Method

Floquet method, which is also known as infinite array method, allows quick simulation of an infinite array that consists of identical elements. The cell is constructed by special boundary conditions that enable the element to be virtually extended into an infinite array, with mutual coupling between the neighboring elements accounted for. With reference to *Figure 2.5*, to build a simulation model, the two vertical walls on the *E* plane are defined as perfect electrical conductor (PEC); while the other two horizontal walls on the *H* plane are perfect magnetic conductor (PMC). By image theory, the element can be viewed as a virtual infinite array, as illustrated in *Figure 2.6*. A *y*-polarized plane wave is then generated for the simulation. *Figure 2.7* shows the electric fields that are propagating in the Floquet cell at z = 0. This method does not impose any restrictions on the element size and wave's incidence angle. Nevertheless, the transmission response of the unit element cannot be verified experimentally at element level and this weakness remains the main disadvantage.

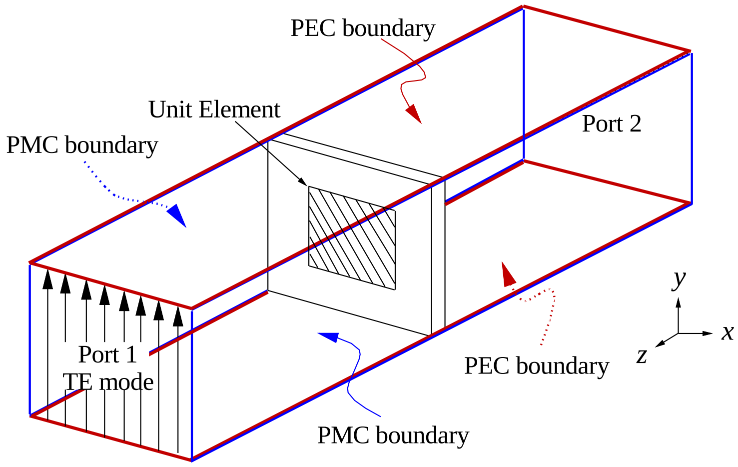

Figure 2.5: Floquet Model with the unit element placed at the center.

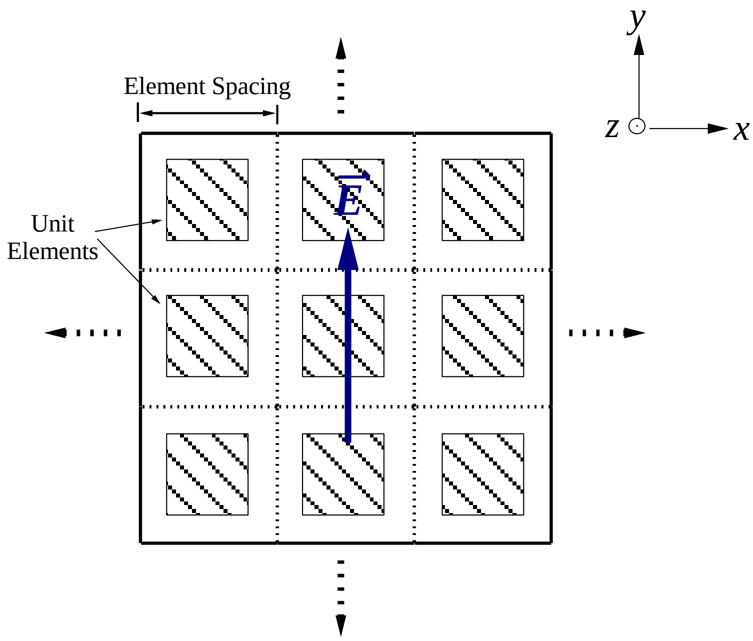

Figure 2.6: Infinite array constructed using Image Theory.

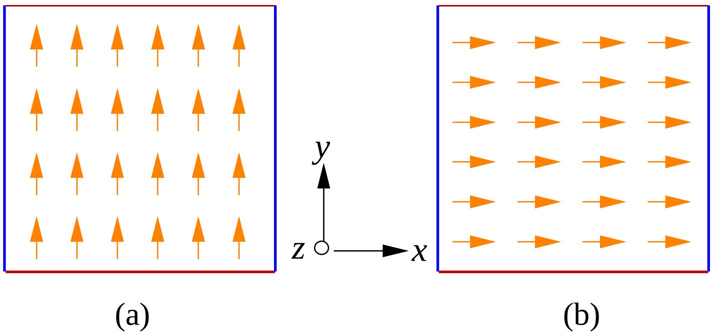

Figure 2.7: Electric fields generated according to Floquet boundary condition at z = 0. (a) *TE* mode, (b) *TM* mode.

Although Floquet model enables the simulation of the unit element in array form; it has some shortcomings that cannot be avoided. First of all, the transmitarray itself is not infinite in practice, and edge effects can cause diffraction and taper losses which are not accounted for by the model. Secondly, the Floquet model assumes mutual coupling to be caused by neighboring unit elements which are identical in shape, but this assumption is not true as all the elements are different. Thirdly, the full transmitarray is designed from the S-curve generated from a Floquet model with normal incidence. But the incident angle is not a constant as the elements are located at different places in an array. This can cause the accuracy of the model to be slightly compromised. According to Abdelrahman et al. (2014), the measured gain and the radiation patterns can be made more accurate and closer to the theoretical analysis by individually considering oblique incident angle of each unit element in simulation.

CHAPTER 3

DESIGN OF LINEARLY AND CIRCULARLY POLARIZED YAGI-UDA-LIKE TRANSMITARRAYS

3.1 Introduction

In the past, the concept of Yagi-Uda has been widely used for designing various types of high-gain antennas such as monopole array (Nascimento, 2008), single-band microstrip array (Nagy, 2010), and multi-band fractal microstrip antenna (Kumar and Malathi, 2007). For the first time, in this project, the Yagi-Uda concept has been applied for designing a linearly polarized (LP) and a circularly polarized (CP) transmitarray. In the proposed design, the transmitarray element is to function as a phase shifter and director simultaneously. The characteristics of the unit elements are first analyzed in Section 3.2.

Floquet cell has been deployed for simulating the transmission characteristics of the unit element, along with electric field analysis. Fitted equations are also provided for estimating the transmission phase range of the LP and CP transmitarray elements. For both cases, the antenna properties are further analyzed in Section 3.3, where the array configurations and the corresponding phase compensation schemes are discussed. The characteristics of the feeder are also examined here. Measurement setup of the proposed transmitarrays is discussed in Section 3.4, following with the experimental verification in Section 3.5. To understand the effects of the geometrical parameters on the radiation performance of the proposed transmitarrays, parametric analysis has been performed on some of the important design parameters.

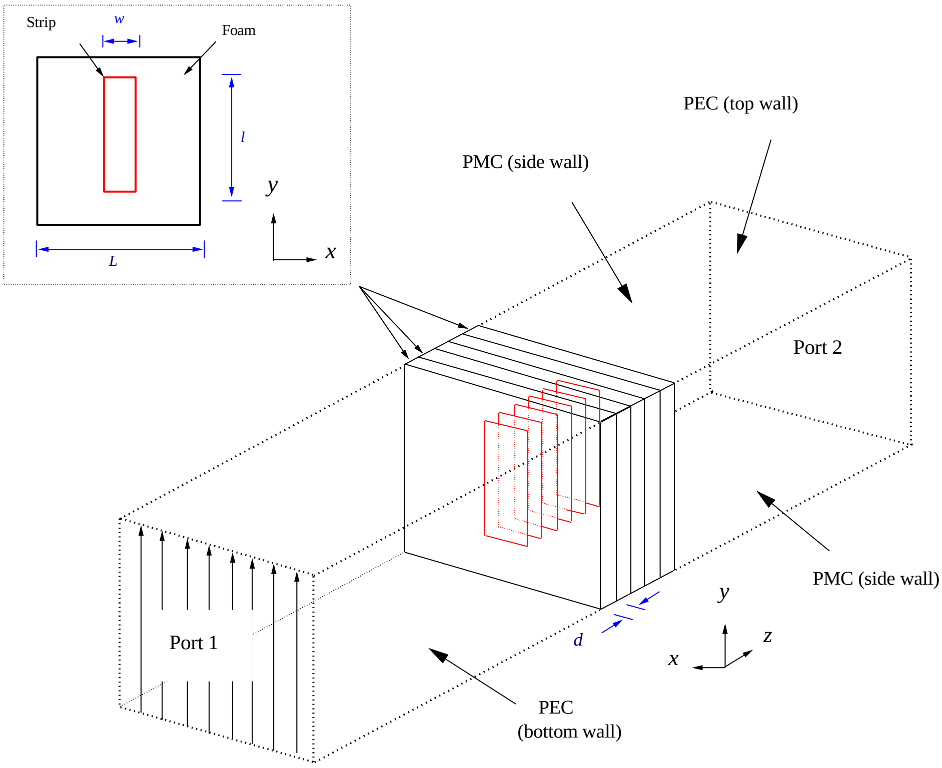

(a)

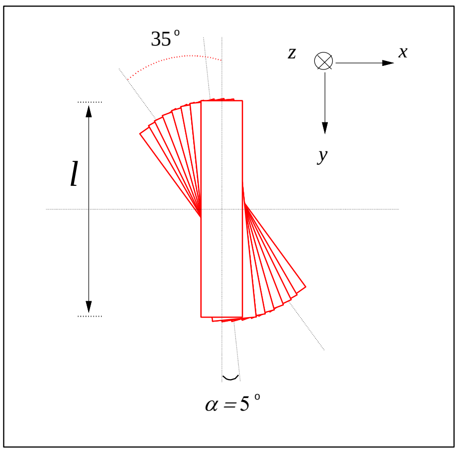

(b)

Figure 3.1: Unit elements for (a) linearly polarized transmitarray (6-layers). (b) Circularly polarized transmitarray (8-layers).

3.2 Unit Element Analysis

CST Design Studio was used to simulate the proposed unit cell elements and the full transmitarrays. The configuration of the linearly polarized (LP) unit element, shown in *Figure 3.1*, is described first. It is composed by six rectangular metal strips ($l \times w$, where $l > w$) of equal length which are stacked in parallel, and the element is placed at the center of a square Floquet cell with a size of $L \times L$ shown in *Figure 3.1(a)*.

The strips are separated by a polystyrene foam with dielectric constant of $\varepsilon_r \sim 1$ and thickness of *S*. Port 1 and 2 are assigned to be Floquet ports, where an *y*-polarized plane wave is launched at Port 1, with a normal incident angle of $\theta = 0^o$, for exciting the array of the strips in the element. The re-radiated wave is moving towards the receiving port (Port 2) located on the other end. The separation distance between the two ports, which is also the length of the Floquet cell, is set to be 160mm in this case, although varying it does not affect the simulation outcome much as the reference plane is always de-embedded to a surface near to the final strip.

With reference to *Figure 3.1(a)*, the top and bottom surfaces of Floquet cell are defined as perfect-electric-conductor (PEC) walls while the side walls are made perfect-magnetic-conductor (PMC) walls. In CST simulation, the unit element that is placed inside the Floquet cell is simulated as an infinite periodic array of its own by taking account of mutual coupling. For this case, the strip length *l* is varied to generate phase change. To make the element produce circularly polarized (CP) wave, every two of the strips are inclined anti-clockwise with an angle of $\alpha = 5^{o}$ starting from the one facing Port 1, as shown in *Figure 3.1(b)*. Again, the strip length is used as the phase shifter for this CP element.

The transmission characteristics of the unit elements are studied by varying the strip length for an incident wave with certain frequency (f_o). For the LP case, the unit cell is designed at the operating frequency of 6GHz. The strip width is set to be w = 5mm and the strips separation is selected to be d = 10mm, with a cell size L of 30mm (0.6λ at 6GHz) defined. By increasing l from 1mm to 24mm, the simulated transmission amplitude ($|S_{21}|$) and phase ($\angle S_{21}$) responses of the LP unit element are shown in *Figure 3.2*. The ports were de-embedded near to the surface of the transmitting elements to keep the phase change below one cycle. For amplitude loss of less than $|S_{21}|$> -3dB, the element is able to provide a maximum transmission phase (ϕ_{max}) of 384^{o}, 382^{o}, 364^{o}, 474^{o}, and 389^{o} at 5GHz, 5.5GHz, 6GHz, 6.5GHz, and 7GHz, respectively, for a maximum useable strip length (l_{max}) of 22.8mm, 20.8mm, 18.8mm, 17.2mm, and 15mm. The length-phase relationship in *Figure 3.2(b)* is also known as S-Curve.

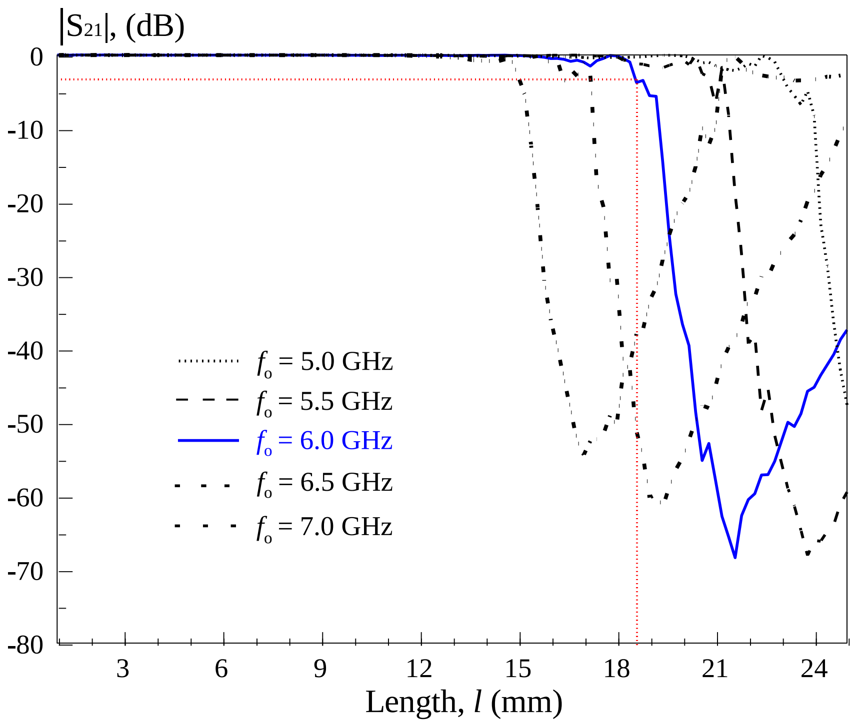

(a)

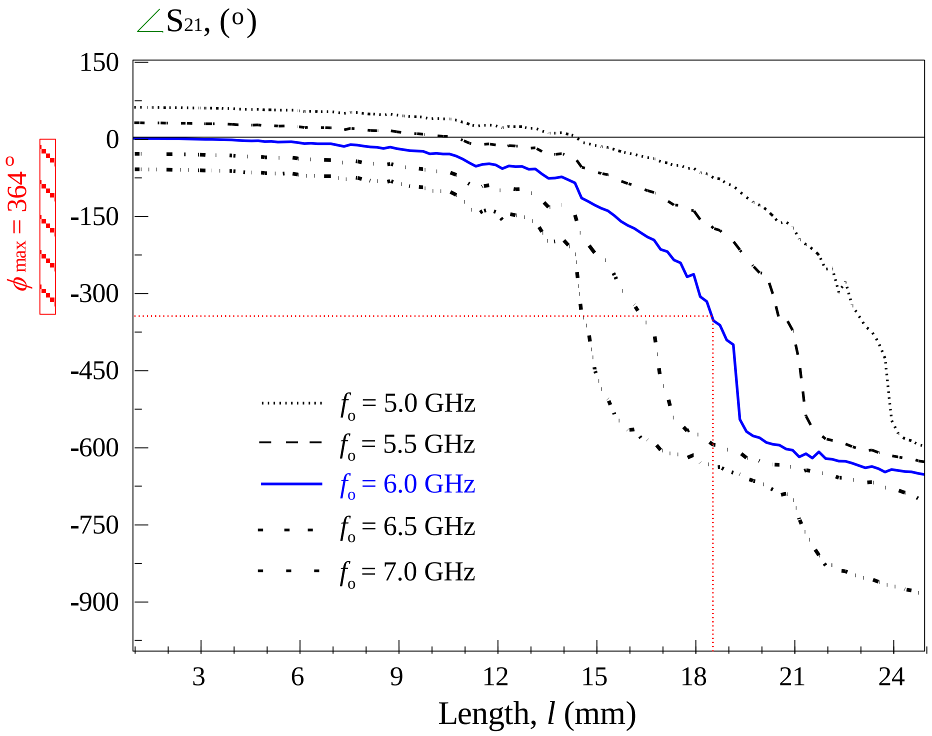

(b)

Figure 3.2: The effect of wave frequency (f_o) on the amplitude and phase of the linearly polarized unit element. (a) Transmission amplitude response. (b) Transmission phase response.

To understand the physical insight better, the current distributions on the strips are illustrated at the frequency of 6GHz for a unit element with l = 12mm (~0.24λ), as shown in *Figure 3.3(a)*. It is observed that electric field of the incident wave first induces currents on the strip facing Port 1 and energy propagates to the subsequent strips through coupling mechanism. The operation principle sounds somewhat like how directors are driven in the conventional Yagi-Uda antenna. To verify it, a reference Yagi-Uda antenna is designed following the guideline given in *Table 3.1*, working at 6GHz, with the detailed dimension given, and the current distribution on its directors are also depicted in *Figure 3.3(b)*. Comparing the two, it is observed that current distributions on the element strips and the Yagi-Uda directors are quite close, showing that the strips of the proposed antenna are able to direct wave through coupling mechanism, functioning like directors in a Yagi-Uda antenna.

Table 3.1: Comparison of the conventional Yagi-Uda antenna to the proposed transmitarrays.

	Conventional Yagi-Uda Antenna	***Linearly Polarized Unit Element (6GHz)***	***Circularly Polarized Unit Element (10GHz)***
Feeder length	(0.47 - 0.49) λ	0.56 λ (28mm)	0.617λ (18.5mm)
Reflector length	(0.5 – 0.525) λ	1 λ (50 mm)	3.33 λ (100mm)
Reflector-feeder spacing	(0.2 – 0.25) λ	0.2 λ (10 mm)	0.167 λ (5mm)
Director Spacing	(0.3 – 0.4) λ	0.2 λ (10 mm)	0.167 λ (5mm)
Director lengths	(0.4 – 0.45) λ	(0.02 – 0.376) λ (1–18.8 mm)	(0.033 – 0.36) λ (1–10.8mm)

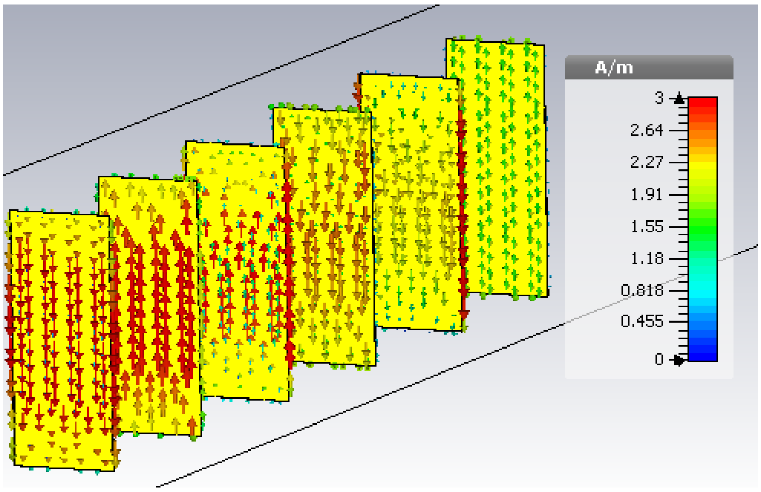

(a)

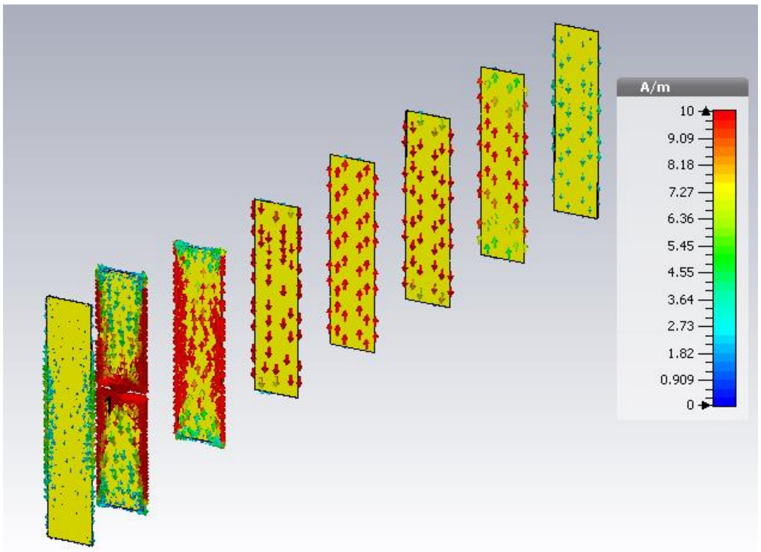

(b)

Figure 3.3: (a) Surface current distribution on the strips for the LP transmitarray cell element. (b) Current distribution on the directors, reflector, and driving dipole of the reference Yagi-Uda antenna.

The layer number is increased and the corresponding maximum reflection phase (ϕ_{max}) at 6GHz is depicted in *Figure 3.4*, which is extracted from the S-Curve by varying the strip length (l). Also, the response is curve-fitted using a simple linear function. It can be seen that the maximum achievable phase range can be estimated by $\phi_{\max} = 60N + 20$ for strip layers of one to eight. With reference to the figure, it can be seen that the phase range can be easily increased by having more layers.

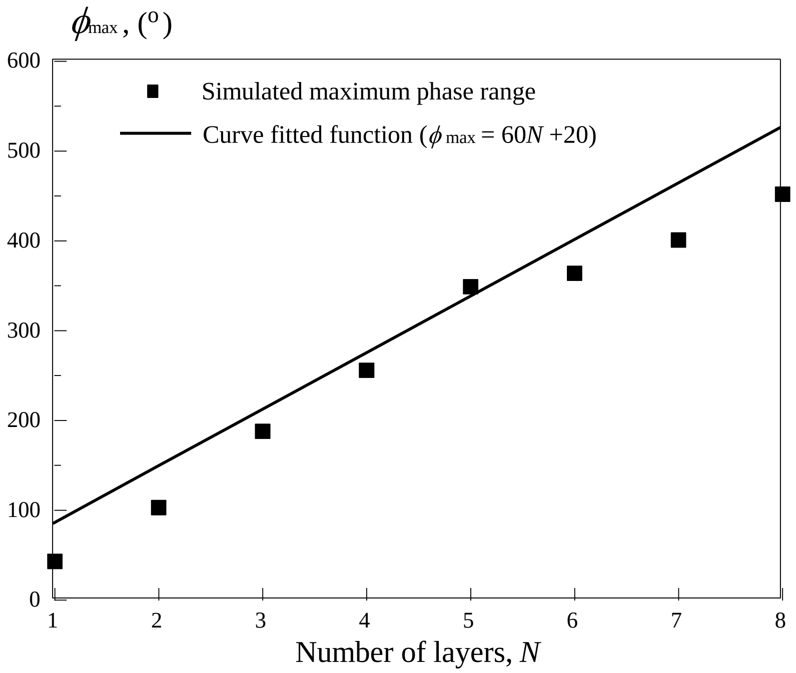

Figure 3.4: Maximum reflection phase range (ϕ_{max}) as a function of layer number at 6 GHz (with w = 5mm and d = 10mm).

The simulated transmission amplitude ($|S_{21}|$) and phase ($\angle S_{21}$) responses of the CP element (with w = 5mm, d = 5mm, and L = 18mm) are shown in *Figure 3.5*. To illustrate the design concept, the transmitarray is designed to operate at 10GHz. This frequency is selected as it can be measured using the X-band CP horns in our lab. We do not have CP horns in other frequency ranges. Increasing the strip length to 10.8mm produces a useable transmission phase range of ϕ_{max} = 412^{o} at 10GHz. The phase responses for an incident wave of 9.8GHz and 10.4GHz are also appended to the same figure, which have shorter available phase ranges (ϕ_{max}) of 192^{o} (for l_{max} = 9.8cm) and 257^{o} (for l_{max} = 9.2cm). Currents on the CP strips for the case of l = 10mm are illustrated in *Figure 3.6* and, again, showing it is coupling mechanism that transfer energy from the first to the last strip, operating like the directors of an Yagi-Uda antenna. With reference to *Figure 3.7*, it can be seen that the maximum phase range with increasing more layers can be estimated by a curve-fitted linear function $\phi_{\max} = 53N + 5$. It is obvious that a larger phase range is obtainable by increasing the number of layers.

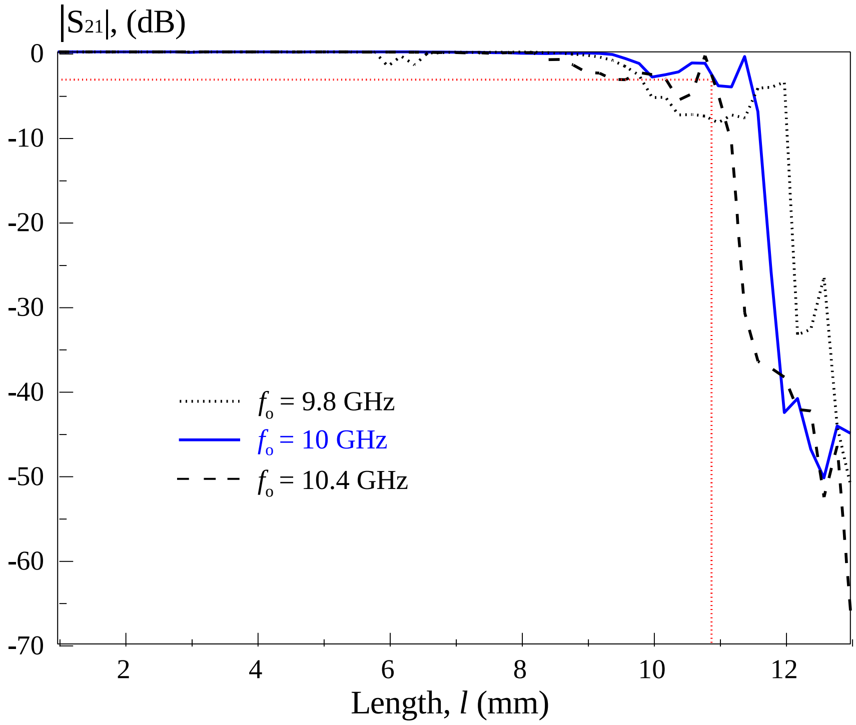

(a)

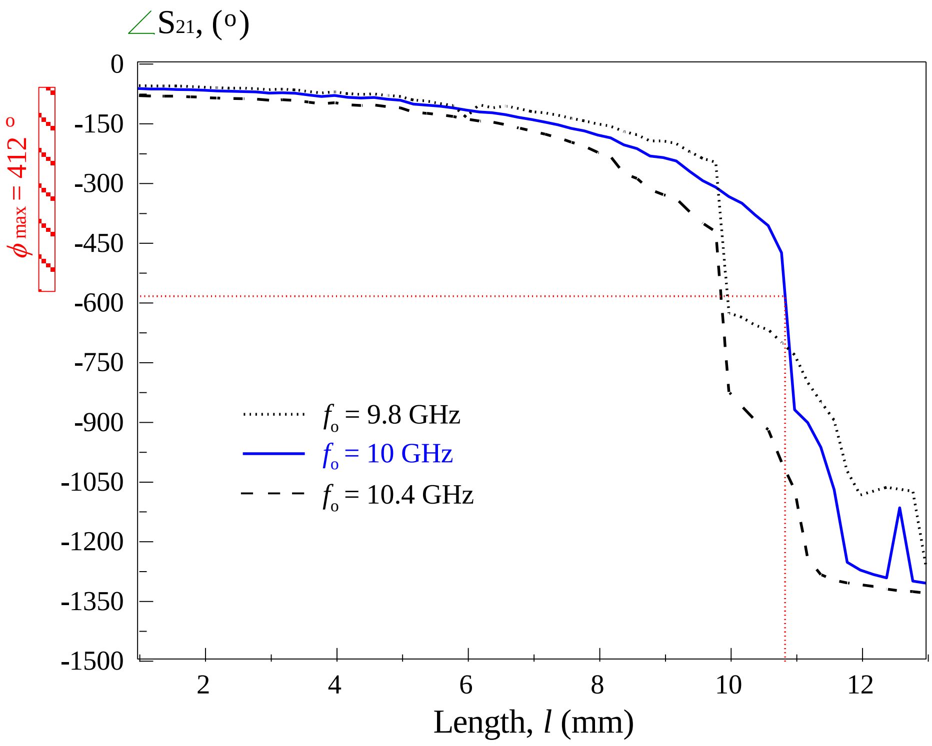

(b)

Figure 3.5: The effect of wave frequency (f_o) on the amplitude and phase of the circularly polarized unit element. (a) Transmission amplitude response. (b) Transmission phase response.

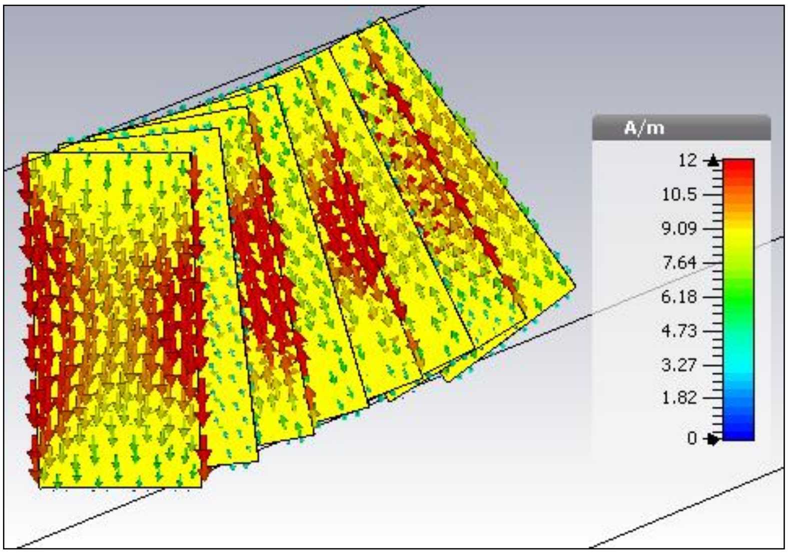

Figure 3.6: Surface current distribution on the strips for the CP transmitarray cell element.

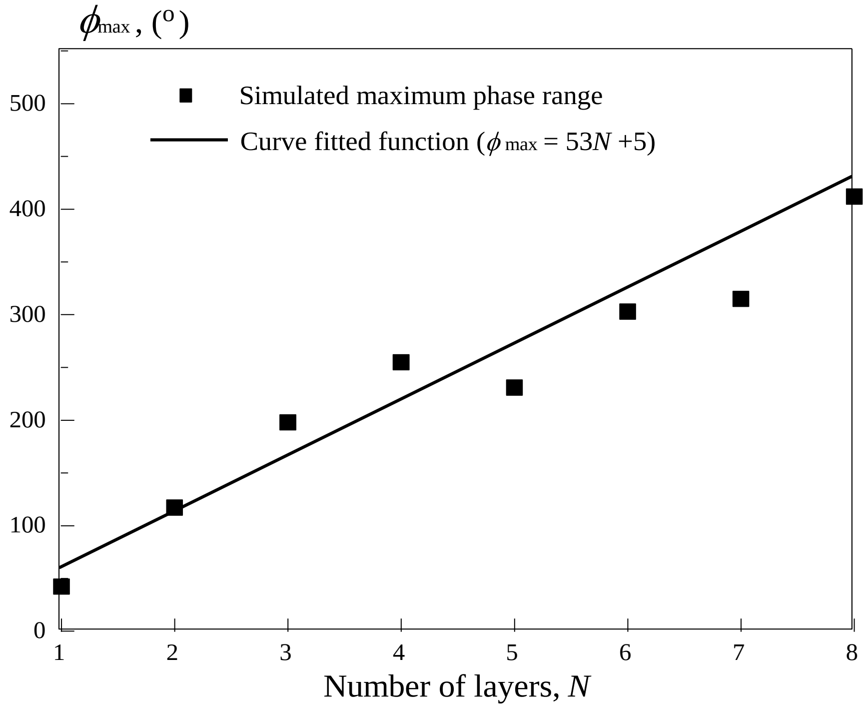

Figure 3.7: Maximum reflection phase range (ϕ_{max}) as a function of layer number at 10 GHz (with w = 5mm and d = 10mm).

3.3 Transmitarray Configuration

Next, the unit elements are explored for designing the linearly polarized (LP) and circularly polarized (CP) transmitarrays. The design procedure of the LP transmitarray is elaborated first. To begin with, the S-Curve at 6GHz (shown as a blue curve in *Figure 3.2(b)*) is selected. In our design shown in *Figure 3.8*, the wave propagation path P_0 from the feeder to the center point of the transmitarray is taken to be the reference as it is the shortest, and the strip length of the central element is made to have l_{max}. Path difference (Δ_N) between the N^{th} element and that for the reference point can be easily calculated as $\Delta_N = P_N - P_0$, which is certainly positive as P_N is longer than P_0. To make the transmitted wave front at the N^{th} element cophasal with that from the center, the additional phase (Δ_N) can be easily compensated by choosing a strip length (on the x – axis of *Figure 3.2(b)*) from curve which can provide a reflection phase of $\phi_{max} + \Delta_N$ on the y-axis.

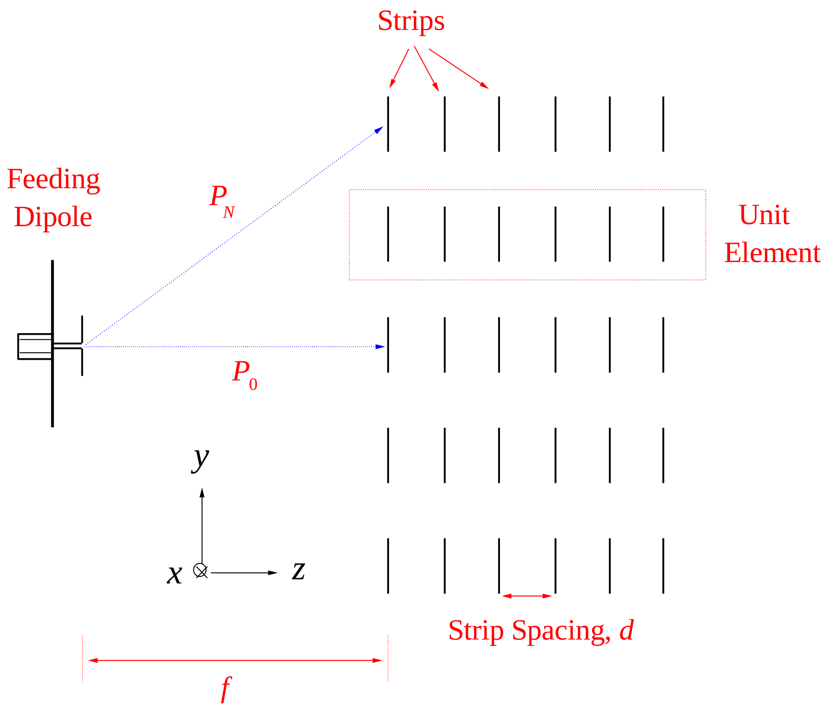

Figure 3.8: Configuration of the proposed linearly polarized transmitarray.

All of the 25 elements of the proposed 5×5 linearly polarized transmitarray are designed following this procedure and they are placed in the far-field zone (f = 55mm) of a metal-backed half-wavelength dipole shown in *Figure 3.9*, which has a dimension of l_1 = 11mm, w_1 = 5mm, g_1 = 3mm, h_1 = 10mm, w_2 = 50mm. As shown in *Figure 3.10*, the isolated dipole has an antenna bandwidth of 28.3%, covering 5.42GHz to 7.22GHz, and it has a peak gain of 8.27dBi along the boresight of the feeder. The backing metal plate is functioning as the ground of the dipole as well as the reflector of the transmitarray. Since the total dimension of the transmitarray is D = 5L = 150mm, the F / D is calculated to be 0.367. Form boards (with ε_r ~ 1) and 3M copper tapes are used to construct a prototype for the LP transmitarray, as shown in *Figure 3.11*. Copper tape with adhesive layer on one side is stuck to a form board with its remaining metal etched away. Six strip-loaded form boards are then stacked in parallel and separated from the feeding dipole using a few supporting form boards.

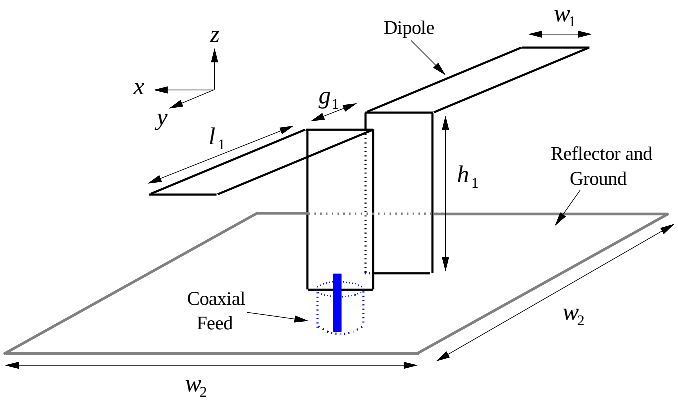

(a)

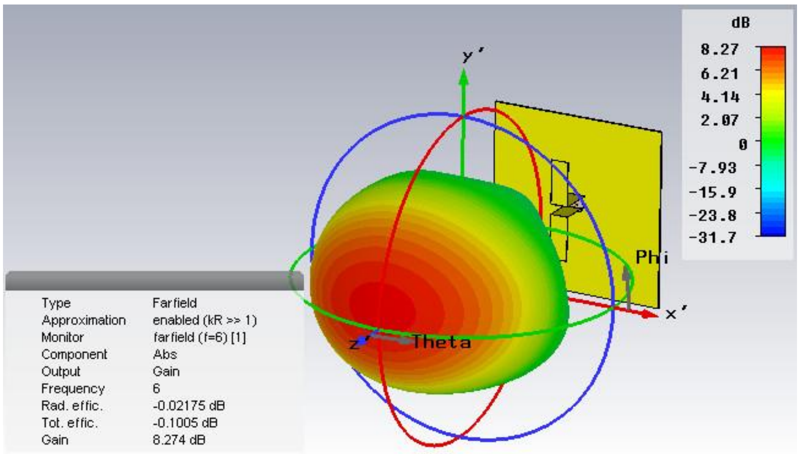

(b)

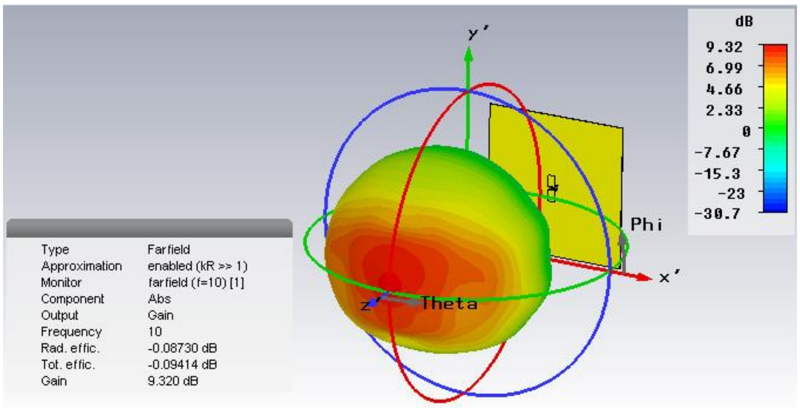

(c)

Figure 3.9: The feeding dipole. (a) Configuration of the half-wavelength dipole; (b) 3D radiation pattern for LP transmitarray at 6GHz; (c) 3D radiation pattern for CP transmitarray at 10GHz.

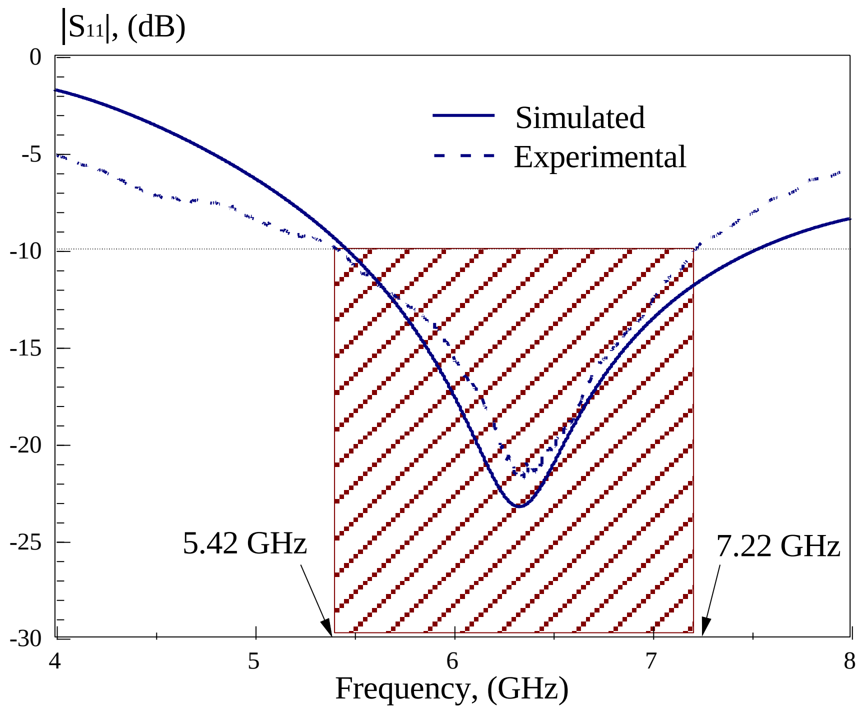

Figure 3.10: Measured and simulated reflection coefficients of the feeding dipole.

With the use of the same design procedure, the 10GHz S-curve in *Figure 3.5(b)* is used to design a 5×5 full CP transmitarray, as shown in *Figure 3.12*. For this case, the feeding dipole, which has a dimension of l_1 = 8.15mm, w_1 = 5mm, g_1 = 2.2mm, h_1 = 5mm, w_2 = 100mm, is placed at a distance f = 122mm from the center point of the transmitarray, resulting an F / D ratio of 1.36, where $D = 5L$ = 90mm. The feeding dipole has an impedance bandwidth of 24.25%, covering 8.89GHz – 11.32GHz, and a peak gain of 9.22dBi near to the boresight. By viewing at the array of strips to function like directors, the design parameters of the proposed LP and CP transmitarrays are compared with those of a conventional Yagi-Uda in *Table 3.1*. It can be seen that the element strip lengths of the transmitarrays are generally shorter than the directors of the conventional Yagi-Uda antenna. As a rule of thumb, the directors of the transmitarrays must be made shorter than their respective feeders to enable energy propagation in the direction of the directors. On the other hand, in our cases, the reflector size of the feeding dipole is made electrically larger than the feeder so that energy can be reflected to the direction of the directors better.

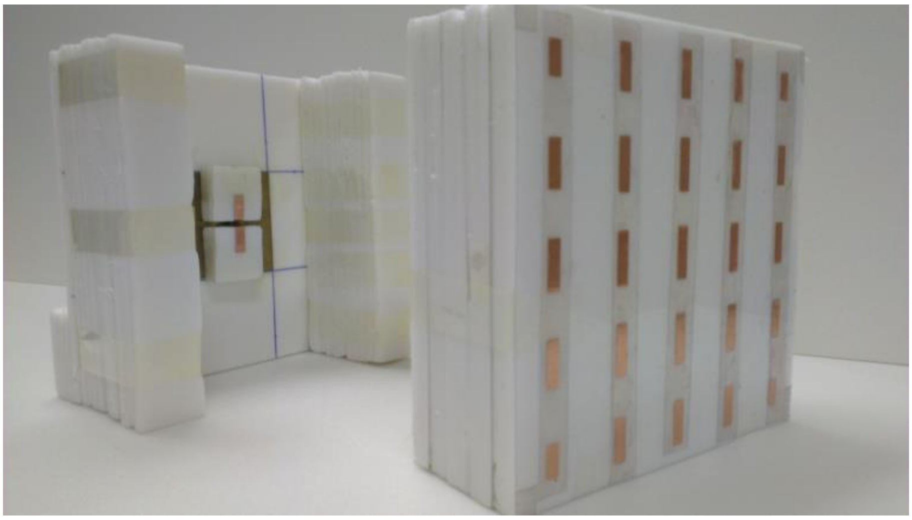

Figure 3.11: Prototype of the linearly polarized transmitarray.

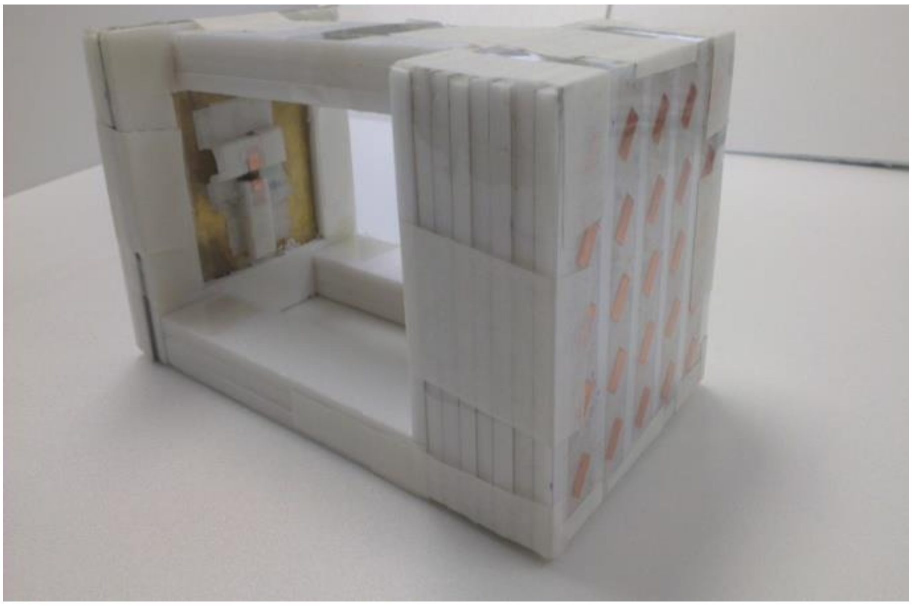

Figure 3.12: Prototype of the circularly polarized transmitarray.

3.4 Measurement Setup

Reflection coefficients and input impedances were measured with a Rohde & Schwarz ZVB8 vector network analyzer. On the other hand, *Figure 3.13* shows the free space experimental setup for measuring antenna gain and radiation patterns. The proposed transmitarray (antenna under test) is connected to a signal generator (Rohde & Schwarz SMB100A) for generating a monotonic microwave signal. A linearly polarized C-band pyramidal horn (ATM PNR137-440-2, 5.85GHz – 8.2GHz), which has a measured antenna gain of 10.47dBi at 6GHz, is placed at a far-field distance R = 1.8m from the transmitarray. It is connected to a spectrum analyzer (Advantest U3771) for capturing the receiving power P_r. In measurement, a 6GHz monotone with a power of P_t = 10dBm was supplied by the signal generator and the receiving horn is rotated around the transmitarray under test in the θ direction. For each elevation angle, the received power P_r was directly read from the spectrum analyzer and the corresponding antenna gain can be calculated using the Friis Transmission equation. Losses in the cables are compensated. Similar measurement setup has been deployed for measuring the circularly polarized transmitarray, except that the receiver is now a left- or right-handed polarized conical horn (XB-CPHA-L/R89).

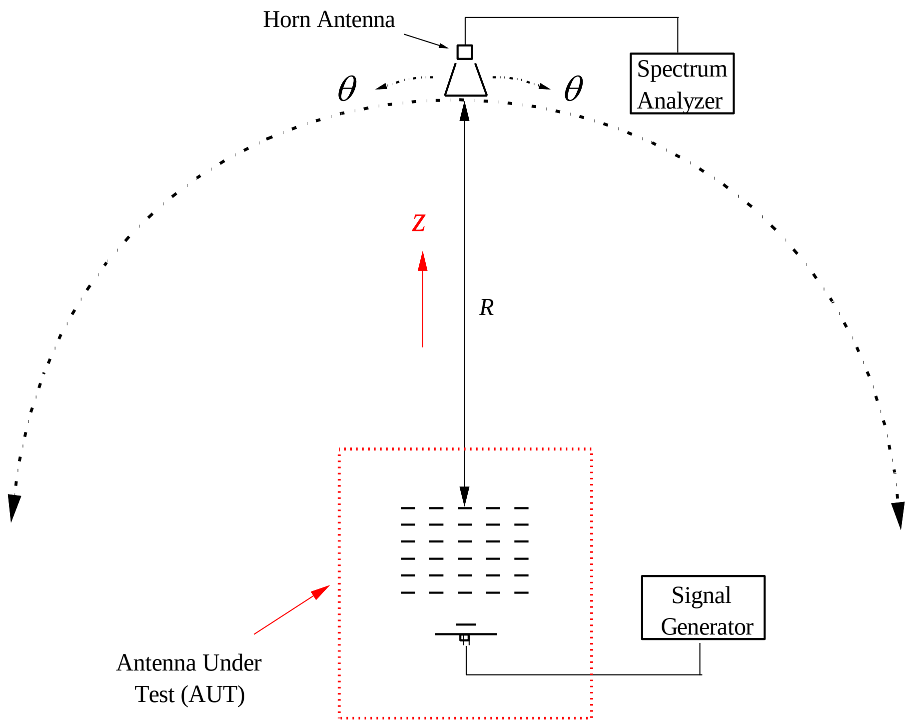

Figure 3.13: Measurement setup for the transmitarray (R = 1.8m).

3.5 Simulated and Experimental Results of Transmitarray

The performance of the proposed linearly polarized transmitarray is analyzed first. *Figure 3.14* shows the measured and simulated input impedances, showing reasonable agreement, and the bandwidth is covering 5.5GHz – 6.81GHz. Discrepancy between the measured and simulated reactance can be caused by fabrication and experimental tolerances as the rectangular metal strips are fabricated and aligned manually. Although significant effort was made to align the multilayer strips in parallel, slight misalignment (which may be in the order of less than 0.1mm) was still unavoidable in preparing the prototype. With the use of the measurement setup, the measured and simulated radiation patterns in the *yz* – plane (*E* plane) and *xz* – plane (*H* plane) are shown in *Figure 3.15* at 6 GHz. Good agreement between simulation and measurement has been obtained. The simulated cross-polarized field is not shown as the signal level is lower than -80dB for all angles. Broadside radiation patterns have been obtained in both with a measured peak gain of 17.7dBi (simulation 17dBi). The co-polarized field is larger than its cross-polarized counterpart by at least 30dB in the boresight direction (θ = 0^0). *Figure 3.16* shows the measured and simulated antenna gain across frequency. The proposed transmitarray has a simulated 1-dB bandwidth of 12.8%, covering 5.9GHz to 6.6GHz, but with a slightly smaller measurement bandwidth of 11.86% (5.6GHz to 6.2GHz).

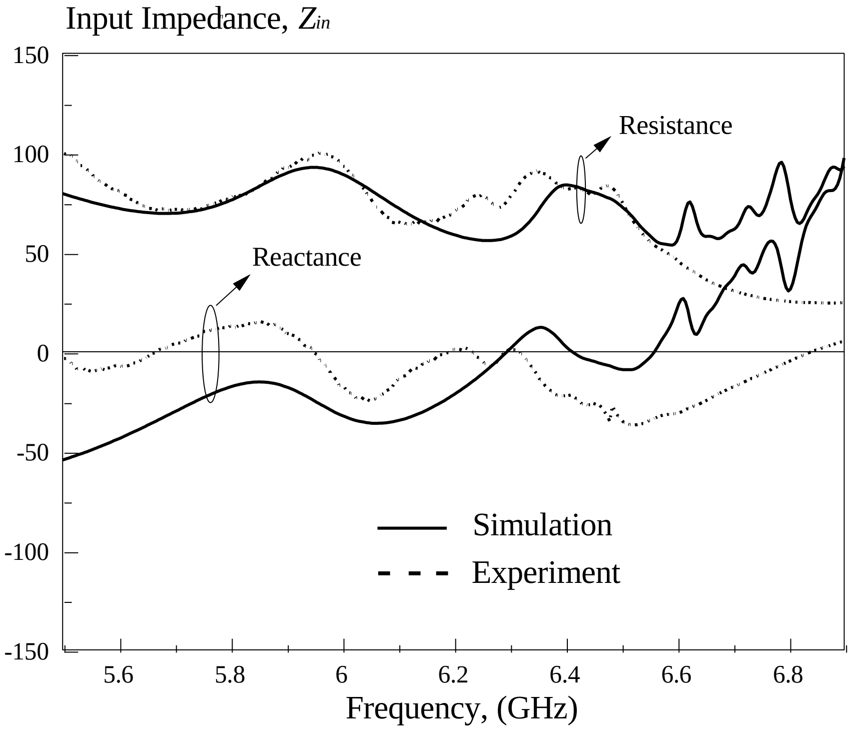

Figure 3.14: Measured and simulated input impedances.

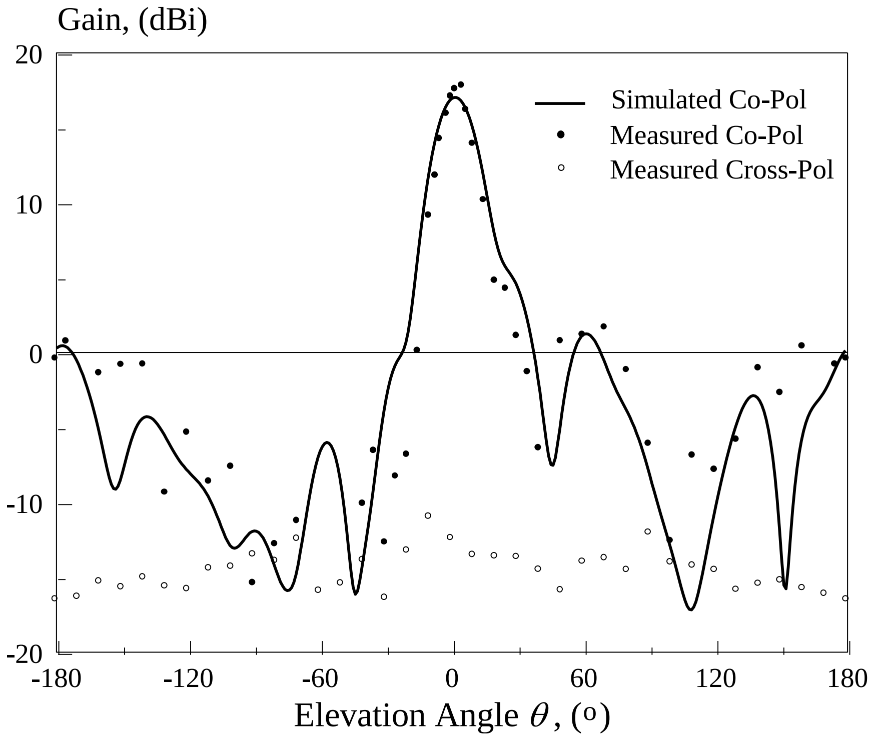

(a)

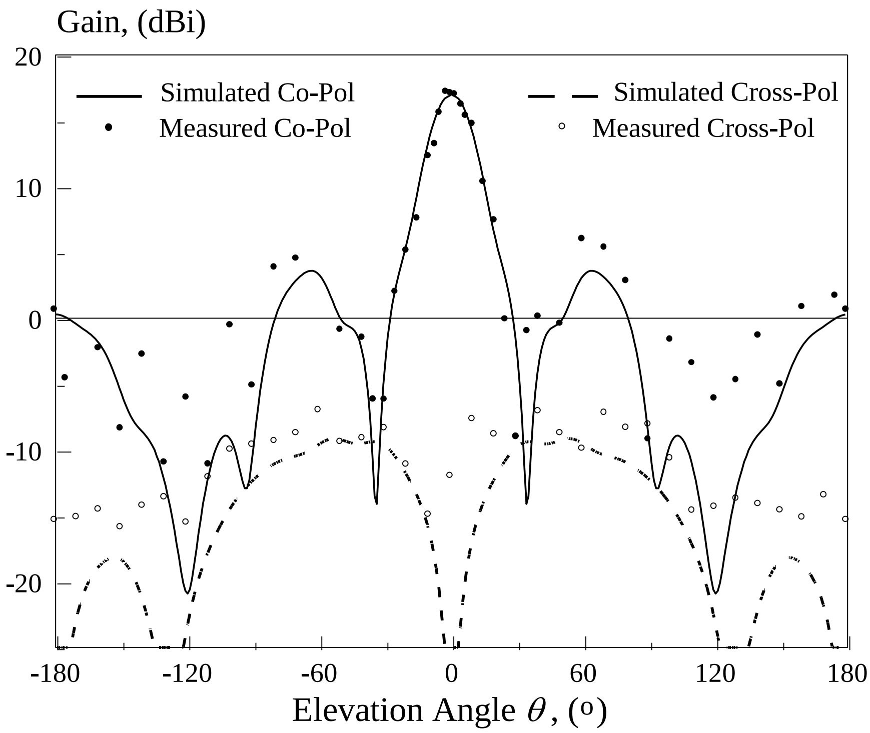

(b)

Figure 3.15: Measured and simulated (a) *E*- and (b) *H*- plane radiation patterns of the proposed LP transmitarray at 6 GHz.

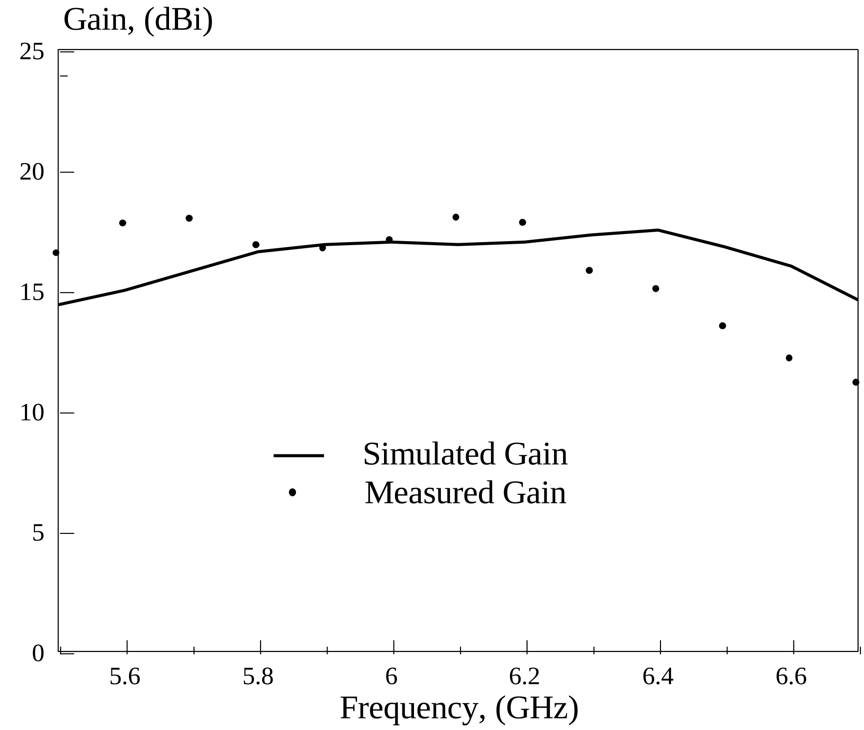

Figure 3.16: Measured and simulated antenna gain of the proposed LP transmitarray with respect to the frequency.

Next, the performance of the proposed CP transmitarray is analyzed. It can be observed from the axial ratio (AX) measurement in *Figure 3.17* that the measured 3-dB axial-ratio bandwidth is ~7%, covering 9.6GHz – 10.2GHz. Although the transmitarray has a very broad impedance bandwidth of 25.3%, the useable CP bandwidth is only 7% limited by its AX performance. The proposed reflectarray has three (3) resonances located at 9.65GHz, 9.9GHz and 10.1GHz. With reference to the figure, the first and second optimum frequencies of the simulated AX curve have combined into one at 10.1GHz, and its third resonance falls on 10.3GHz. The measured AX curve has three distinguished resonances. Discrepancy between the simulated and measured AXs can be caused by strips misalignment, which is very difficult to avoid in experiment.

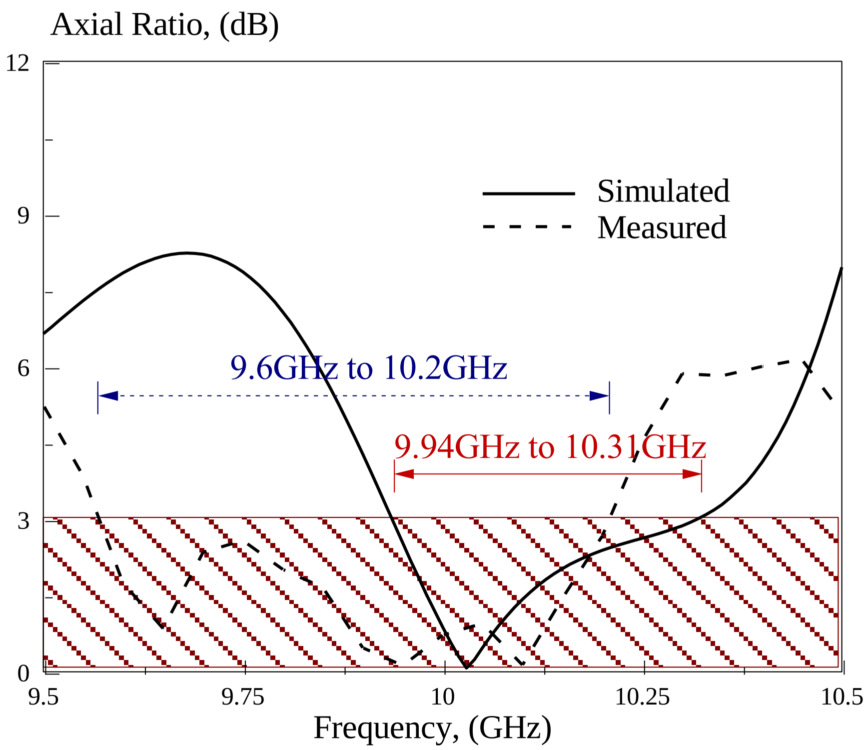

Figure 3.17: Measured and simulated axial ratios of the CP transmitarray.

Figure 3.18 illustrated the measured and simulated radiation patterns in both of the *E* and *H* planes. This is a left-handed circularly polarized (LHCP) transmitarray, showing broadside patterns with a maximum measured antenna gain of 16.2dBi (simulation 16.6dBi). For both planes, the LHCP fields are larger than their RHCP counterpart by at least 18dBi in the boresight direction. The characteristics of the antenna gain are shown in *Figure 3.19*. It has a measured 1-dB bandwidth of ~ 4% (9.7GHz – 10GHz), which is slightly lower than its simulated bandwidth of ~ 5% (9.8GHz – 10.2GHz).

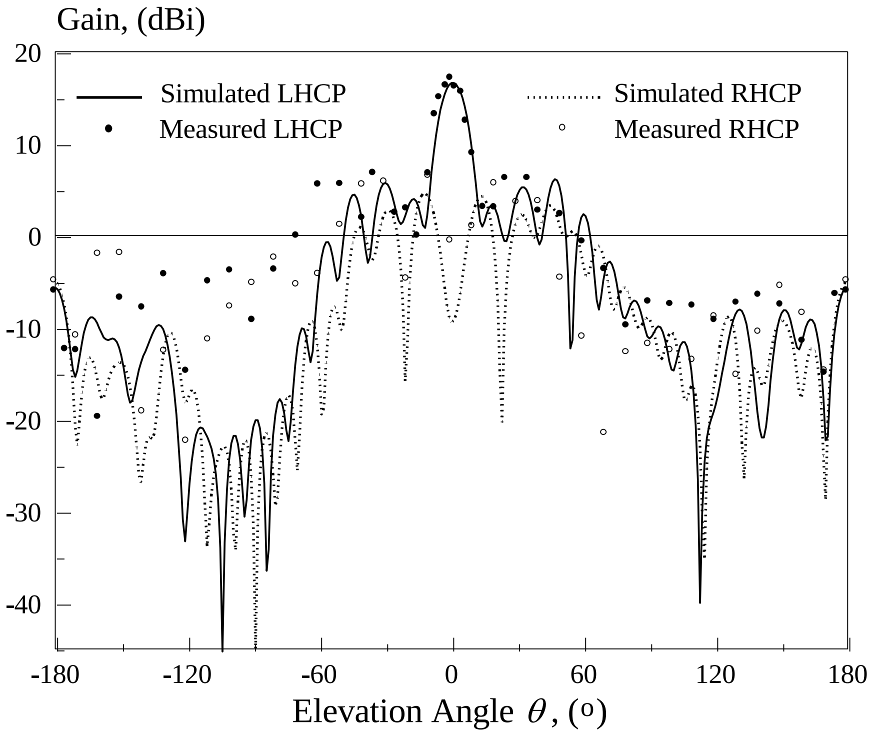

(a)

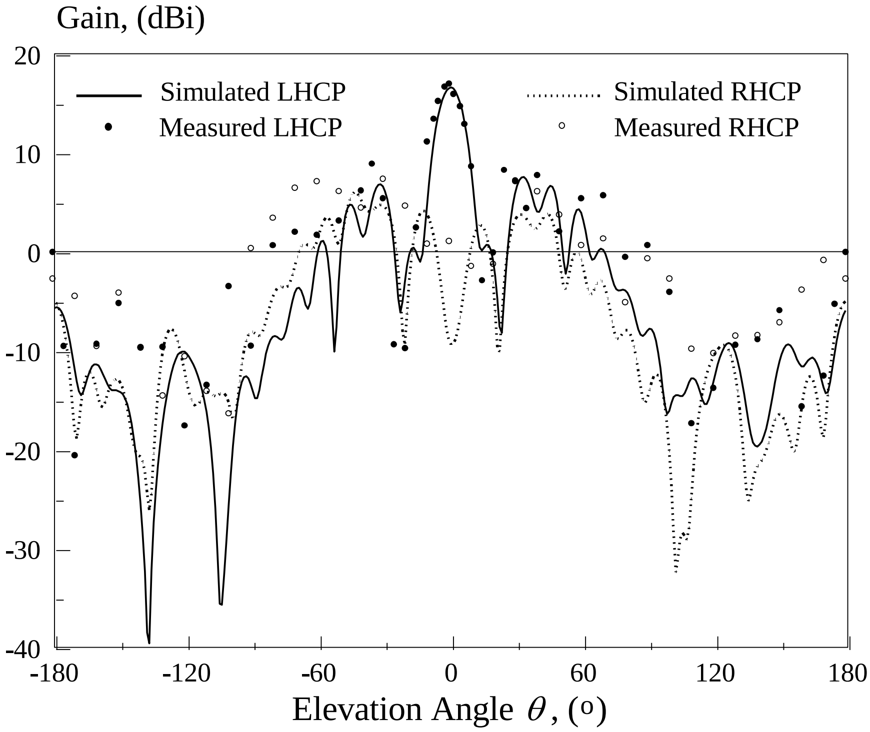

(b)

Figure 3.18: Measured and simulated (a) *E*-plane and (b) *H*- plane radiation patterns of the proposed CP transmitarray at 10 GHz.

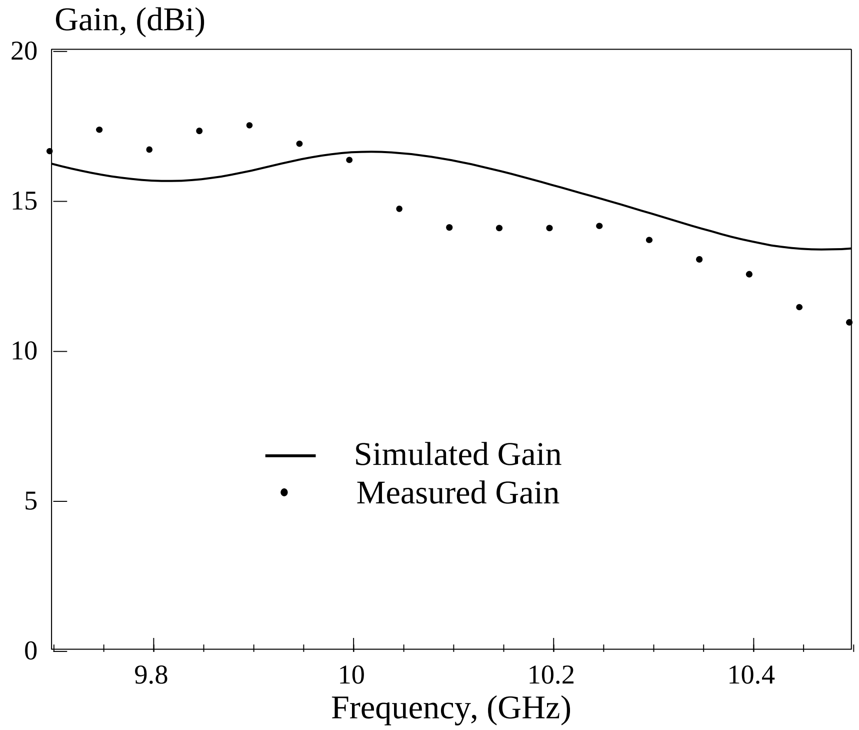

Figure 3.19: Measured and simulated antenna gain of the proposed CP transmitarray as a function of frequency.

3.6 Parametric Analysis

To understand the characteristics of the proposed transmitarrays, parametric analysis has been performed on a collective of important design parameters. The effects of the design parameters will be studied in this section.

3.6.1 Analysis on Linearly Polarized Transmitarray

The LP transmitarray is analyzed first. To begin, the director spacing (d) is varied and the element response is illustrated in *Figure 3.20*. It can be seen from the transmission amplitude and phase responses that director spacing of

5mm, 10mm, and 15mm enable a transmission phase range of 384^o, 364^o, and 238^o. Reduction in phase range can be due to the decrease of capacitance when the strips split further. In our experiment, a director spacing is selected to be 10mm (~ 0.2λ), which is slightly smaller than the director distance of 0.3λ – 0.4λ. The element is not designed into a full reflectarray as the phase range for the case of d = 15cm is not sufficient.

Next, the effect of the cell size (L), which is translated into the separation distance when extended into a full transmitarray, is studied. Analysis is started by setting L = 0.5λ, 0.55λ, and 0.6λ at 6GHz and the simulated results are illustrates in *Figure 3.21*. It is obvious that changes in cell size don't affect its transmission response much. However in this case, as can be seen in the full transmitarray simulation in *Figure 3.22*, the front-to-back increases when L is increased. This can be due to the increase of scattered field from the strip elements when they get closer. It is observed that the back lobe is the lowest for L = 0.6λ , as can be observed in *Figure 3.22*. It was observed from simulation that the antenna gain of the LP transmitarray is not affected much by the change of L in the range of 0.5λ - 0.6λ.

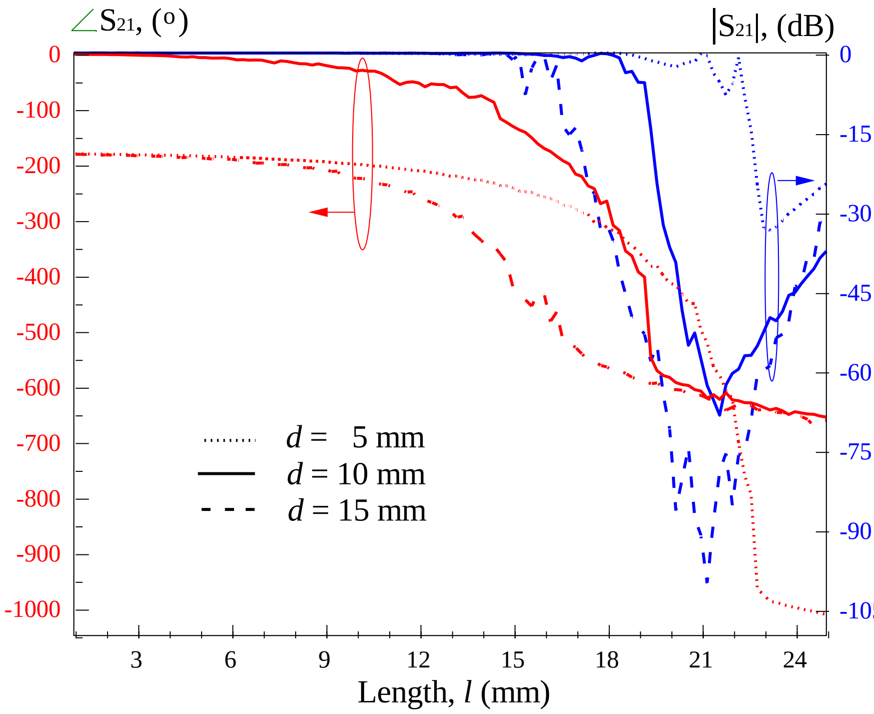

Figure 3.20: The effect of director spacing, (*d*) on the transmission amplitude and phase responses of the LP unit cell.

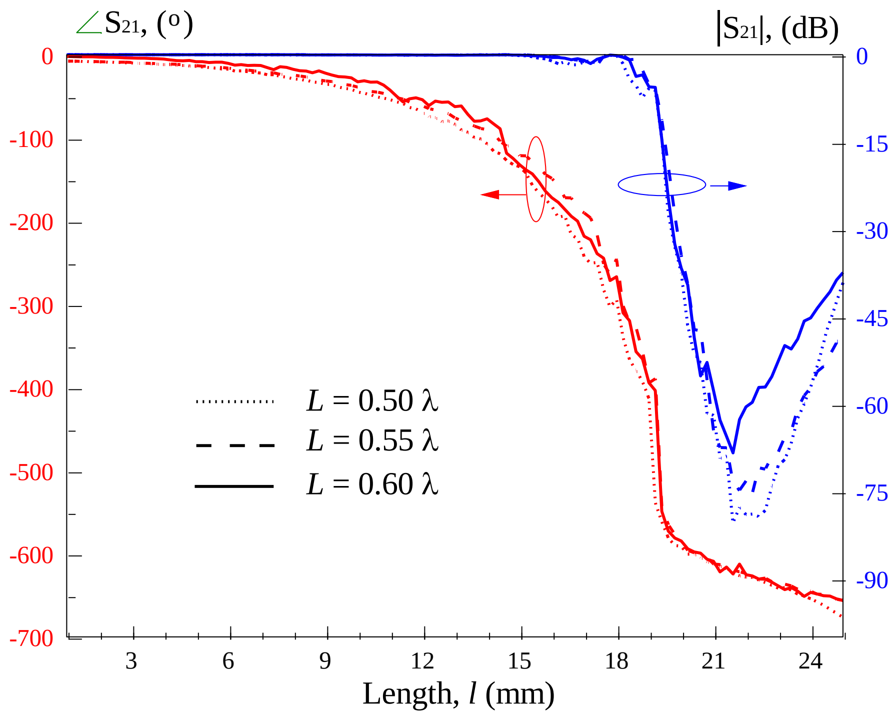

Figure 3.21: The effect of unit cell dimension (*L*) on the transmission amplitude and phase responses of the LP element simulated using unit cell.

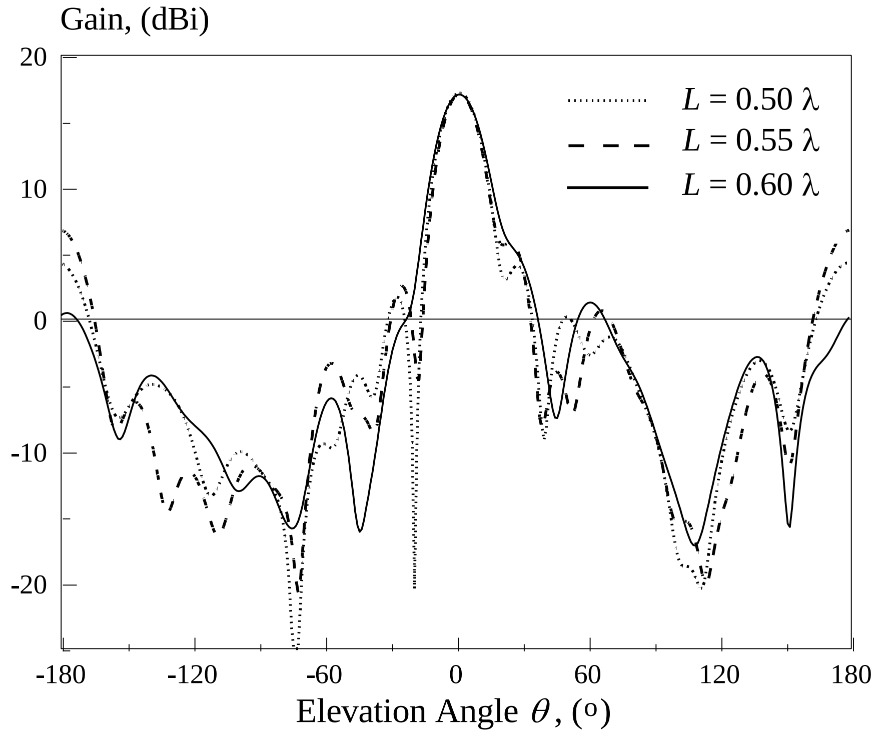

(a)

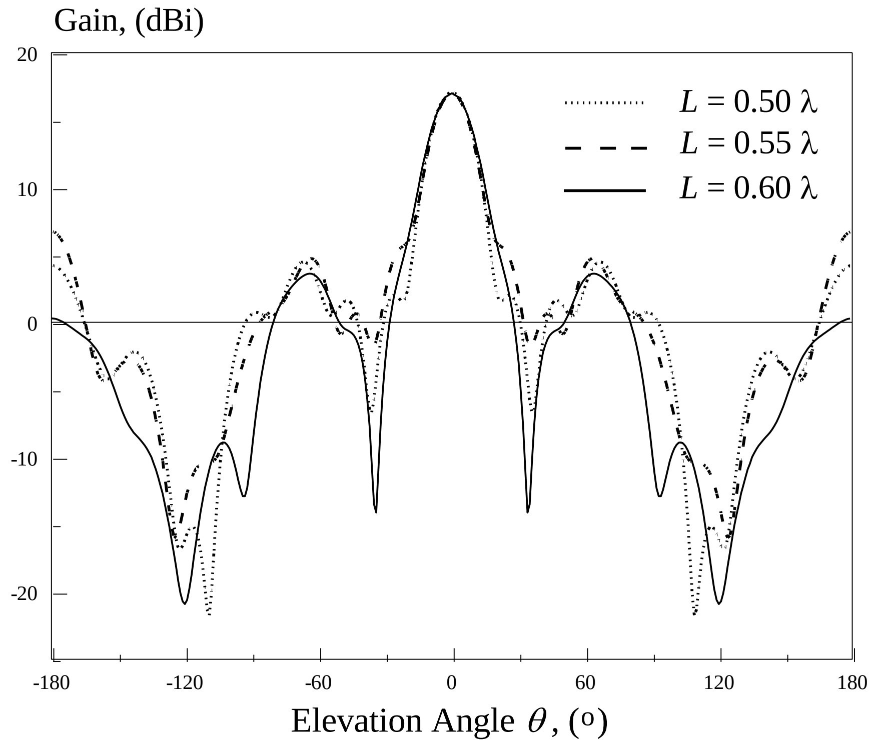

(b)

Figure 3.22: Radiation patterns of the proposed LP transmitarray with different unit cell sizes at 6GHz. (a) *E* - and (b) *H* - planes.

By maintaining the cell size at $L = 0.60\lambda$ and array dimension D = 150mm, the effect of the F / D ratio is inspected at the frequency of 6GHz. The corresponding radiation patterns are illustrated in *Figure 3.23*, and the antenna gain and half-power beamwidth (HPBW) are compared in *Table 3.2*. The optimized F / D ratio is found to be 0.36, which is equal to a feeding distance of 155cm (1.1λ at 6GHz). Changes in the F / D ratio can cause the radiation performance to deteriorate due to spillover losses, quantization losses, and taper losses.

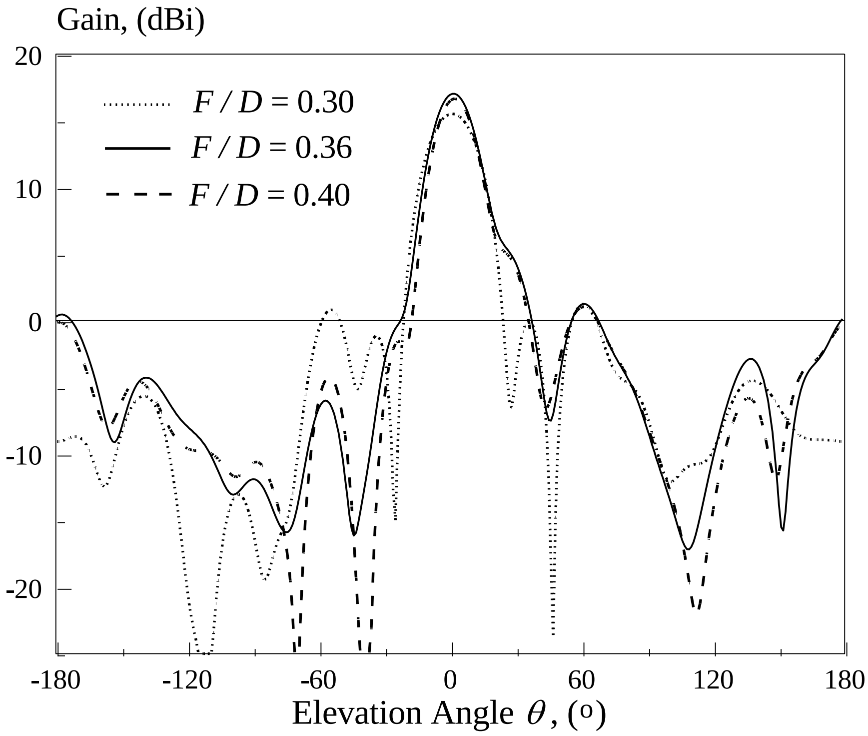

(a)

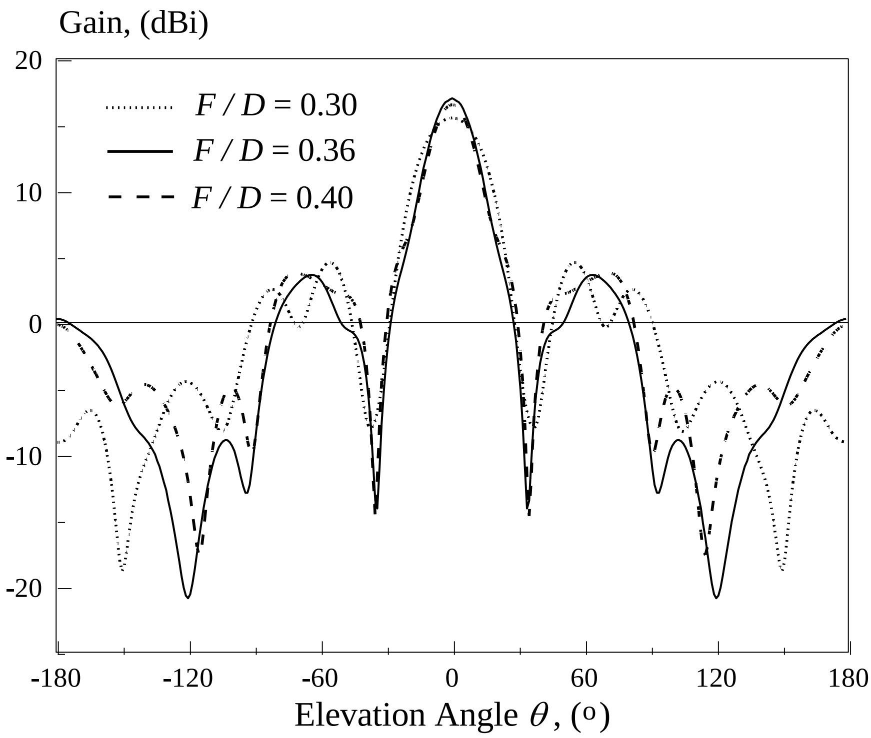

(b)

Figure 3.23: Radiation patterns of the proposed LP transmitarray with different F / D ratio. (a) E - and (b) H - planes.

Table 3.2: LP transmitarray performance for different *F / D* ratios.

F/ D	***E* - plane**		***H* - plane**	
	Gain(dBi)	**HPBW(°)**	**Gain(dBi)**	**HPBW(°)**
0.30	15.5	23.7	15.5	29.0
0.36	17.0	19.0	17.0	19.5
0.40	16.6	18.0	16.5	19.0

The effect of the reflecting metallic plate ($R \times R$), which is also used as the ground of the half-wavelength dipole, is analyzed and the results are shown in *Figure 3.24*. It acts like a reflector as if that for the conventional Yagi-Uda antenna. In experiment, the plate is designed to have 50mm × 50mm, which is ~ 1λ of the operating frequency. When the reflector size is made much smaller than 1λ (~30mm), as can be seen in *Figure 3.24*, a small portion of the signal gets spill over to the reverse side, resulting in larger backlobe and sidelobes. The radiation performances are compared in *Table 3.3*. Obviously, increasing reflector size is good for enhancing antenna gain and suppressing the field components going beyond ± 60°, but with the price of a larger antenna size and a narrower HPBW.

Table 3.3: LP transmitarray performance for different reflector size *R*.

Reflector size, R (mm × mm)	***E* - plane**		***H* - plane**	
	Gain(dBi)	**HPBW(°)**	**Gain(dBi)**	**HPBW(°)**
30 × 30	16.0	18.3	16.0	20.4
50 × 50	17.0	19.0	17.0	19.5
150 × 150	18.3	17.0	18.3	18.5

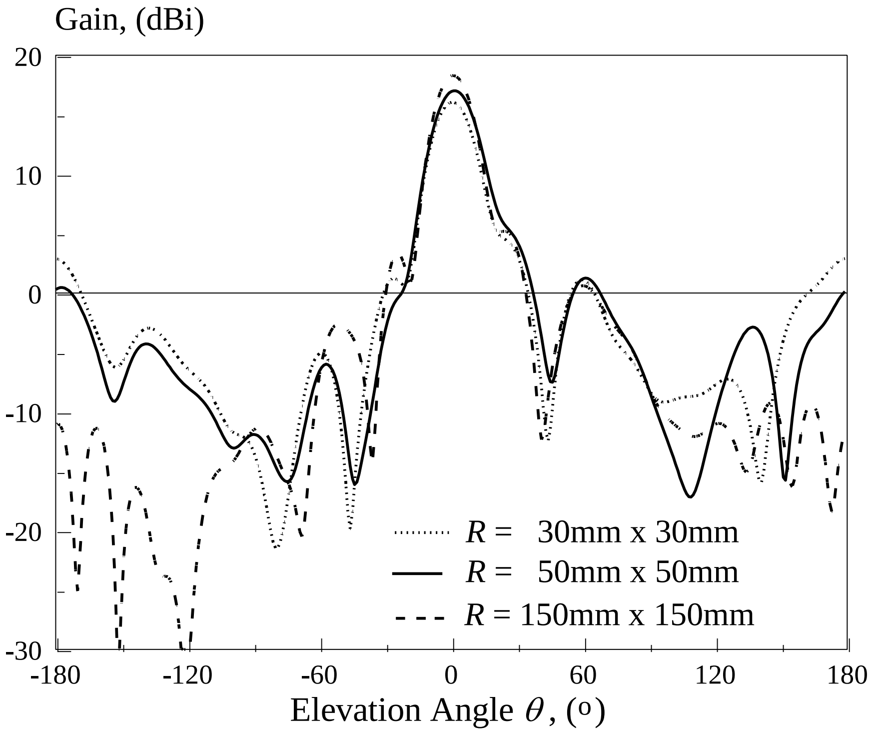

(a)

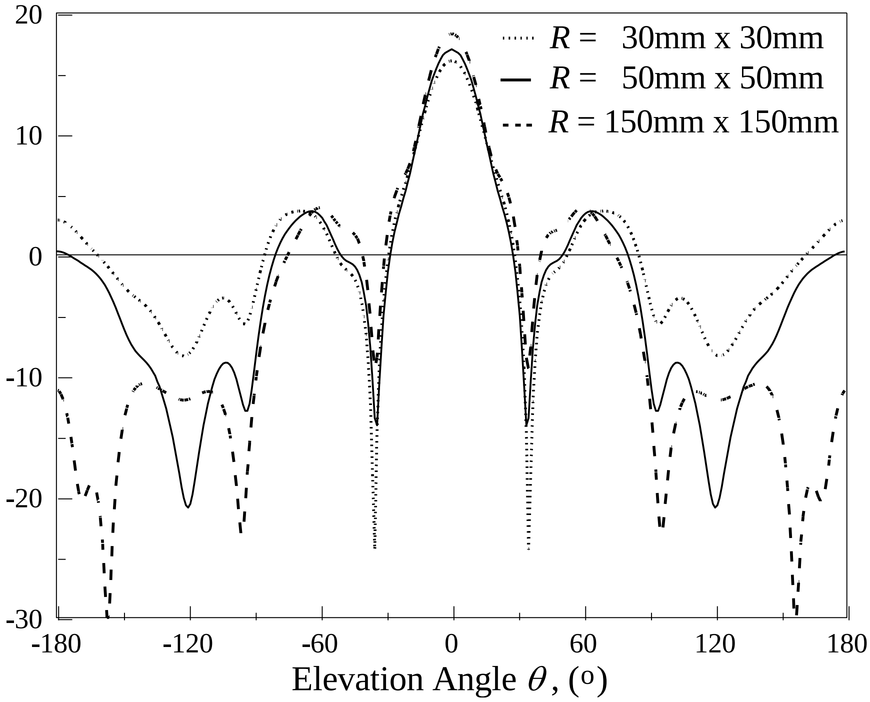

(b)

Figure 3.24: Radiation patterns of the proposed LP transmitarray for different reflector plate sizes (*R*) at 6GHz. (a) *E*- and (b) *H*- planes.

The properties of the strip element, which is also functioning as the director of the transmitarray, are studied here. It was observed from *Figure 3.25* that the strip width (W) does not affect the transmission amplitude and phase responses much. However, the strip width does have some effect on the radiation performance of the transmitarray. With reference to *Figure 3.26*, it is observed that broader strip width is good for enhancing antenna gain, but it causes the backlobe and sidelobes to increase as well. In our design, a tradeoff is made by selecting W = 5mm (~ 0.1λ).

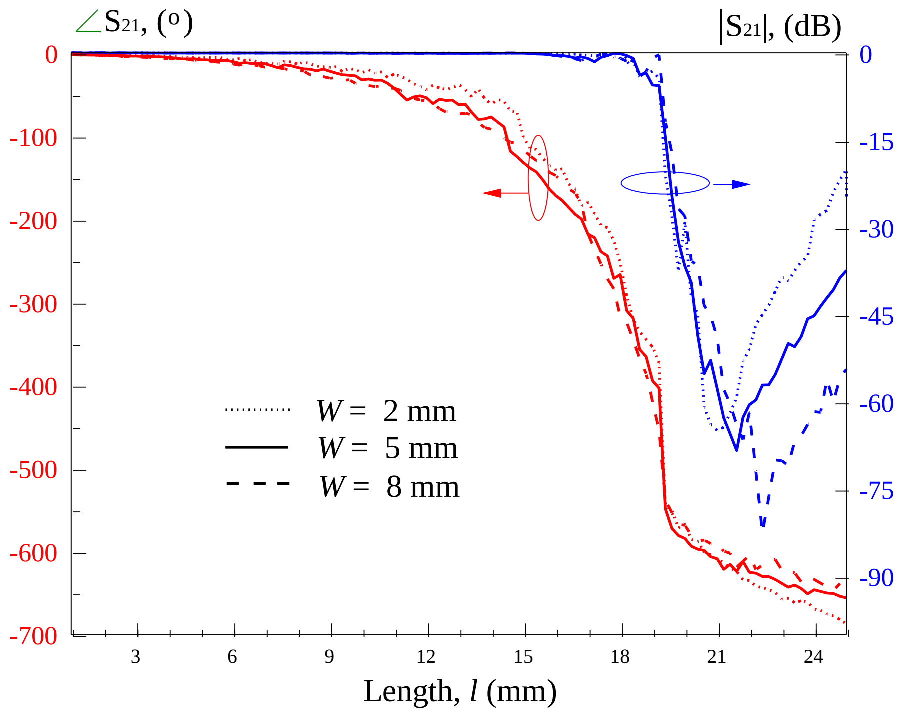

Figure 3.25: The effect of strip width (W) on the amplitude and phase responses of the LP unit cell.

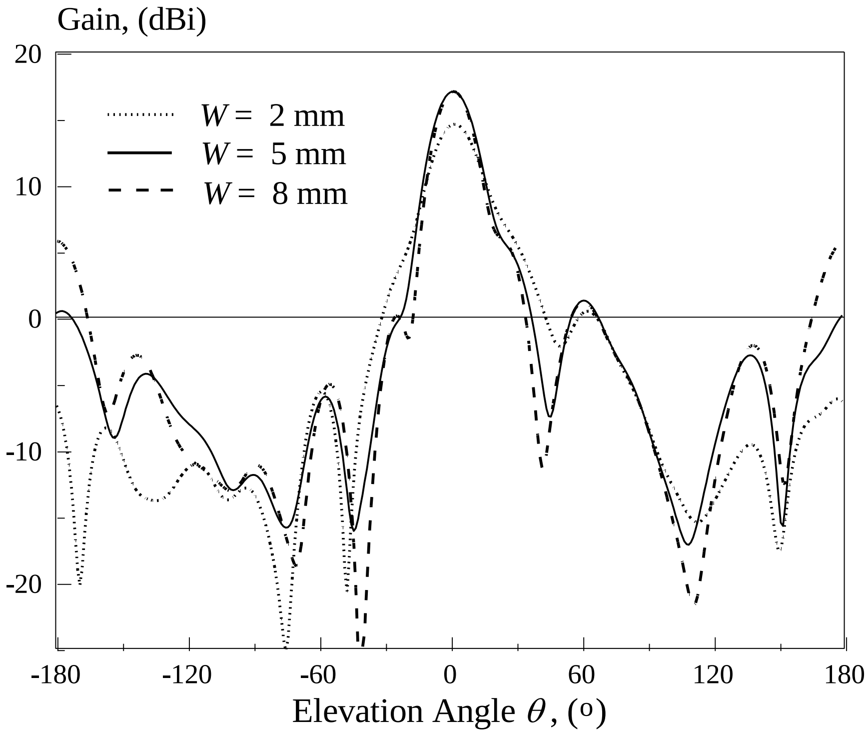

(a)

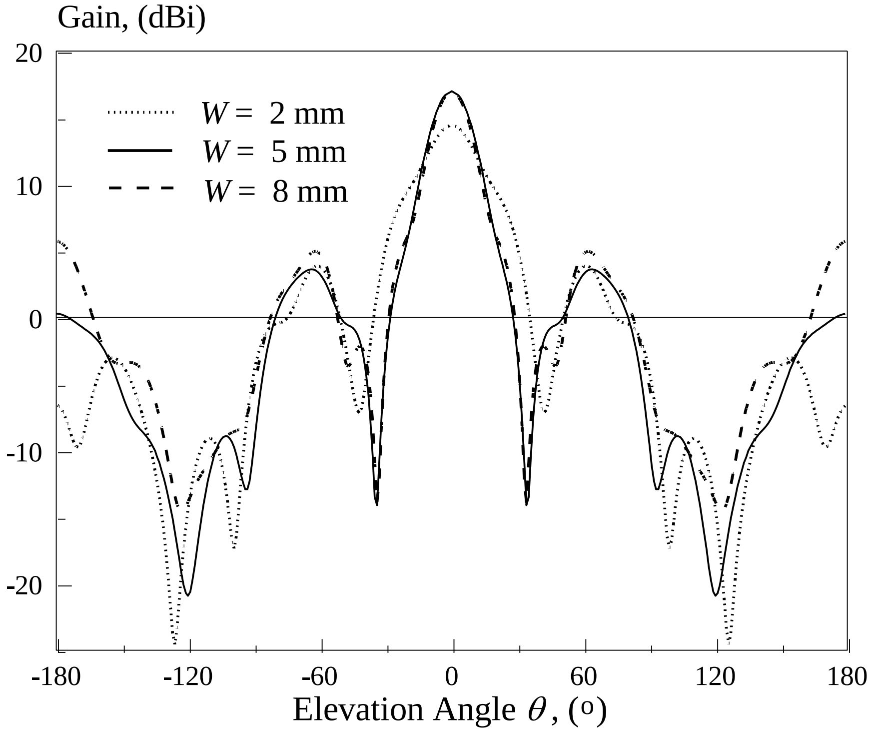

(b)

Figure 3.26: Radiation patterns of the proposed LP transmitarray for different director widths (*W*) at 6 GHz. (a) *E* - and (b) *H* - planes.

Finally, the suspension distance (h_1) between the feeding dipole and its ground plate is varied and studied. The corresponding radiation patterns are shown in *Figure 3.27* and compared in *Table 3.4*. Optimum spacing was found to be around 10 mm (~ 0.2 λ), falling within the typical separation range (0.2λ - 0.25λ) of the directors a conventional Yagi-Uda antenna. Increase in h_1 causes the antenna gain to reduce and the sidelobe level to increase.

Table 3.4: LP transmitarray performance for different reflector-feeder spacing h_1.

Spacing h_1 (mm)	***E* - plane**		***H* - plane**	
	Gain(dBi)	**HPBW(°)**	**Gain(dBi)**	**HPBW(°)**
5	17.0	19.0	16.8	20.9
10	17.0	19.0	17.0	19.5
15	15.8	19.0	15.8	18.9

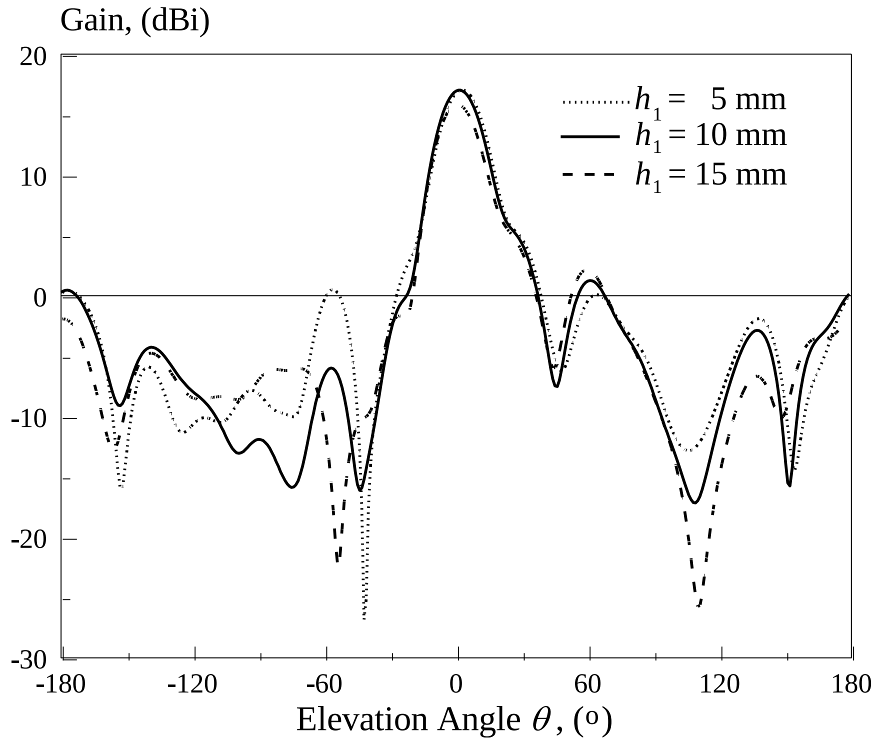

(a)

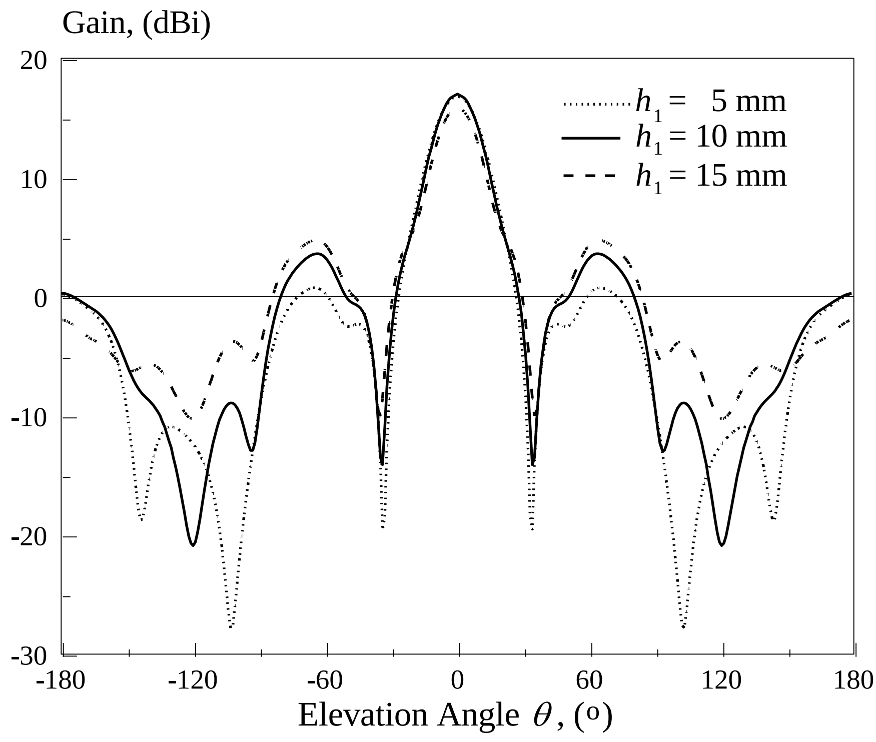

(b)

Figure 3.27: Radiation patterns of the proposed LP transmitarray for different reflector-feeder spacing (h_1) at 6 GHz. (a) E - and (b) H - planes.

3.6.2 Analysis on Circularly Polarized Transmitarray

Parametric analysis is also performed on the circularly polarized unit element and the full transmitarray. The director spacing (*d*) is varied and the effects are studied in *Figure 3.28*. When *d* is increased from 3mm, 5mm, to 10mm, the useable phase range is also reducing from 439°, 412°, and 136°. Similar to the LP case, small spacing is more favorable for achieving a broader phase range. However, the thickness of the 5mm is selected for our design as 3mm is not commercially available.

The effect of the element cell size (*L*), or transmitarray separation distance in the full transmitarray, is then studied. It is observed that this parameter does not affect the transmission characteristics much. For *L* of 0.5λ, 0.55λ, 0.6λ, and 0.65λ, as can be seen from *Figure 3.29*, the phase range is able to reach 414°, 429°, 412°, and 393° respectively. The simulated antenna gain and axial ratio for the CP transmitarray are also shown in *Figure 3.30* and *Figure 3.31*. Obviously, the CP transmitarray is much more sensitive to the change in separation distance. Such deterioration is expected as all other parameters are optimized for *L* = 0.6λ. Radiation patterns for the cases of 0.5λ, 0.55λ and 0.65λ are not further explored as their antenna gains see a sharp drop of greater than 4dB in the broadside direction and it is not worthwhile to investigate further.

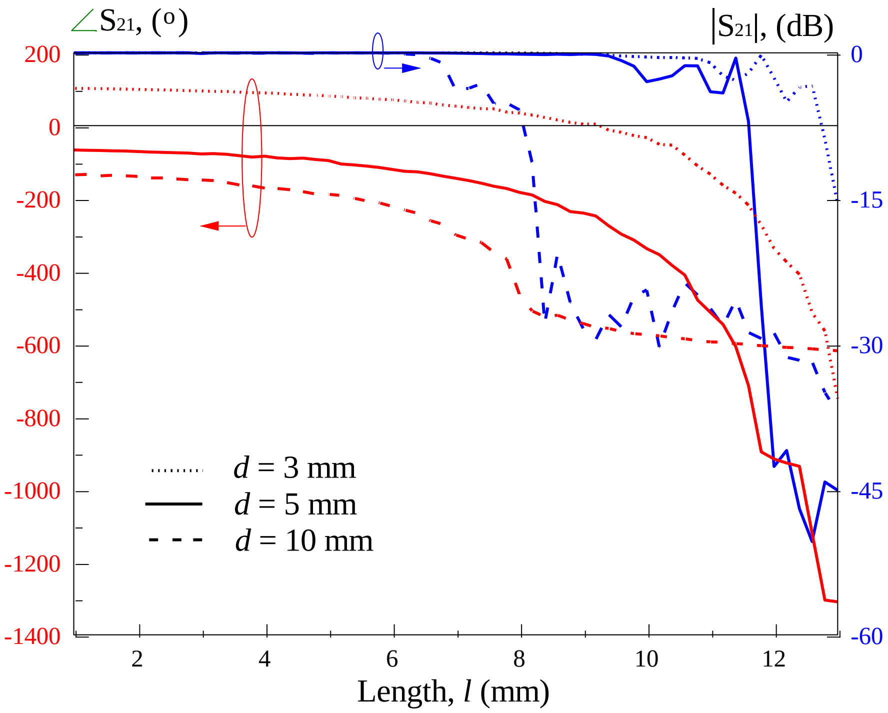

Figure 3.28: The effect of director spacing, (d) on the amplitude and phase responses of the CP unit cell.

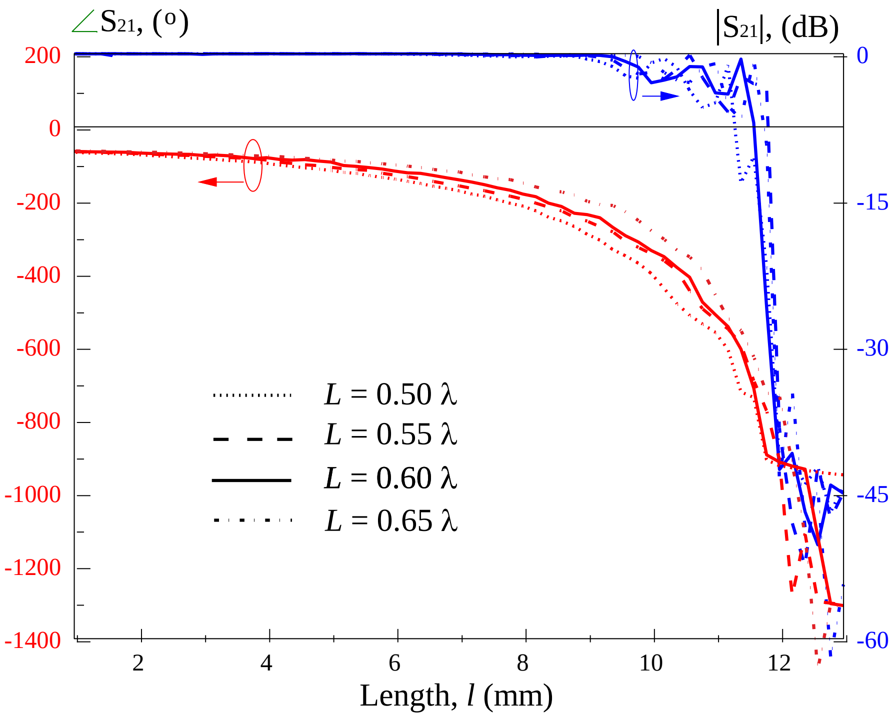

Figure 3.29: The effect of unit cell dimension (L) on the transmission amplitude and phase responses of the CP element simulated using unit cell.

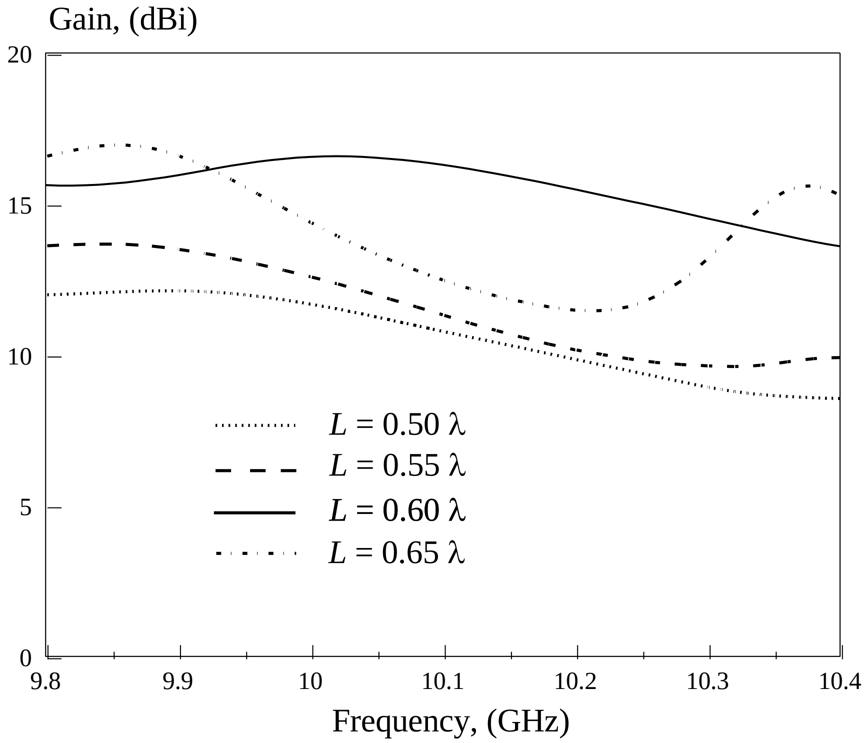

Figure 3.30: The effect of separation distance (L) on the antenna gain of the CP transmitarray.

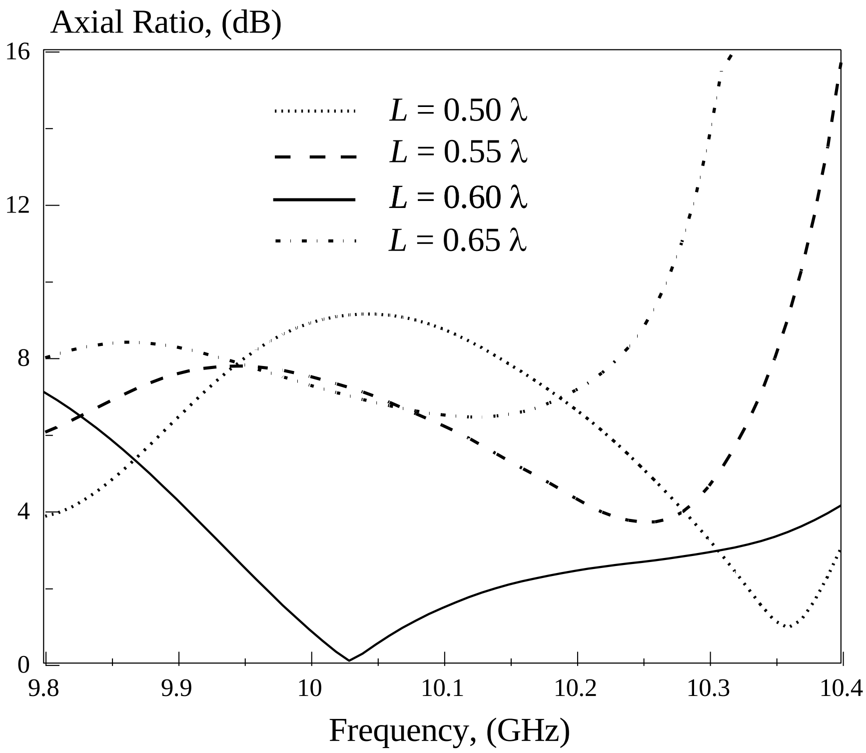

Figure 3.31: The effect of separation distance (L) on the antenna axial ratio of the CP transmitarray.

Analysis is also performed to study the sensitivity of *F / D* for the CP transmitarray. By keeping the cell dimension at *L* = 0.60λ and array dimension *D* = 90mm, three transmitarrays are designed at the *F / D* ratios of 1.00, 1.356, and 1.389 and the simulated radiation patterns at 10GHz are shown in *Figure 3.32*. The respective antenna gains and HPBW are compared in *Table 3.5*. It can be seen that making *F / D* = 1 can result in a larger antenna again, but it also causes the backlobe and the side lobes to increase. In our design, the *F / D* = 1.356 is selected as a tradeoff. Changing *F / D* also causes the antenna gain and the axial ratio to drift. It can be seen in *Figure 3.33* that a sacrifice of ~1dB is made on the antenna gain by choosing *F / D* = 1.356, comparing with that of unity. On the other hand, it is observed from *Figure 3.34* that the axial ratio has achived the best performance around 10GHz for *F / D* = 1.356.

Table 3.5: CP transmitarray performance for different *F / D* ratios.

F/ D ratios	**E-plane**		**H-plane**	
	Gain(dBi)	**HPBW(º)**	**Gain(dBi)**	**HPBW(º)**
1.000	17.5	12.5	17.4	12.7
1.356	16.6	11.5	16.6	11.7
1.389	16.5	11.2	16.5	11.7

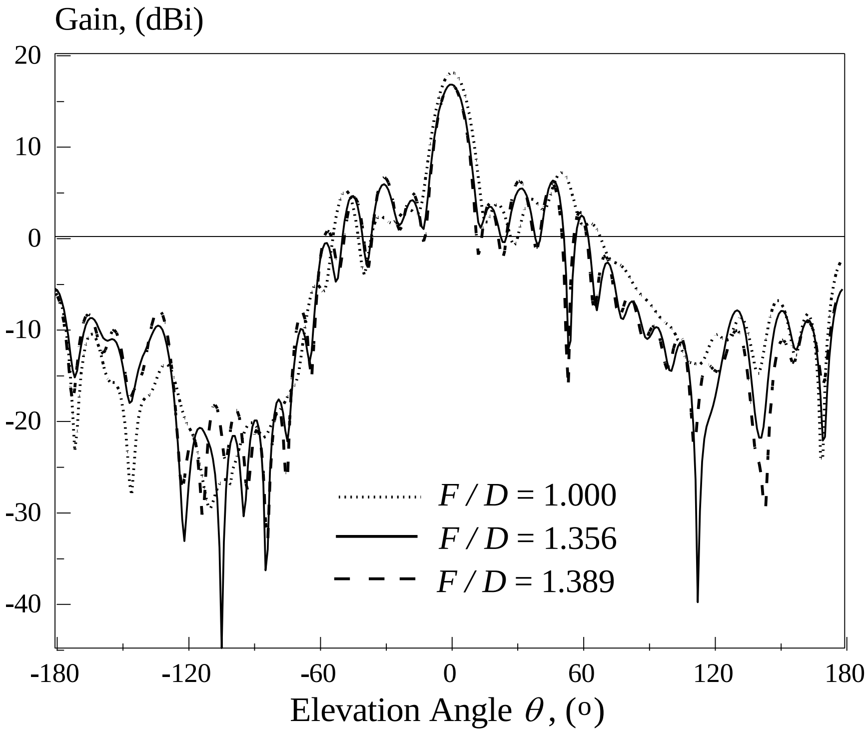

(a)

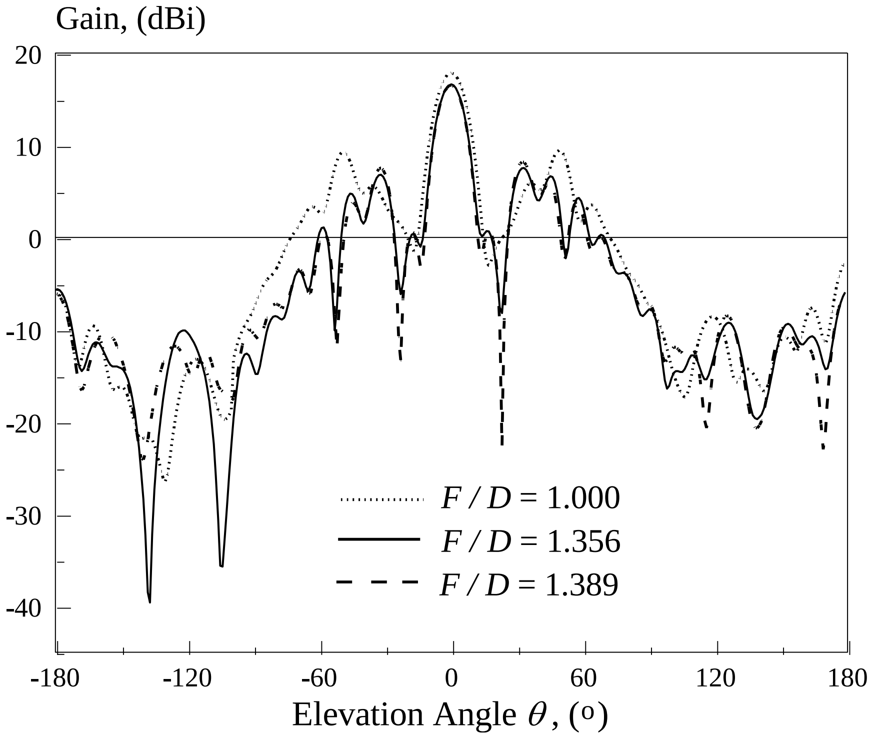

(b)

Figure 3.32: Radiation patterns of the proposed transmitarray with different F / D ratio. (a) E - and (b) H - planes.

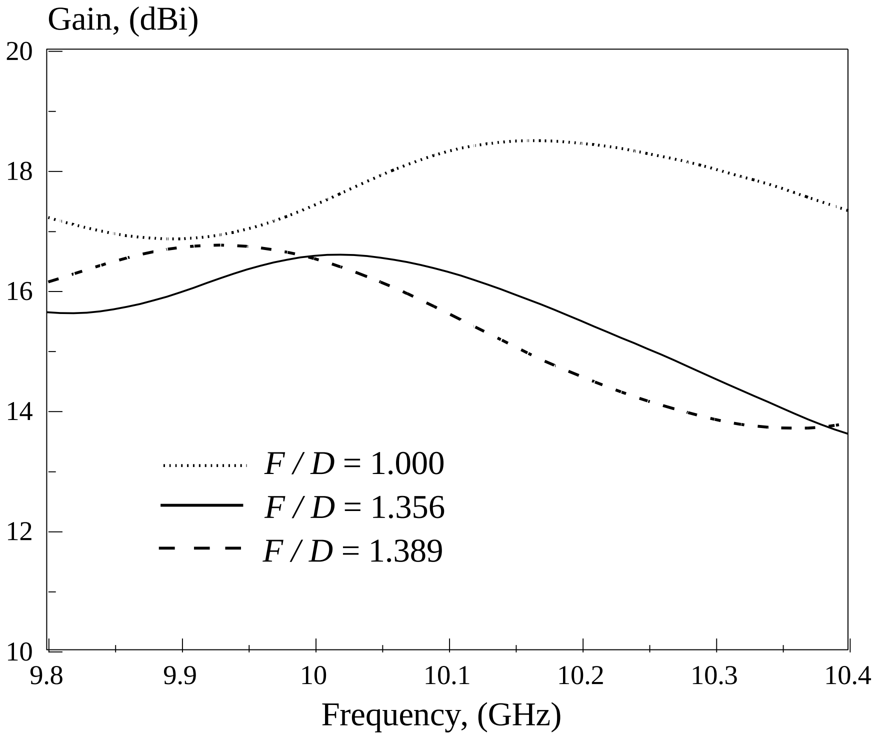

Figure 3.33: The effect of F / D ratio on the antenna gain of the CP transmitarray.

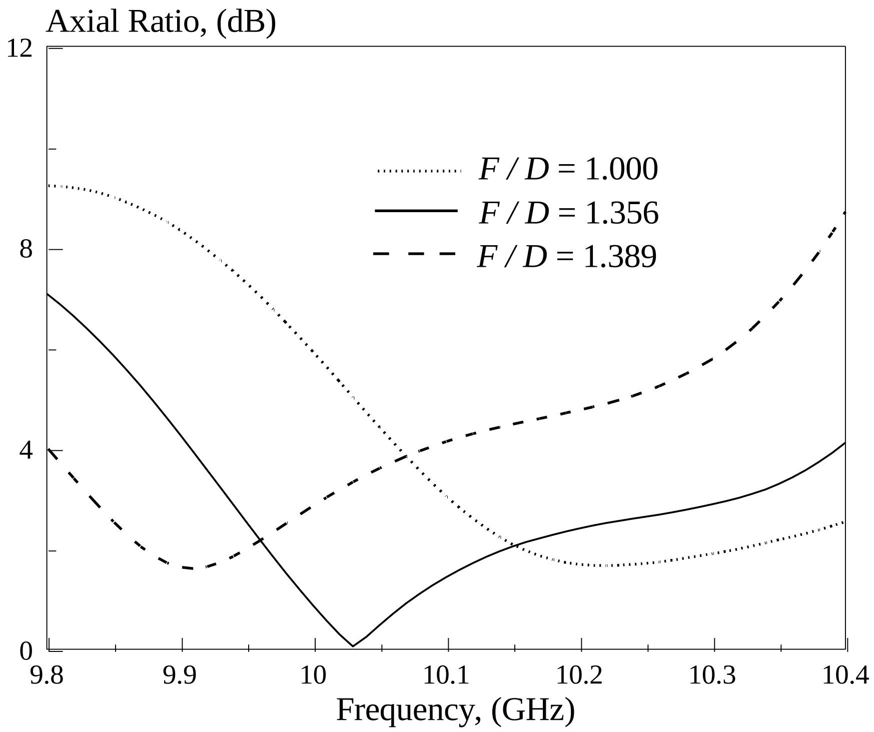

Figure 3.34: The effect of F / D ratio on the antenna axial ratio of the CP transmitarray.

The effect of the ground size ($R \times R$), which is also the reflector of the CP transmitarray, is now studied. Similar to its LP counterpart, as can be seen in *Table 3.6*, increasing ground size is good for enhancing the antenna gain and achieving a narrower beamwidth, but it also causes the backlobe and sidelobes to increase. The antenna gain and axial ratio performance is also checked across the frequency range of 9.8GHz to 10.4GHz in *Figure 3.35* and *Figure 3.36*, respetively. It is found that the utilization of the a larger reflective ground facilitates the enhancement of antenna gain. The case for R = 100mm has the best axial ratio bandwidth and it is selected for our design.

Table 3.6: CP transmitarray performance for different reflector size *R*.

Reflector Plate, *R* (mm × mm)	**E-plane**		**H-plane**	
	Gain(dBi)	**HPBW(º)**	**Gain(dBi)**	**HPBW(º)**
30 × 30	15.6	11.7	15.5	12.5
100 × 100	16.6	11.5	16.6	11.7
150 × 150	17.4	10.6	17.4	10.9

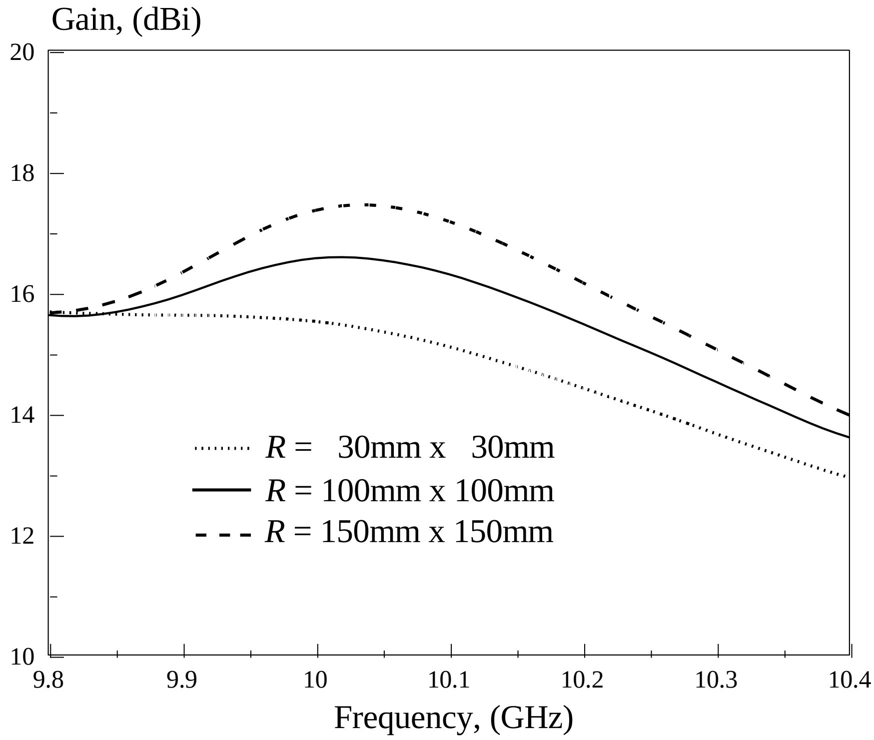

Figure 3.35: The effect of ground size on the antenna gain of the CP transmitarray.

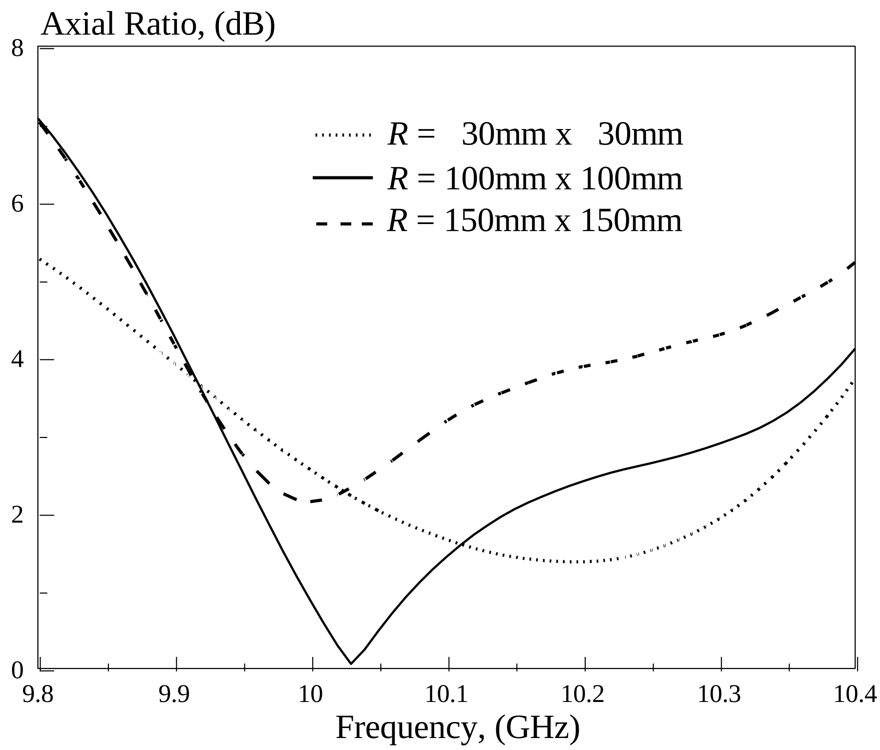

Figure 3.36: The effect of ground size on the axial ratio of the CP transmitarray.

The strip element (*W*), which is also a dual-functional director for the CP transmitarray, is further studied and the radiation patterns are shown in *Figure 3.37*. With reference to the figure, the case of the shorter strip length has resulted in a larger antenna gain, where the corresponding antenna gain and HPBW for different cases are compared in *Table 3.7*. It is opposite to what was observed for the LP case. Nevertheless, it does not have much effect on the backlobe and sidelobes. It is very interesting to note from *Figure 3.38* and *Figure 3.39* that the antenna gain and axial ratio are very sensitive to the change of strip width. Both deteriorate significantly when the strip width is increased from 5mm.

Table 3.7: CP transmitarray performance for different strip width *W*.

Width, *W* (mm)	**E-plane**		**H-plane**	
	Gain(dBi)	**HPBW(º)**	**Gain(dBi)**	**HPBW(º)**
5	16.6	11.5	16.6	11.7
8	11.1	15.0	11.1	15.2
10	8.77	10.3	8.71	10.9

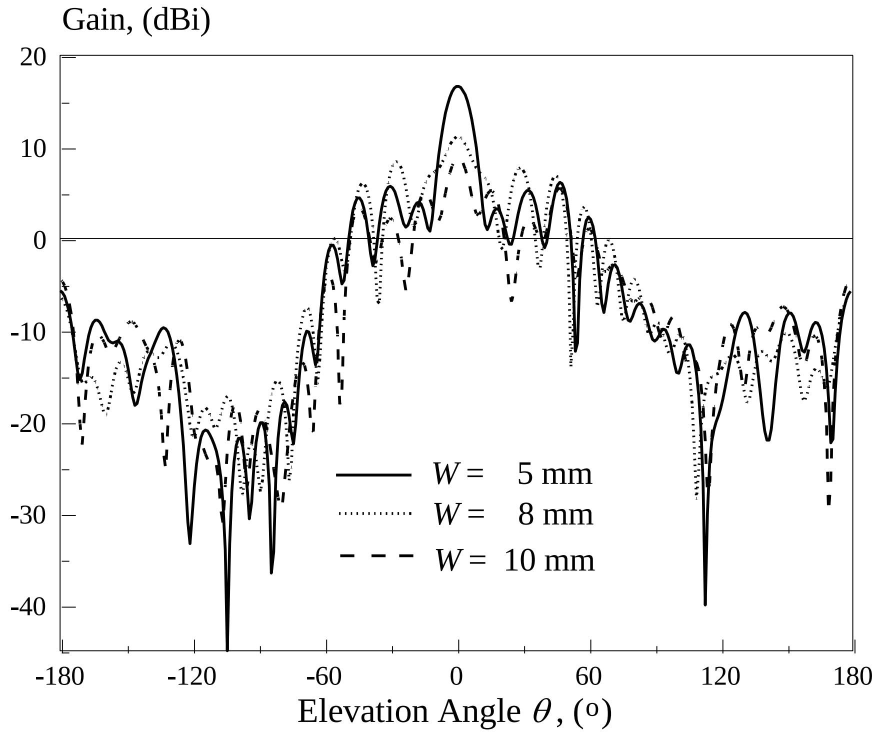

(a)

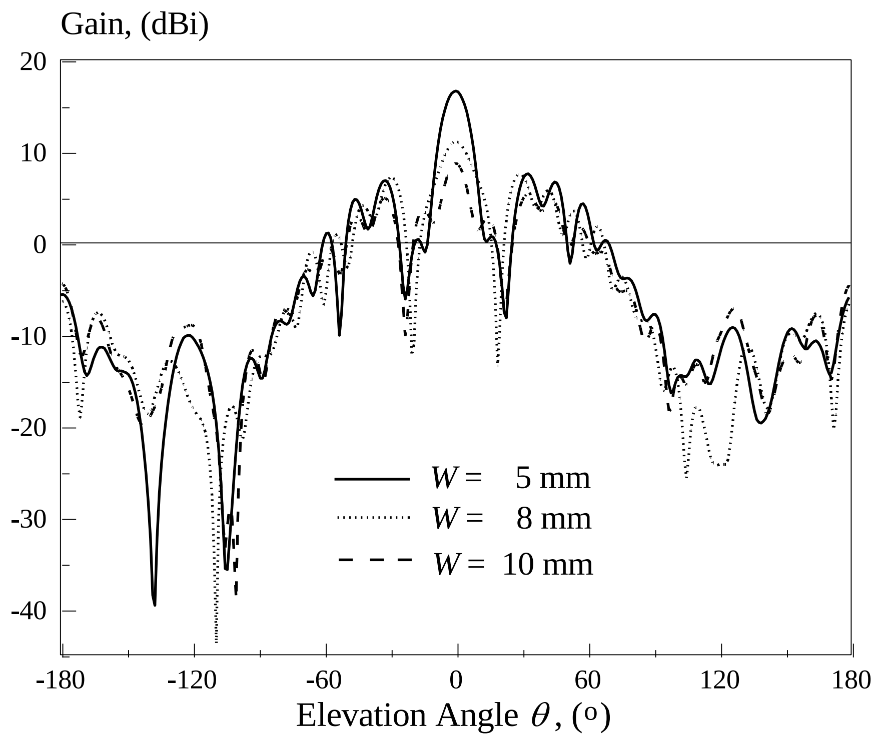

(b)

Figure 3.37: Radiation patterns of the proposed CP transmitarray for different director widths (W) at 10 GHz. (a) E - and (b) H - planes.

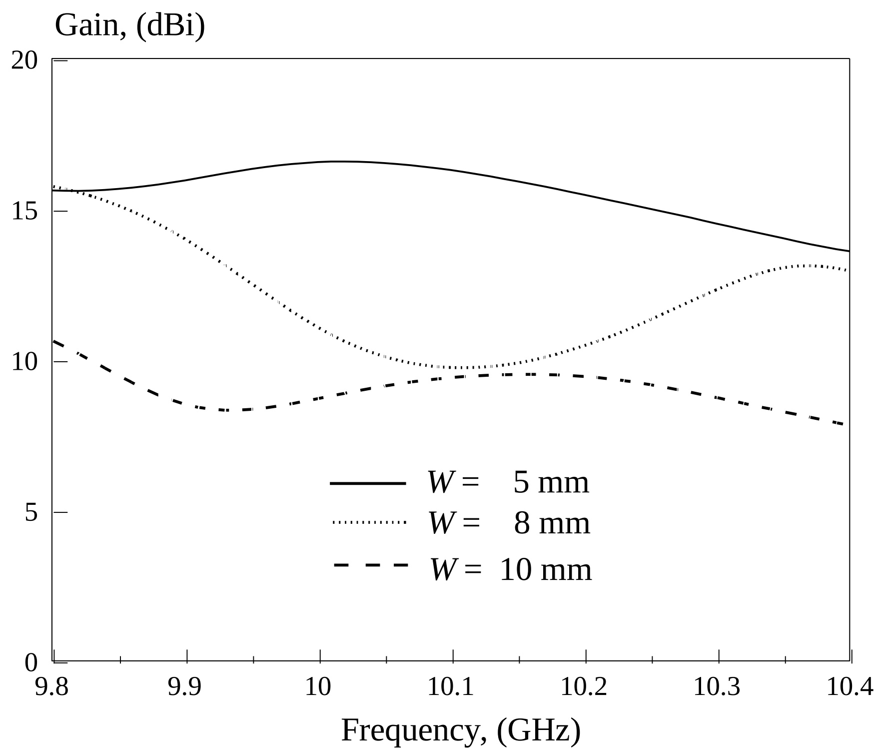

Figure 3.38: The effect of strip width (*W*) on the antenna gain of the CP transmitarray.

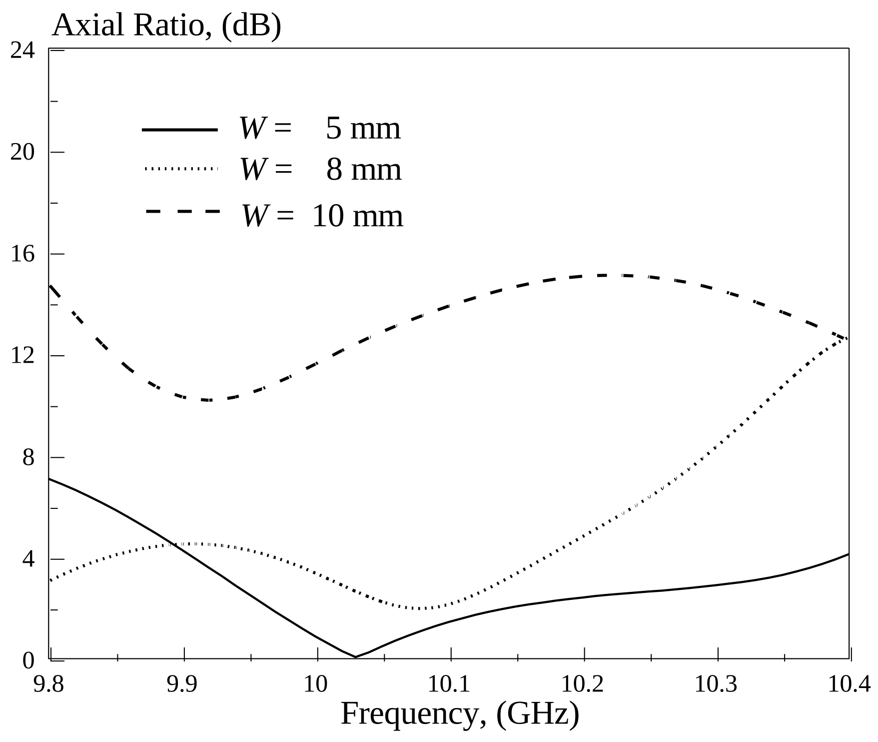

Figure 3.39: The effect of strip width (*W*) on the axial ratio of the CP transmitarray.

For the CP transmitarray, the radiation patterns of the transmitarray are studied for different feeding dipole height (h_1), with the results illustrated in *Figure 3.40*. The antenna gains and HPBW are also compared in *Table 3.8*. It can be seen that the antenna gains and sidelobe levels are the most optimum for h_1 = 5mm (~0.2λ). Again, changing h_1 causes the antenna gain to drop and the sidelobe level to increase. The antenna gain and axial ratio also degrade when this design parameter is varied, as can be seen *Figure 3.41* and *Figure 3.42*.

Table 3.8: LP transmitarray performance for different reflector-feeder spacing h_1.

Height, h_1 (mm)	**E-plane**		**H-plane**	
	Gain(dBi)	**HPBW(°)**	**Gain(dBi)**	**HPBW(°)**
2	14.4	12.2	14.1	12.5
5	16.6	11.5	16.6	11.7
10	13.5	11.1	13.5	11.9

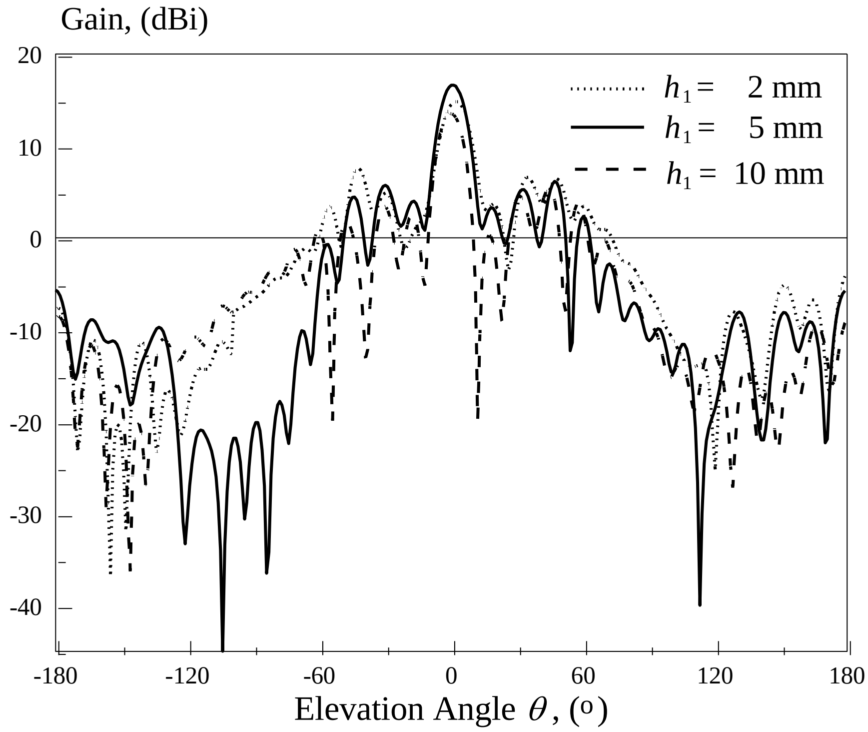

(a)

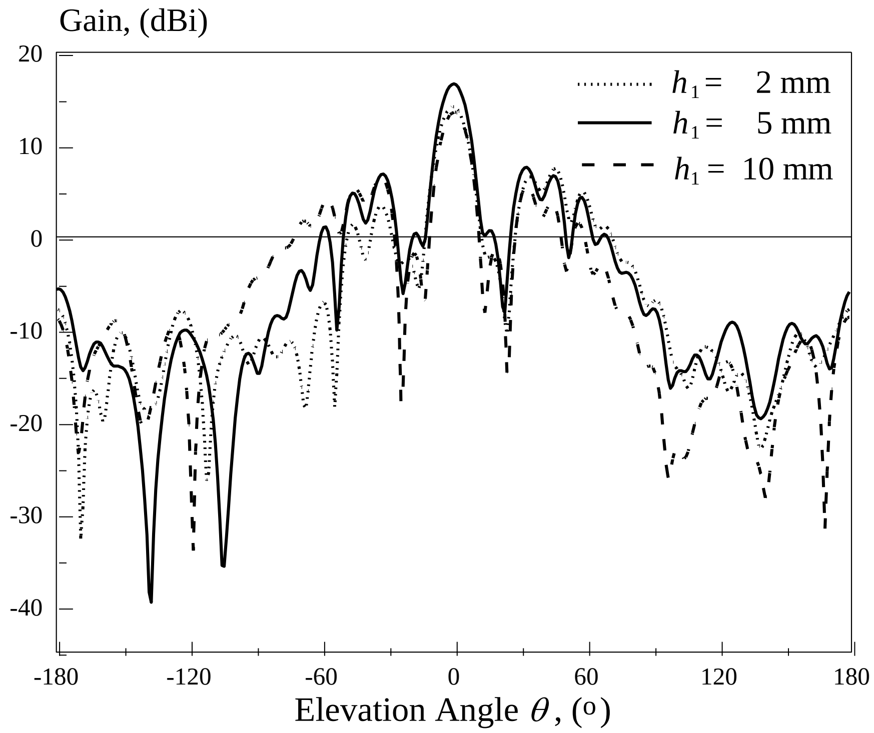

(b)

Figure 3.40: Radiation patterns of the proposed CP transmitarray for different reflector-feeder spacing (h_1) at 10GHz. (a) *E* - and (b) *H* - planes.

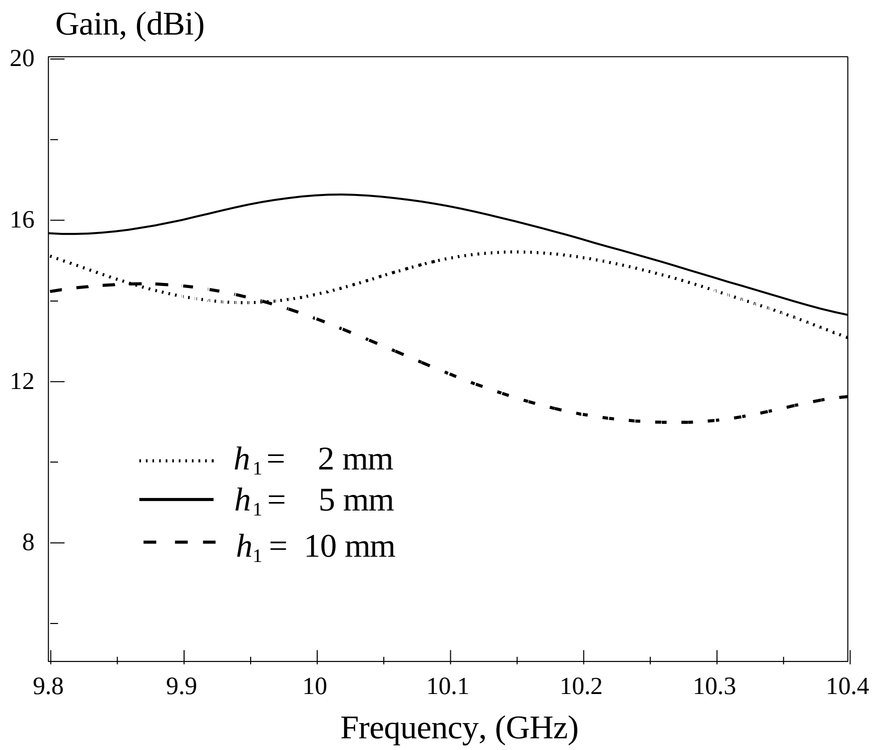

Figure 3.41: The effect of feeding dipole height (h_1) on the antenna gain of the CP transmitarray.

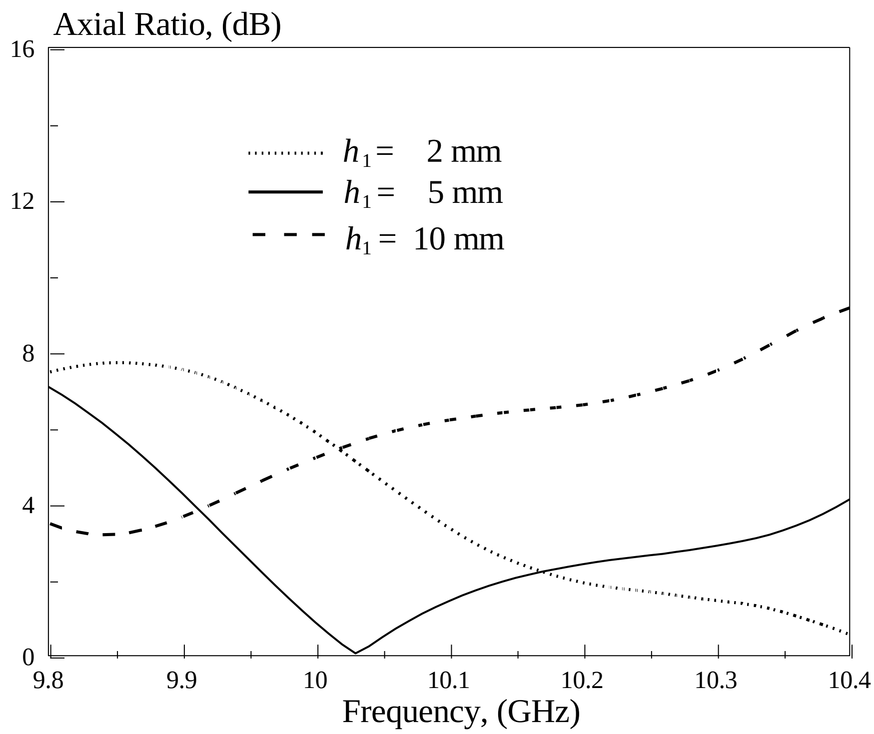

Figure 3.42: The effect of feeding dipole height (h_1) on the axial ratio of the CP transmitarray.

3.7 Conclusion

Two novel Yagi-uda-like transmitarrays have been proposed for linearly polarized (LP) and circularly polarized (CP) operations. The transmitarray element is composed by multiple strips, which are stacked in parallel for achieving broad transmission phase range. To demonstrate the working principle, a 6-layer unit element is first simulated using the Floquet method and it is found that the LP case has a transmission phase range of 364^o. By introducing rotational offset between the stacking strips, the element is found to be able to generate circular polarization yielding a useable phase range of 412^o. When designed into a 5×5 full transmitarray, the LP case is able to produce an antenna gain of ~ 17dBi with a broad 1-dB bandwidth of 11.86%. For the same array dimension, the CP transmitarray has a measured antenna gain of 16.6dBi and a 1-dB bandwidth of ~ 4%.

A design guideline has been given and comprehensive parametric analysis has been conducted on both and it was found that the side and back lobes of both of the transmitarrays can be easily suppressed by tuning some of the geometrical parameters. With the use of design concept of the Yagi-Uda director, the transmitarray elements are made to provide the functions of phase shifter and director at the same time. Different from the conventional transmitarrays, no dielectric substrate is required by the proposed designs. Also, the proposed CP and LP transmitarrays have wider bandwidth than the conventional ones (Abdelrahman et. al., 2014).

CHAPTER 4

DESIGN OF ANNULAR RING-SLOT TRANSMITARRAY

4.1 Introduction

Usually, transmitarray elements are designed by using printed resonators such as loop, patch, dipole, or any other geometry which can be mounted on a supporting substrate. (Lam et. al., 1997; Ryan et. al., 2010). Due to its low Q factor, different slot resonators (Abdelrahman et. al., 2013; Abdelrahman et. al., 2014) have also been explored for designing transmitarrays. Similar to reflectarray, the main drawback of the microstrip transmitarray is its limited bandwidth, which is inherent to its composing element itself (Huang and Encinar, 2007). In recent years, much effort has been done to improve bandwidth and phase performances of the transmitarray (Abdelrahman et. al., 2015). To provide sufficient compensating phases to all elements, the change of a particular geometrical structure is required to generate a transmission phase of at least 360^o, while maintaining low transmission loss in the desired frequency passband. Since a single layer of transmitarray element is usually able to yield a transmission phase of less than 90^o (Abdelrahman et. al., 2014), multilayer structures have been commonly used for increasing the phase range of the transmitarray. In this project, the multilayer annular ring-slot resonator is explored for designing a linearly polarized transmitarray for the first time.

This chapter is organized as follows. The geometry of the proposed unit-cell and an analysis of its transmission characteristics are presented in Section 4.2. Floquet cell is deployed for simulating the transmission response and generating the S-curve. The curve is then utilized for designing a 9 × 9 transmitarray in Section 4.3. Finally, measurement is conducted to verify the simulation models in Section 4.4, and parametric analysis on some of the important design parameters is shown in Section 4.5. Throughout the entire chapter, the CST Microwave Studio has been used for all simulations.

4.2 Unit Cell Configuration and Analysis

Figure 4.1 shows the configuration of the proposed transmitarray element. It is composed by a 3-layer annular ring-slot resonator made by stacking two pieces of Duroid RO5870 (ε_r = 2.33 and thickness of h = 1.57mm) substrates. With reference to the figure, the cell size is L = 23mm (0.6λ at 7.8GHz) and the outer diameter of the annular-slot is S = 16mm. By keeping S a constant, the inner diameter (d) of the slot is deployed as the phase-changing parameter. The transmission characteristics of the element is simulated using a Floquet cell which imitates an infinite array by taking account of the intercoupling mechanism between the elements, as depicted in *Figure 4.2*. In such settings, with reference to *Figure 4.2*, the top and bottom surfaces are defined to be perfect electric conductor (PEC) boundaries and perfect magnetic conductor (PMC) boundaries, respectively. A normal incident wave ($\phi = 0^o$ and $\theta = 0^o$) is launched at Port 1 and it is moving towards Port 2. In simulation, the port is de-embedded to a surface near to the transmitting element so that the phase change can be kept below one cycle.

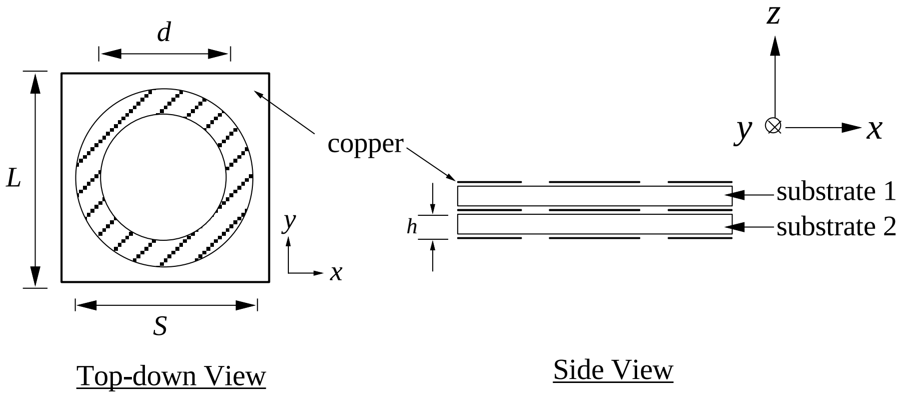

Figure 4.1: Configuration of the transmitarray element.

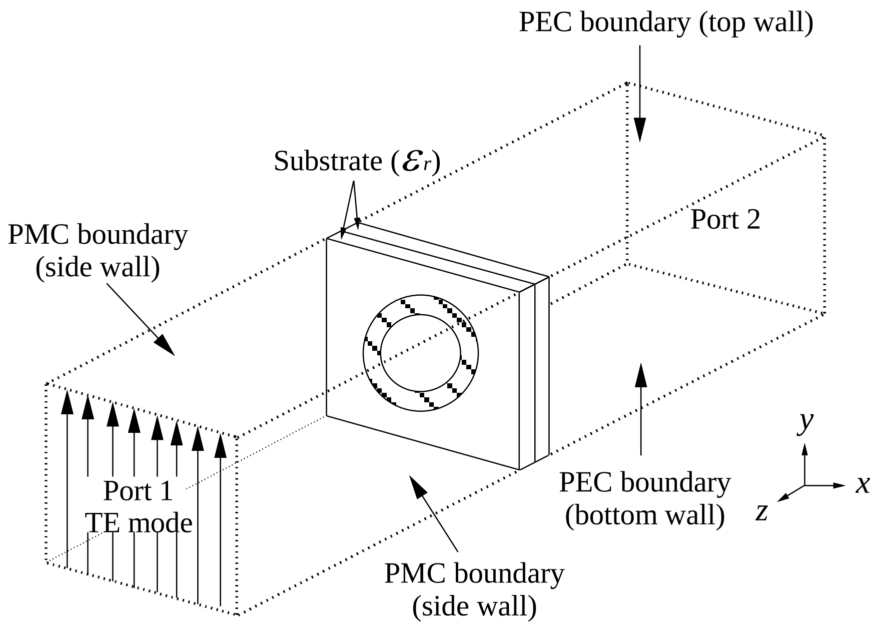

Figure 4.2: Unit cell model of the transmitarray element.

By changing *d* from 0.5mm to 15.5mm, the transmission magnitude and phase responses are simulated for the unit element with different number of layers. The transmission amplitude and phase responses are shown in *Figure.4.3*. It is found annular ring-slot resonator has larger loss and the phase range is taken at the amplitude threshold of -6dB. With reference to the figure, it is found that the phase ranges are 103^o, 228^o; 395^o, and 445^o with useable ranges of 0.5mm-13.3mm, 0.5mm-13.9mm, 2.1mm-13.9mm, and 2.1mm-13.7mm for one-layer, two-layer, three-layer, and four-layer annular ring-slot resonators at 7.8GHz. The phase range increases when more layers are involved, but with the price of increasing the material costs.

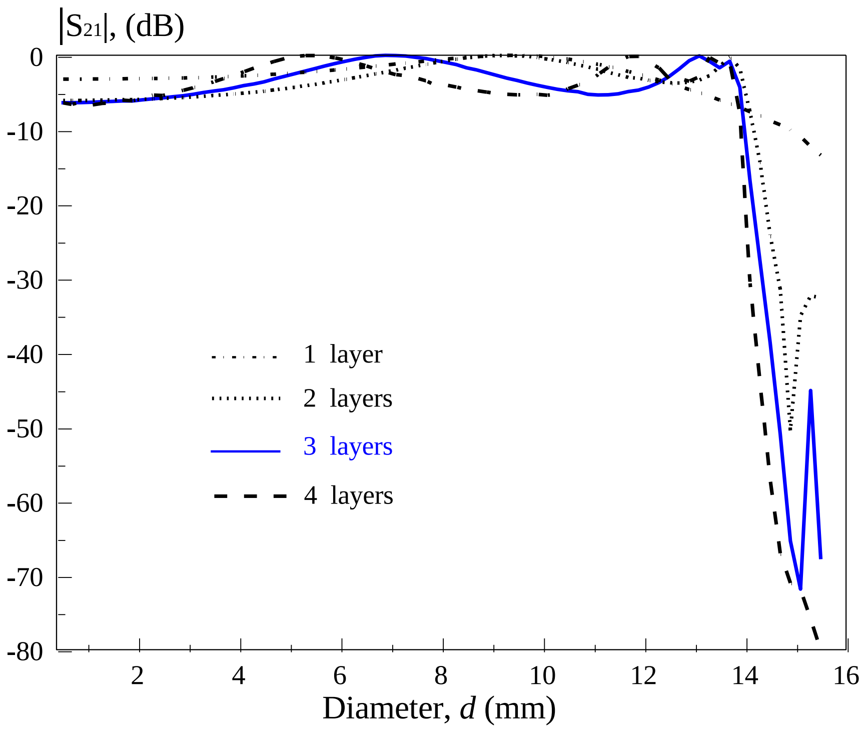

(a)

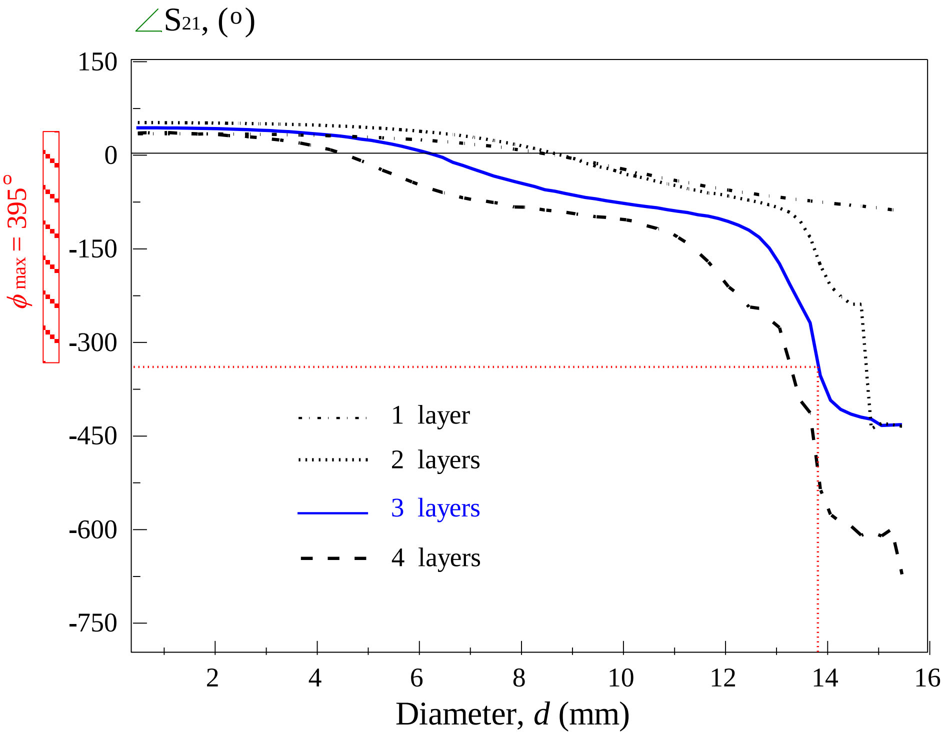

(b)

Figure 4.3: The effect of layer number on the transmission of the unit element at 7.8 GHz. (a) Transmission amplitude response. (b) Transmission phase response.

The characteristics of the multilayer annular ring-slot resonator are further explored. For an annular ring-shaped slot (with inner diameter d and outer diameter S) made on a substrate (ε_r), its resonant frequency can be calculated using $f_{nm0} = \frac{c_o k_{nm}}{\pi(S+d)\sqrt{\varepsilon_{eff}}}$, where c_o is the speed of light in free space, and k_{nm} are the roots of Bessel functions with mode indexes n and m. The effective dielectric constant is defined to be $\varepsilon_{eff} = 1 + q\ (\varepsilon_r - 1)$, where q is the correction factor by taking account of different dielectric materials on two sides of the annular-ring slot. A correction factor of 0.082 is here and it was proven to be correct for the narrow annular ring slot antenna (Chew, 1982). $\pi\,(S + d)$ is the mean circumference of the annular ring slot. An annular ring-slot shaped antenna can resonate at the fundamental [TE_{110}] as well as the higher order modes [TE_{210}, TE_{310}, …] (Eriksson et. al., 2001). Next, the magnetic field distribution for the TE_{110} of an annular ring-slot with d = 12 mm, S = 16 mm, and L = 23 mm is illustrated in *Figure 4.4*, which is the fundamental TE_{110} mode. The resonance frequency f_{mn0} is calculated to be 5.96GHz, with k_{11} = 1.8412, and it is agreeing quite well with that (5.848GHz) simulated using CST in a unit cell model.

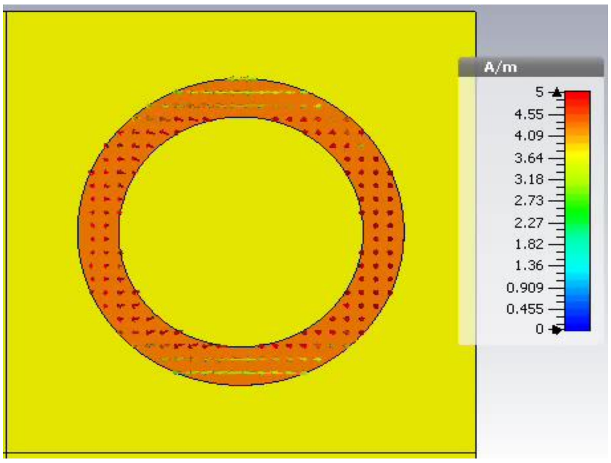

Figure 4.4: Magnetic field distribution on the annular ring-slot transmitarray element (d = 12 mm, S = 16 mm, L = 23 mm, and $\theta = 0^o$ at 7.8 GHz).

The characteristics of the three-layer case (shown in *Figure 4.2*) are now analyzed. *Figure 4.5* shows the effect of the cell for different wave frequencies. It can be seen that the phase range is able to reach 407°, 395°, and 391° for the incident wave of 7.6GHz, 7.8GHz, and 8GHz. Frequency of 7.8GHz was selected for our design as it has reasonable transmission phase range and slow gradient, which is good for designing a transmitarray with better dimension resolution. Size of the unit element (L), which is translated into the separation distance of the elements when designed into a full-fledge transmitarray, is also studied and the results are shown in *Figure 4.6*. The phase ranges are 316°, 395°, and 117°, respectively, for L of 0.52λ, 0.60λ, and 0.78λ. A cell size of 0.60λ is chosen as it can provide a phase range of greater than 360°. Both of the transmission phase range and slope deteriorate when the separation distance becomes larger (0.78λ). *Figure 4.7* shows the change of transmission amplitude and phase range when the outer diameter (S) of the slot is varied. Transmission amplitude increases when S is made larger. Nevertheless, the phase range is changing in the reverse trend. The phase range for the case of 22mm, 20mm, and 18mm are 249.5^o, 332^o, and 357^o, respectively, and they are not sufficient for compensating the transmission phase of a large array. As a result, the outer slot with diameter of 16mm is used as it is able to provide a phase range of 397^o.

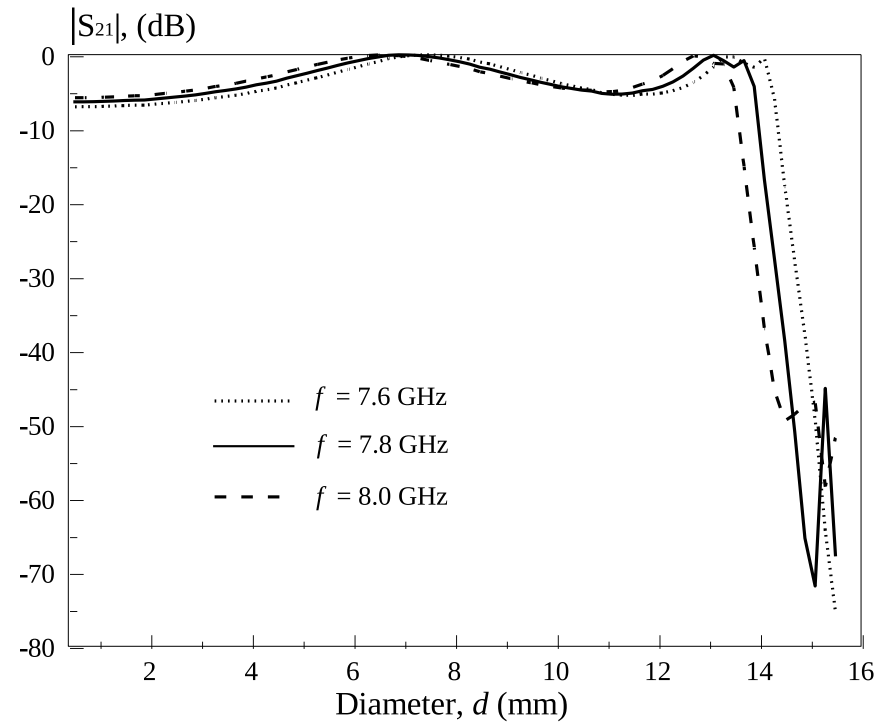

(a)

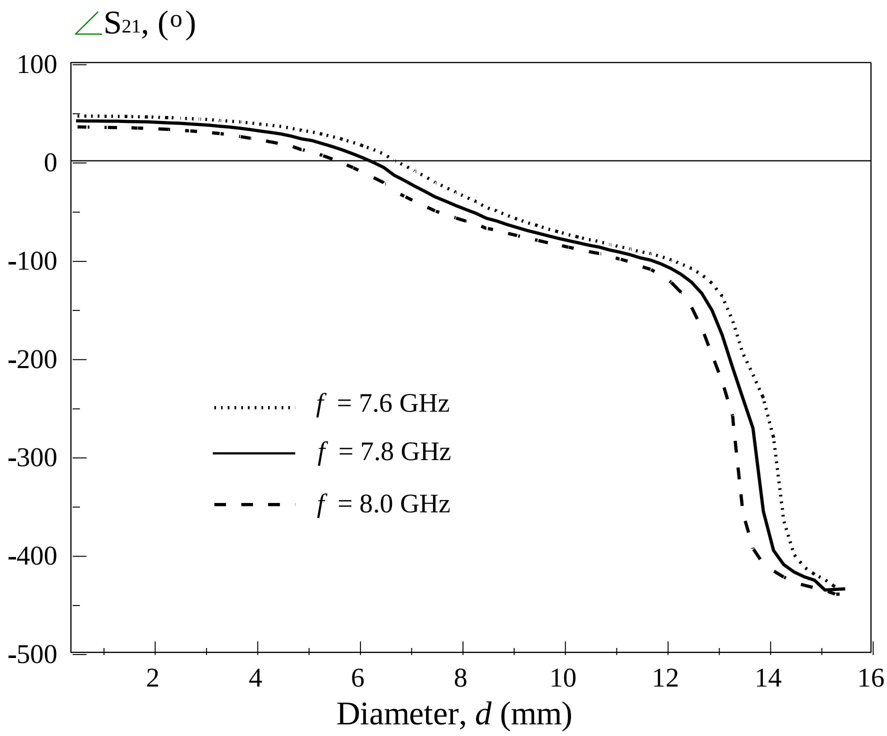

(b)

Figure 4.5: The effect of frequency (f) on the transmission of the unit cell. (a) Transmission amplitude response. (b) Transmission phase response.

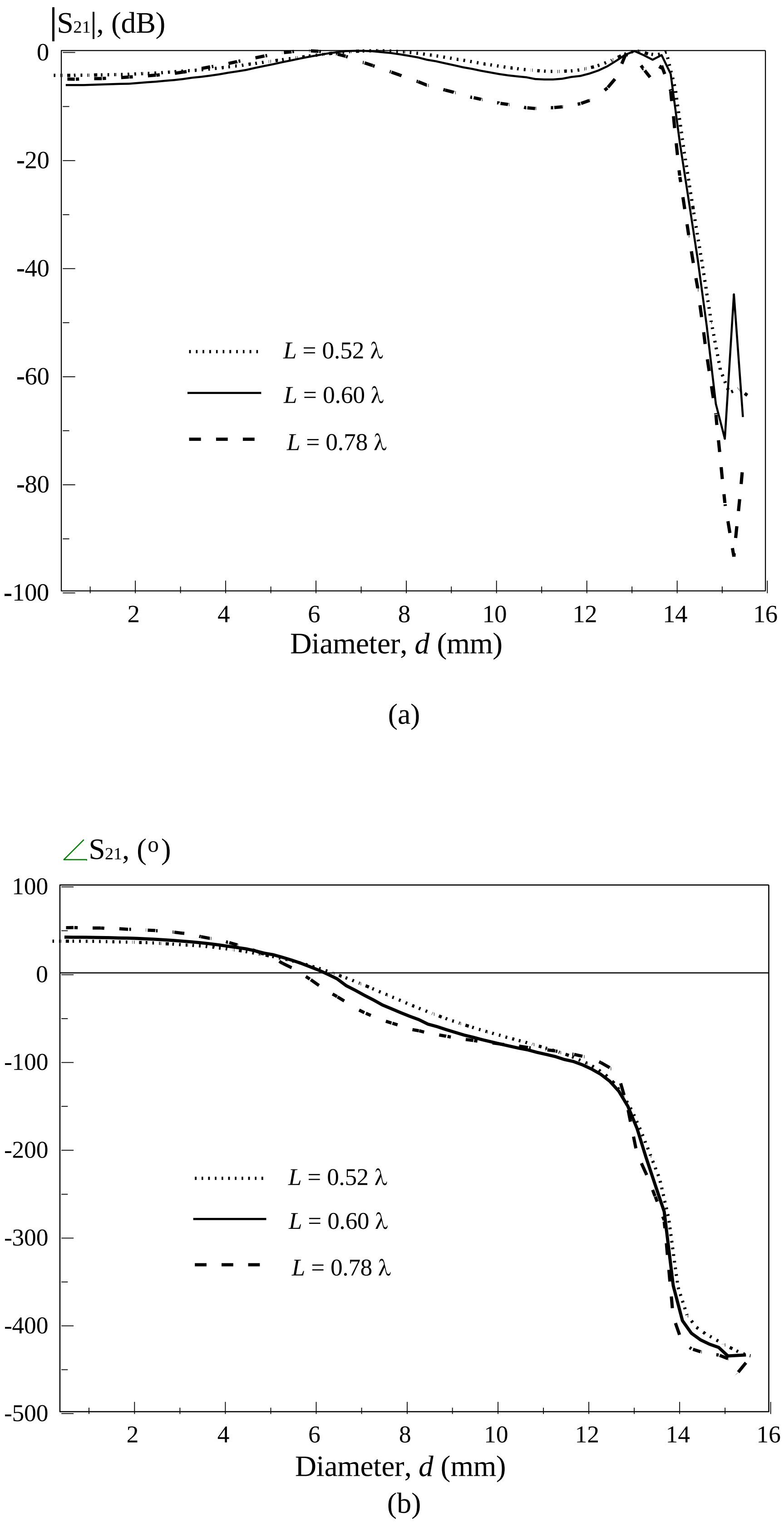

Figure 4.6: The effect of separation distance (L) on the transmission of the unit cell. (a) Transmission amplitude response. (b) Transmission phase response.

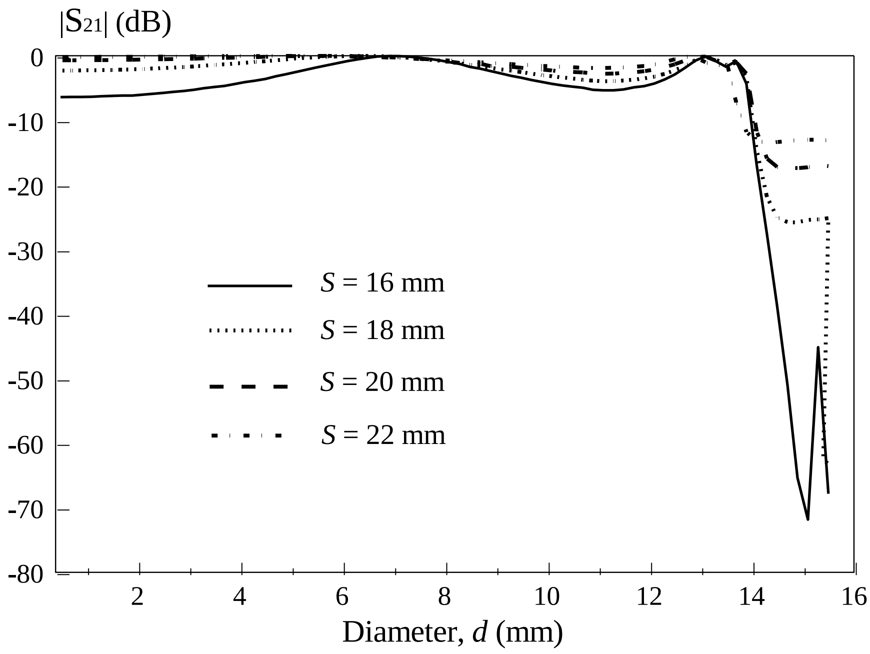

(a)

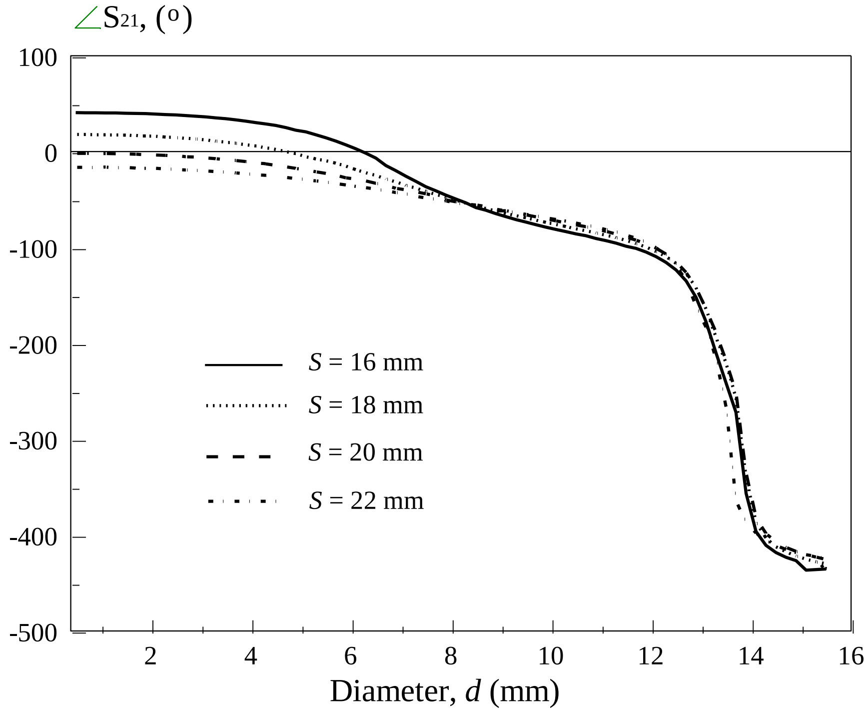

(b)

Figure 4.7: The effect of the outer slot diameter (*S*) on the transmission of the unit cell. (a) Transmission amplitude response. (b) Transmission phase response.

4.3 Transmitarray Configuration

The aforementioned three-layer annular ring-slot resonator is now used for designing 9 × 9 transmitarray, as depicted in *Figure 4.8*. Two substrates are deployed to accommodate the three-layer transmitting elements. In this case, spacing between any two elements is taken 0.6λ at 7.8GHz, resulting a total transmitarray dimension of D = 207mm. It has an F / D ratio of 0.87. The elements are fed by a linearly polarized C-band pyramidal horn (ATM PNR137-440-2, 5.85GHz – 8.2GHz) suspended at a distance f = 180mm from the center point of the transmitarray with an inclination angle of $\theta = 0^{o}$. The horn is arranged such that a y-polarized wave is launched to the H - plane.

By taking the center point to be the reference, the transmission phase ψ_i that is required by the i^{th} element can be calculated using $\psi_i = k(R_i - \vec{r_\mathrm{I}}\,.\,\vec{r_o})$, where k is the propagation constant, R_i is the distance from the feed horn to the i^{th} element, and while $\vec{r_\mathrm{I}}$ is the position vector of the i^{th} element. The transmitarray is designed to have broadside direction where the vector product is ($\vec{r_\mathrm{I}}\,.\,\vec{r_o} = 0$) for the reference element position at the center. After obtaining the required transmission phase for each element, the corresponding d that is able to give this phase can be easily found out from the x-axis of *Figure 4.3(b)*. Finally, the prototype of the proposed annular ring-slot transmitarray is shown in *Figure 4.9*. Copper tape is used to connect the metal layers at the four edges so that they are electrically shorted maintaining at the same potential.

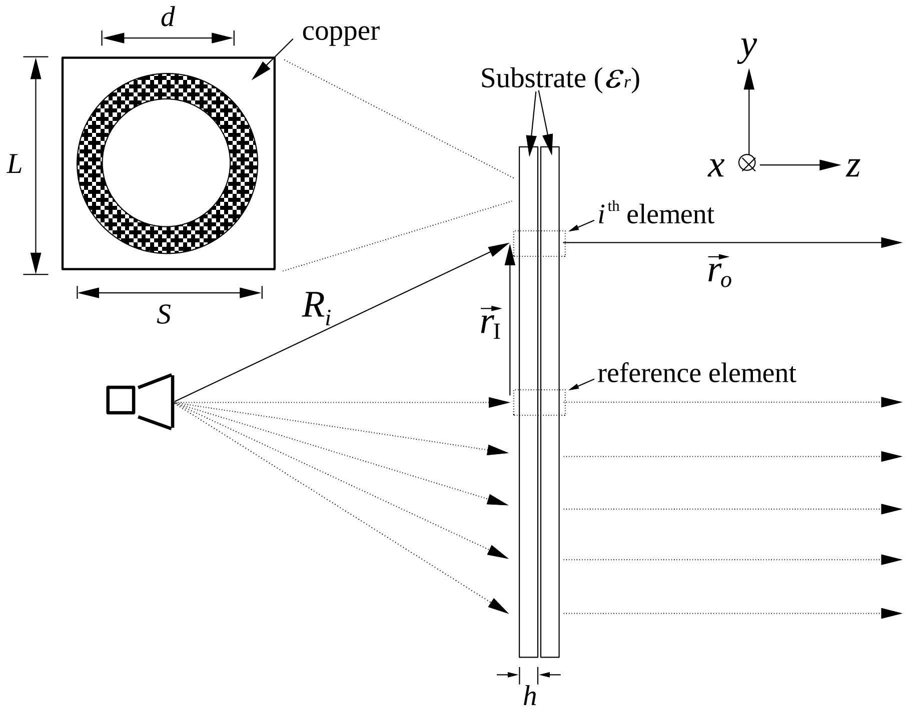

Figure 4.8: Configuration of the full transmitarray.

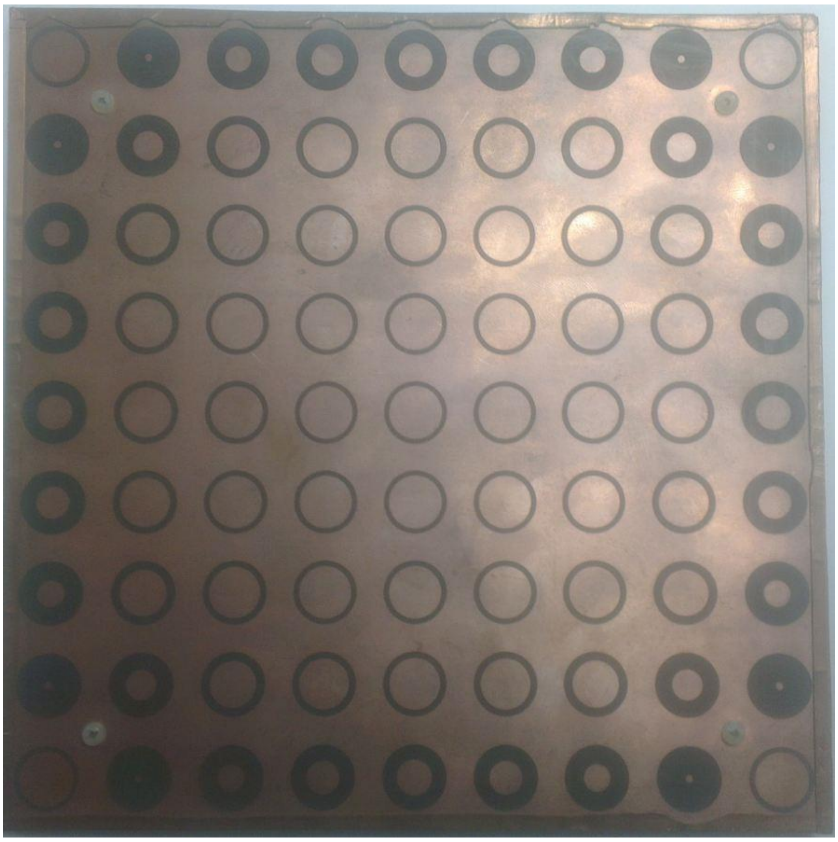

Figure 4.9: Photograph of the proposed three-layer transmitarray. Copper tape is used to connect the metal parts of all layers so that they have the same potential.

4.4 Simulated and Measured Results of Transmitarray

Antenna performance of the proposed transmitarray is measured using the experimental setting shown in *Figure 4.10*. Rohde & Schwarz SMB100A Signal Generator (100kHz -12.75GHz) is used to generate a monotone microwave signal which is connected to the feed horn ($G_r{}^H$=12.61dBi at 7.8GHz) of the transmitarray. Also, the transmitted signal is received by a similar measuring horn antenna that is placed at the far-field distance of 4.64m. As can be seen from the figure, the measuring horn antenna is connected to an Advantest U3771 Spectrum Analyzer (9kHz – 31.8GHz) to receive power at different angles (θ). The transmitarray is supplied with an input power of $P_t{}^T$= 10 dBm at 7.8GHz, and the received power is denoted as $P_r{}^H$. With the use of Friis transmission equation, the antenna gain ($G_t{}^T$) of the transmitarray can be calculated using *equation (4.1)*.

$$G_t{}^T = G_r{}^H + 10\log(P_t{}^T) - 10\log(P_r{}^H) \tag{4.1}$$

The radiation pattern of the transmitarray can then be measured by turning the rotation angle θ. Measurement was performed in the two major cut-planes.

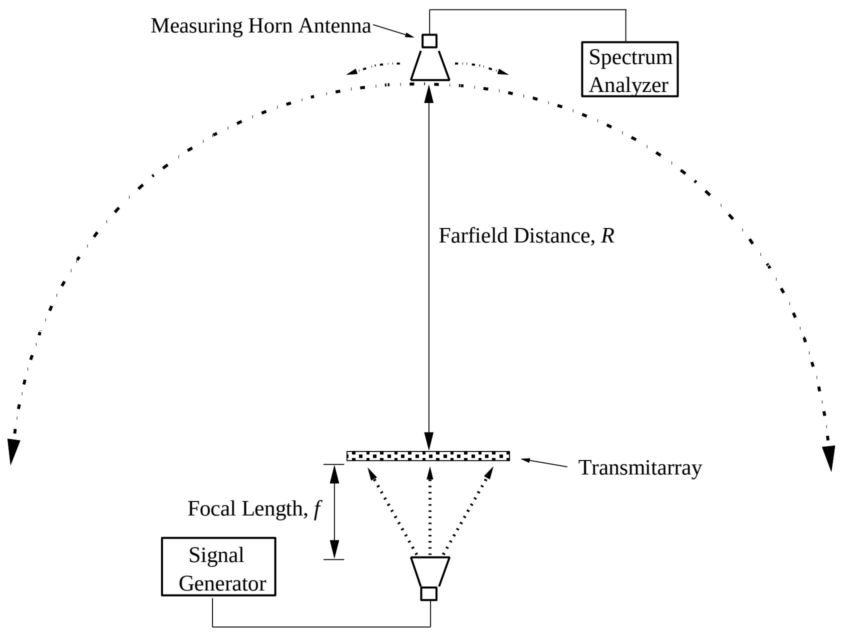

Figure 4.10: Measurement setup for the transmitarray.

Figure 4.11 shows the simulated and measured radiation patterns of the proposed 9×9 annular ring-slot transmitarray in the *E*- and *H*-planes. Reasonable agreement is seen between simulation and measurement. For both planes, it has achieved a maximum measured gain of 22.47dBi and 22.34dBi (simulation 21dBi) in the broadside direction (θ = 0^o) at 7.8GHz. The co-polarized field is larger than its cross-polarized counterpart by at least ~30dB in the broadside. With reference to the figure, the theoretical cross-polarized components are not provided as the level is lower than -30dBi. It can be seen from *Figure 4.12* that the measured 1-dB gain bandwidth of the proposed transmitarray is ~ 2.58%, which is lower than its simulated value of 5.16%.

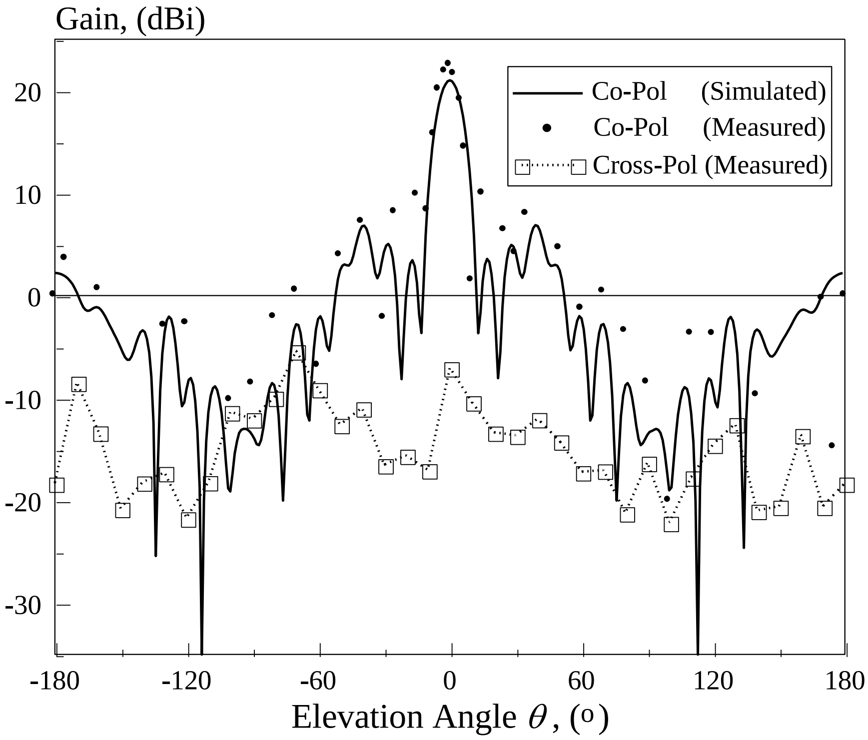

(a)

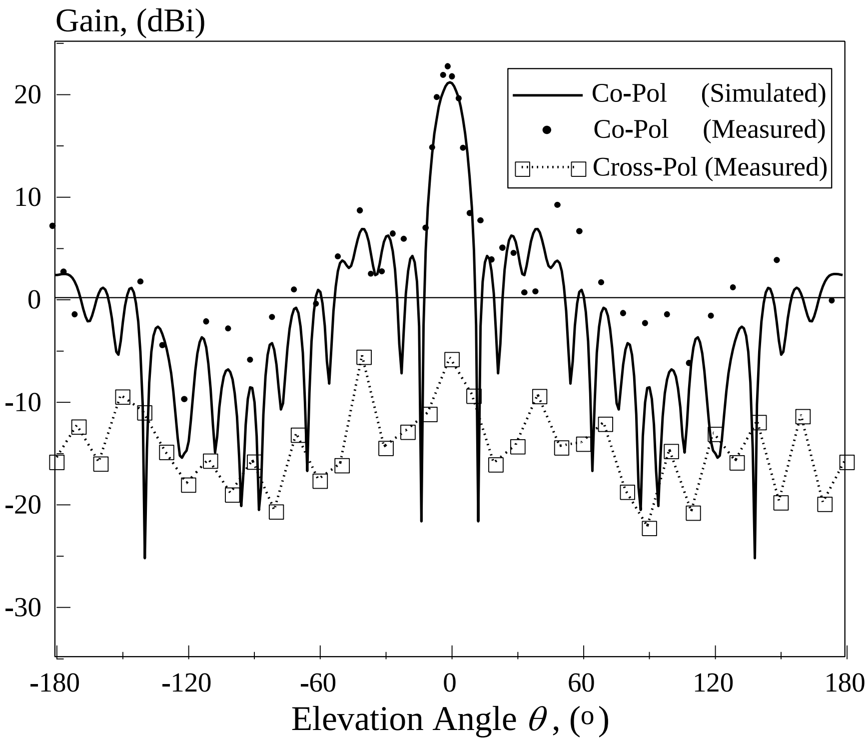

(b)

Figure 4.11: Simulated and measured (a) *E*- and (b) *H*- plane radiation patterns of the proposed transmitarray at 7.8GHz.

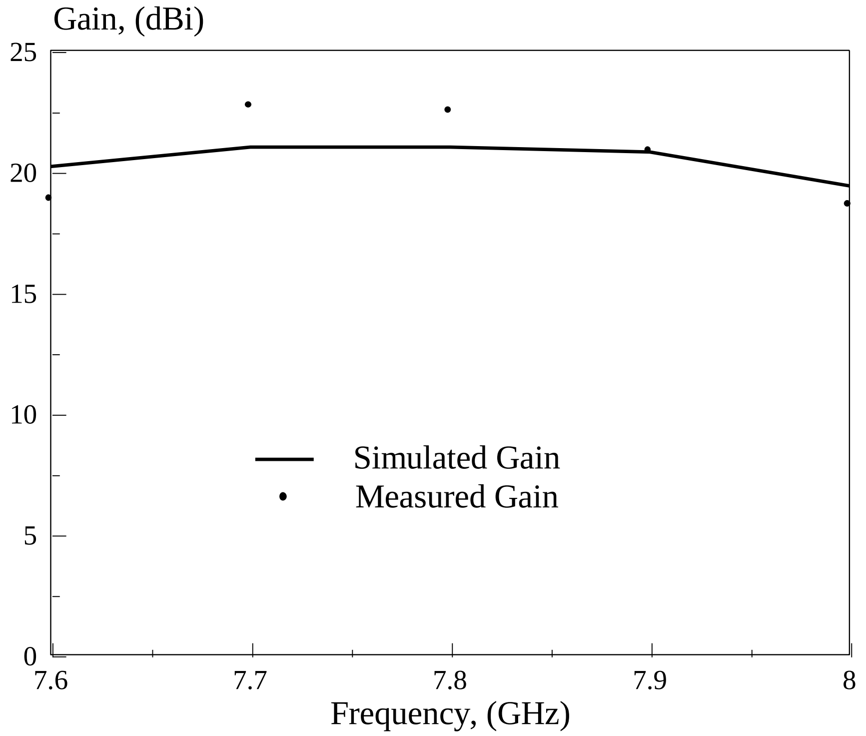

(a)

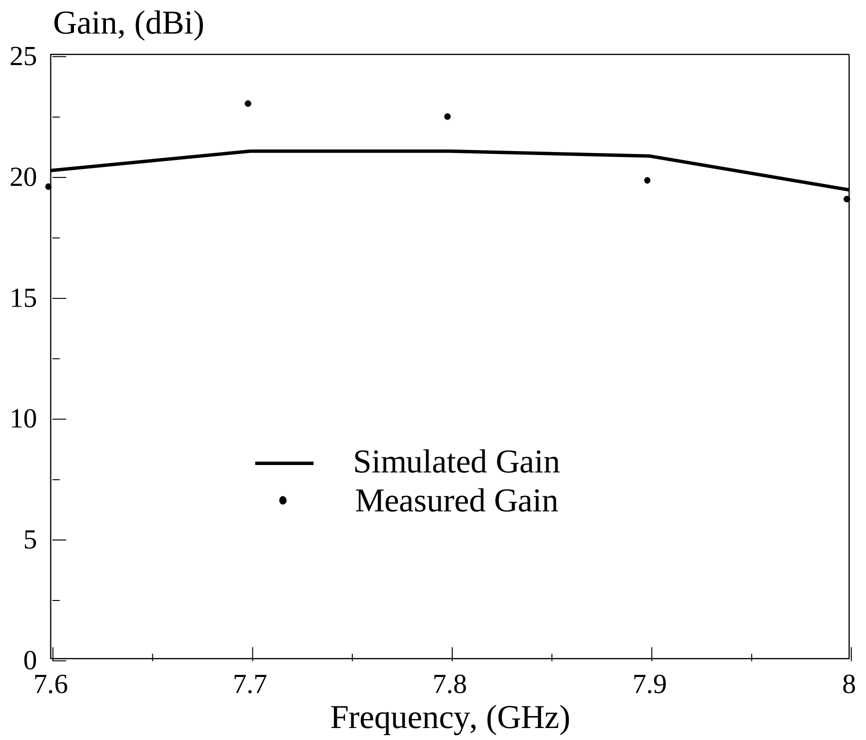

(b)

Figure 4.12: Simulated and measured 1-dB bandwidth of the proposed transmitarray at 7.8GHz. (a) *E*-plane and (b) *H*- plane.

4.5 Parametric Analysis

Parametric analysis is performed on the transmitarray. The holistic effect of the separation distance (L) between the elements is studied. *Figure 4.13* illustrates the radiation patterns of the proposed transmitarray when L is varied from 0.52λ, 0.60λ, to 0.78λ. In this case, the transmitarray is made to have a constant ratio of $F / D = 1$ at 7.8GHz and a comparison is made and summarized in Table I. The two cases which have the separation distance of 0.5λ - 0.6λ are able to produce better antenna gain and wider HPBW angle. Although transmitarrays with 0.52λ and 0.60λ are able to give an antenna gain of greater than 20dBi, the one with 0.60λ is selected because it has lower side-lobes and back-lobe.

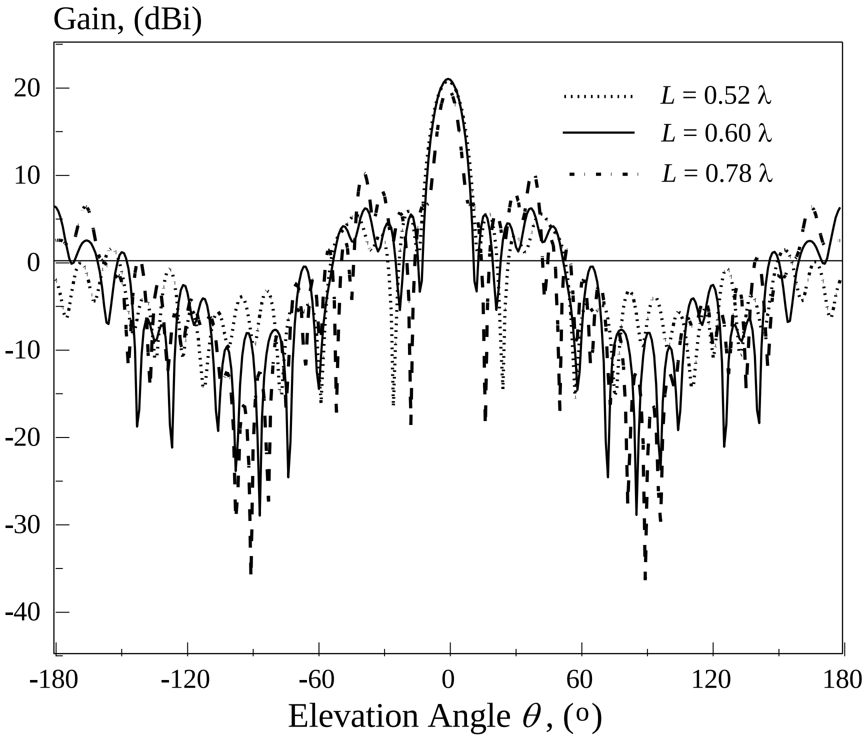

(a)

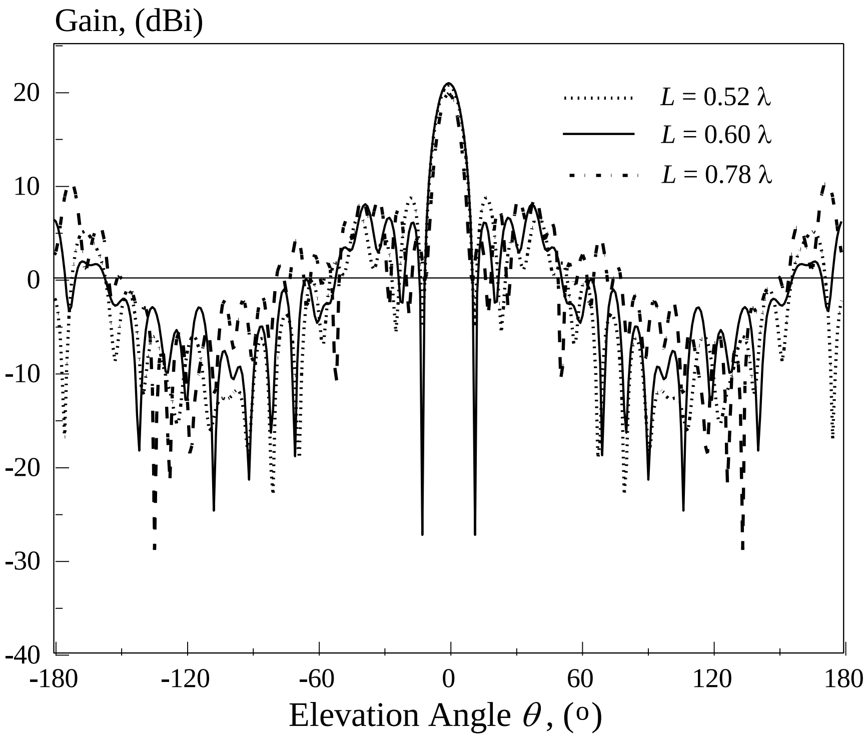

(b)

Figure 4.13: Radiation patterns of the proposed transmitarray with different element separations (L) at 7.8 GHz. (a) E- and (b) H- plane.

Table 4.1: Antenna gain and half-power beamwidth (HPBW) for the transmitarray with different separation distances (*L*).

Separation Distance, *L*	***E* plane**		***H* plane**	
	Gain(dBi)	**HPBW(°)**	**Gain(dBi)**	**HPBW(°)**
0.52 λ	20.6	11.9	20.6	10.5
0.60 λ	20.8	11.0	20.8	10.5
0.78 λ	19.7	7.9	19.7	8.7

By keeping the separation distance at $L = 0.60\lambda$ and the array dimension at D = 207mm, again, the F / D ratios of the proposed 9×9 transmitarray is varied from 0.87, 1, to 1.2 at 7.8GHz. Radiation patterns are shown in *Figure 4.14* as a function of elevation angle (θ), and the antenna performances are compared in Table II. With reference to the figure, smaller F / D ratio is seen to result in higher gain in the broadside direction. As can be seen in the figure, also, increase in the F / D ratio causes the backlobe to deteriorate.

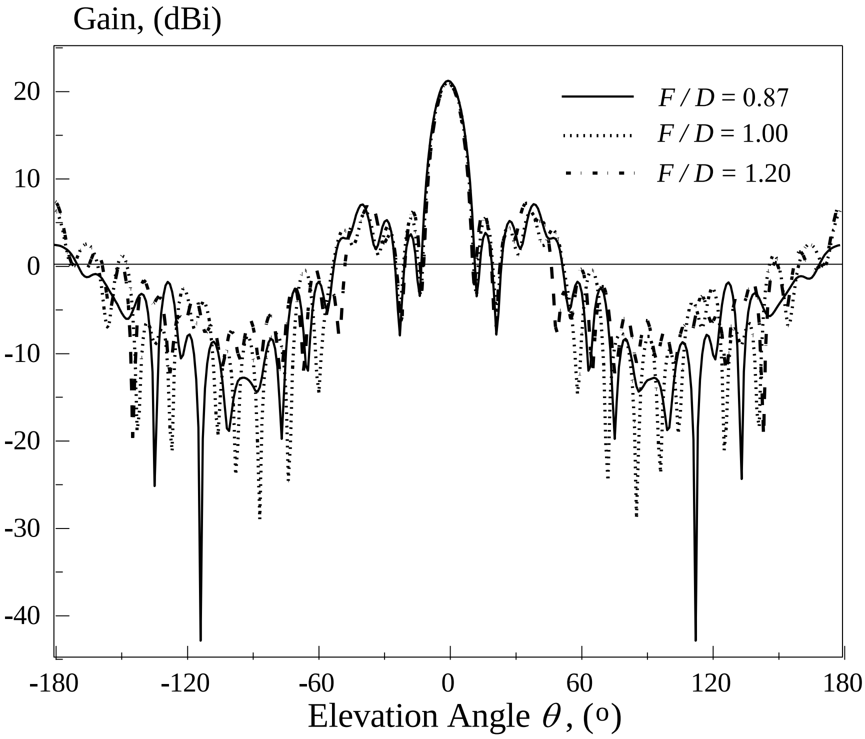

(a)

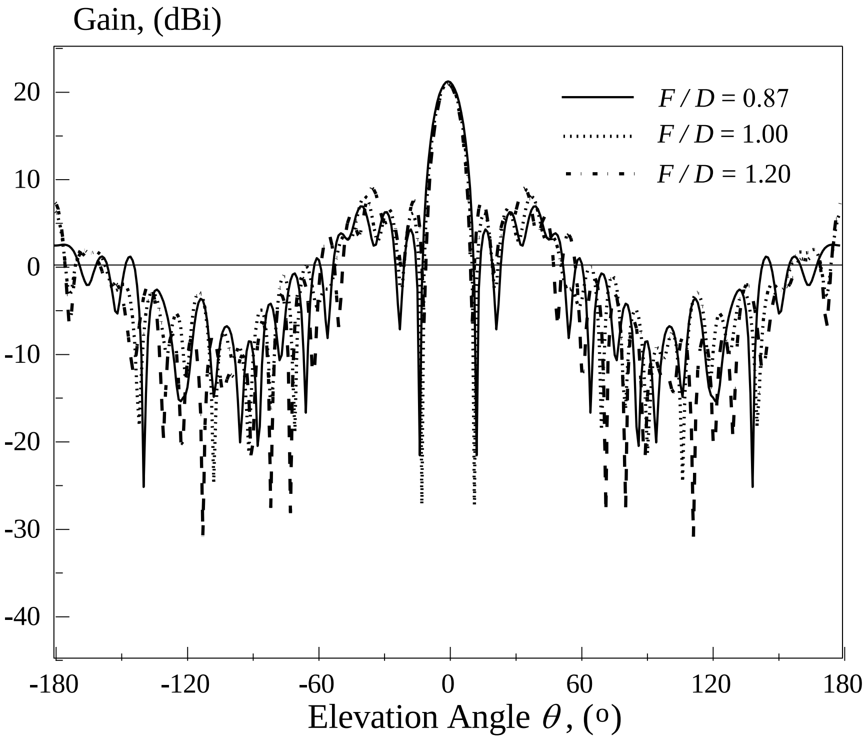

(b)

Figure 4.14: Radiation patterns of the proposed transmitarray with different F / D ratios at 7.8 GHz. (a) *E*- and (b) *H*- plane.

Table 4.2: Antenna gain and half-power beamwidth (HPBW) for the transmitarray with different *F / D* ratios.

F / D ratios	***E* plane**		***H* plane**	
	Gain(dBi)	**HPBW(°)**	**Gain(dBi)**	**HPBW(°)**
0.87	21.0	11.1	21.0	11.0
1.00	20.8	11.0	20.8	10.5
1.20	20.7	10.5	20.7	9.8

4.6 Conclusion

The annular ring-slot resonator has been successfully deployed for designing a 9×9 transmitarray, which has achieved a measured gain of 22.4dBi and a 1dB bandwidth of 2.58%. Reasonable agreement is obtained between the simulated and measured results. All the design parameters have been studied and analyzed systematically in this chapter. Although this type of resonator has slightly larger insertion loss, it can still be used for designing a transmitarray with an antenna gain of greater than 20dBi when appropriate parameters are chosen.

CHAPTER 5

SUMMARY AND DISCUSSION

In this dissertation, two different transmitarray resonators have been proposed and studied numerically and experimentally. In the first part, the Yagi-Uda concept has been applied for designing a Linearly Polarized (LP) transmitarray. In this design, the polarization can be easily modified into Circularly Polarized (CP) transmitarray by making every two of the strips inclined anti-clockwise with an angle of 5^{o}. A 5×5 full-fledge LP transmitarray able to provide antenna gain of ~17dBi with a broad 1dB bandwidth of 11.86% whereas CP transmitarray has a measured gain of 16.6dBi and 1dB bandwidth of 4%. In the second part, an annular ring-slot resonator has been deployed for designing a 9×9 multilayer transmitarray. It was found that an antenna gain of 22.4dBi can be easily achieved in the broadside direction. The design procedures and key performance indicators of transmitarrays have been presented and discussed in detail. Reasonable agreement has been observed between all the simulations and measurements.

REFERENCES

Abbaspour-Tamijani, A., Sarabandi, K., Rebeiz, G. M., 2007. A millimeter-wave bandpass filter-lens array. *IET Microwaves, Antennas and Propagation*, vol. 1, pp. 388-395.

Abdelrahman, A. H., Elsherbeni, A. Z. and Yang, F., 2014. Transmitarray Antenna Design Using Cross-Slot Elements with no Dielectric Substrate. *IEEE Antennas and Wireless Propagation Letter*, vol. 13, pp. 177-180.

Abdelrahman A. H., Yang F., Elsherbeni A. Z., and Khidre A., 2013. "Transmitarray Antenna Design using Slot-Type Element", *IEEE Antennas and Propagation Society International Symposium (APSURSI)*, pp. 1356-1357.

Abdelrahman, A. H., Yang, F., and Elsherbeni, A. Z., 2014. Transmission Phase Limit of Multilayer Frequency Selective Surfaces for Transmitarray Designs. *IEEE Transaction on Antennas and and Propagation*, vol. 62, pp. 690-697.

Abdelrahman A. H., Nayeri P., Elsherbeni A. Z., Yang F., 2014. "Analysis and Design of Wideband Transmitarray Antennas with Different Unit-Cell Phase Ranges", *IEEE Antennas and Propagation Society International Symposium (APSURSI)*, pp. 1266-1267.

Abdelrahman A. H., Nayeri P., Elsherbeni A.Z., Yang F., 2015. Bandwidth Improvement Methods of Transmitarray Antennas. *IEEE Transaction on Antennas Propagation*, vol. 63, no. 7, pp. 2946-2954.

Almajali, E., McNamara, D. A., Shaker, J. and Chaharmir, M. R., 2014. Feed Image Lobes in Offset-Fed Reflectarrays: Diagnosis and Solution. *IEEE Transactions Antennas and Propagation*, vol. 62, no. 1, pp. 216-227.

Arrebola, M., Encinar, J. A. and Barba, M., 2008. Multifed printed reflectarray with three simultaneous shaped beams for LMDS central station antenna. *IEEE Transactions on Antennas and Propagation*, vol. 56(6), pp. 1518-1527.

Berry, D., Malech, R. and Kennedy, W., 1963. The reflectarray antenna. *IEEE Transactions Antennas and Propagation*, 11(6), pp. 645-651.

Bhattacharyya, A. K., 2006. *Phased Array Antennas: Floquet Analysis, Synthesis, BFNs, and Active Array Systems*, John Wiley & Sons, Inc., Hoboken, New Jersey.

Bozzi M., Germani S., and Perregrini, 2004. A Figure of Merit for Losses in Printed Reflectarray Elements. *IEEE Antennas and Wireless Propagation Letter*, vol. 3, no. 1, pp. 257-260.

Capozzoli, A., Curcio, C., D'Elia, G. and Liseno, A., 2010. Fast phase-only synthesis of conformal reflectarrays. *IET Microwaves, Antennas and Propagation*, vol. 4(12), pp. 1989-2000.

Chew W. C., 1982. A Broad-Band Annular Ring Microstrip Antenna. *IEEE Transactions Antennas and Propagation*, vol. 30, pp. 918-922.

Clemente, A., Dussopt, L., Sauleau, R., Potier, P. and Pouliguen, P., 2012. Focal Distance Reduction of Transmit-Array Antennas Using Multiple Feeds. *IEEE Transactions Antennas and Propagation*, vol. 11, pp. 1311-1314.

Dussopt, L., Kaouach, H., Lanteri, J. and Sauleau, R., 2011. Circularly-Polarized Discrete Lens Antennas in the 60-GHz Band. *Radioengineering*, December 2011, vol. 20, issue 4, pp. 733-738.

Encinar, J. A., 2001. Design of Two-layer Printed Reflectarrays using Patches of Variable Size. *IEEE Transactions on Antennas and Propagation*, vol. 49, no. 10, pp. 1403-1410.

Eriksson A., Linner P., and Gevorgian S., 2001. Mode chart of electrically thin parallel-plate circular resonators. *IEEE Proceedings Microwaves Antennas and Propagation*, vol. 148, no. 1, pp. 51-55.

Friedlander, F. G., 1946. A dielectric-lens aerial for wide-angle beam scanning. *IEE Electrical Engineers-Part IIIA: Radiolocation*, vol. 93, no. 4, pp. 658-662.

Gao, S., Luo, Q. and Zhu, F., 2014. *Circularly Polarized Antennas*. John Wiley & Sons, Inc, United Kingdom.

Hansen, R. C., 2009. *Phased Array Antennas*, 2nd ed. John Wiley & Sons, Inc., Hoboken, New Jersey.

Hollung, S., Cox, A. E., and Popovic, Z. B, 1997. A Bi-Directional Quasi-Optical Lens Amplifier. *IEEE Transactions on Microwave Theory and Techniques*, vol. 45, no. 12, pp. 2352-2357.

Huang, J. and Encinar, J. A., 2007. *Reflectarray Antennas*, John Wiley & Sons, Inc., Hoboken, New Jersey.

Ikonen, P., Karkkainen, M., Simovski, C., Belov, P., and Tretyakov, S., 2006. Light-weight base station antenna with artificial wire medium lens. *IEE Proceedings Microwaves*, *Antennas and Propagation*, vol. 153, no. 2 , pp. 163-170.

Jasik, H. 1961. *Antenna Engineering Handbook*, In: Chapters 12 and 15. New York: MaGraw-Hill.

Kaouach, H., Dussopt, L., Lanteri, J., Koleck, T. and Sauleau, R., 2011. Wideband Low-Loss Linear and Circular Polarization Transmit-Arrays in V-Band, *IEEE Transactions on Antennas and Propagation*, vol. 59, no. 7, pp. 2513-2523.

Ku B.-H., Schmalenberg P., Inac O., Gurbuz O. D., Lee J. S., Shiozaki K., and Rebeiz G. M., 2014. A 77-81-GHz 16-Element Phased-Array Receiver with ±50^{o} Beam Scanning for Advanced Automotive Radars, *IEEE Transactions on Microwave Theory and Techniques,* vol. 62, no. 11, pp. 2823-2832.

Kumar R. R. and Malathi P., 2007. Design of Multi-band Microstrip Yagi Uda Antenna, *IEEE Applied Electromagnetics Conference (AEMC2007),* pp. 1-4.

Khoury, K. and Heane, G. W., 1991. High performance lens horn antennas for the millimeter bands. *IEE Colloquium on Radiocommunications in the Range 30-60 GHz*, pp. 10/1-10/9.

Lam, K. W., Kwok S.-W., Hwang, Y. and Lo, T. K.-C., 1997. Implementation of Transmitarray Antenna Concept by using Aperture-Coupled Microstrip Patches. *Asia Pacific Microwave Conference*, *1997. APMC'97*, 1997 Asia Pacific, vol. 1, pp. 433-436.

Lyer, A. K., and Eleftheriades, G. V., 2007. A Multilayer Negative-Refractive-Index Transmission-Line (NRI-TL) Metamaterial Free-Space Lens at X Band, *IEEE Transactions on Antennas and Propagation*, vol. 55, no. 10, pp. 2746-2753.

McGrath, D. T., 1986. Planar three-dimensional constrained lenses. *IEEE Transactions on Antenna and Propagation*, vol. 34, no. 1, pp. 46-50.

Nagy L., 2010. "Low Profile Circular Yagi-Uda Array," in *Proceeding of the Fourth European Conference*, pp. 1-5.

Nascimento D. C., Schildberg R., and Lacava J. C. da S., 2008. "Low-Cost Yagi-Uda Monopole Array," *IEEE Antennas and Propagation Society International Symposium AP-S2008,* pp. 1-4.

Petosa, A., Thirakoune, S., Minin, I. V., and Minin, O. V, 2006. Array of hexagonal Fresnel zone plate lens antennas, *Electronics Letters*, vol. 42, no. 15, pp. 834-836.

Pozar, D. M., 1996. Flat lens antenna concept using aperture coupled microstrip patches. *Electronics Letters*, vol. 32, no. 23, pp. 2109-2111.

Rajagopalan H., and Rahmat-Samii Y., 2008. Dielectric and Conductor Loss Quantification for Microstrip Reflectarray Simulations and Measurements", *IEEE Transactions on Antennas and Propagation*, vol. 56, no. 4, pp. 1192-1196.

Rajagopalan H., Xu S., and Rahmat-Samii Y., 2012. On Understanding the Radiation Mechanism of Reflectarray Antennas: An Insightful and illustrative Approach. *IEEE Journals & Magazines*, vol., 54, no. 5, pp. 14-38.

Reinhart R. C., Johnson S. K., Acosta R. J., Sands S., 2003. Phased Array Antenna-Based System Degradation at wide scan angles, *IEEE International Symposium on Phased Array System and Technology*, pp. 446-451.

Ruze, J., 1950. Wide-Angle Metal-Plate Optics, *Proceedings of the IRE*, vol. 38, pp. 53-59.

Ryan, C. G. M., Chaharmir, M. R., Shaker, J., Bray, J. R., Antar, Y. M. M. and Ittipiboon, A., 2010. A wideband Transmitarray using Dual-Resonant Double Square Rings. *IEEE Transactions Antennas and Propagation,* vol. 58, no. 5, pp. 1486-1493.

Shaker, J., Chaharmir, M. R. and Ethier, J., 2014. *Reflectarray Antennas: Analysis, Design, Fabrication, and Measurement*, Artech House, Boston, London.

Thornton, J. and Huang, K.-C., 2013. *Modern Lens Antennas for Communications Engineering*, John Wiley & Sons, Inc., Hoboken, New Jersey.

Toh, B. Y., Cahill, R. and Fusco, V. F., 2003. Understanding and measuring circular polarization, *IEEE Transactions on Education*, vol. 46, pp. 313-318.

Yijing, F., Ban-Leong, O., Hristov, H. D., and Mook-Seng, L., 2010. Compound Diffractive Lens Consisting of Fresnel Zone Plate and Frequency Selective Screen. *IEEE Transactions on Antennas and Propagation*, vol. 58, no. 6, pp. 1842-1847.

Yu, A., Yang, F., Elsherbeni, A. Z., Huang, J. and Rhamat-Samii, Y., 2009. Aperture Efficiency Analysis of Reflectarray Antennas, *Mircowave and Optical Technology Letters*, vol. 52, no.2, pp. 364-3972

Zhou, M., Sorensen, S. B., Kim, O. S., Jorgensen, E., Meincke, P. and Breinbjerg, O., 2013. Direct optimization of printed reflectarrays for contoured beam satellite antenna applications. *IEEE Transactions Antennas and Propagation*, 61(4), pp. 1995-2004.

Zhou, Y., Rondineau, S., Popovic, D., Sayeed, A., and Popovic, Z., 2005. Virtual Channel Space-Time Processing with Dual-Polarization Discrete Lens Antenna Arrays. *IEEE Transactions Antennas and Propagation*, vol. 54, no. 8, pp. 2444-2455.